ABSTRACT

CARPENTER, SCOTT. Advancing Connected Vehicle Technologies by Improving Vehicular Channel Model Accuracy and Safety Performance Measures. (Under the direction of Dr. Mihail L. Sichitiu).

Wireless communications technologies allow vehicles to exchange information and thus create connected vehicle networks that enable safety applications, such as accident avoidance, thereby reducing damage and injuries caused by moving vehicle collisions. The most promising technologies in the U.S. that will enable such a vehicular ad hoc network (VANET) are collectively referred to as Dedicated Short-Range Communications (DSRC). While standards evaluation units exist, deployment has been limited to prototype testing, forcing VANET researchers to rely on simulation tools and supporting models, with mixed results. Results from inaccurate models can threaten the evaluation of safety applications, with existing performance metrics often only evaluating communications Quality of Service (QoS) measures while ignoring vehicular mobility.

In this dissertation, we explore common deterministic and stochastic vehicular channel models (VCMs), comparing their performance to measurement data from a real-world testbed, and evaluating their impact to safety performance metrics. First, we contribute to the *ns-3* simulator an implementation of a VCM that supports obstacle shadowing using geodata and provide simulation results that compare the performance of the deterministic obstacle shadowing model to other common stochastic fading and shadowing models. Second, we study the packet-level performance of DSRC safety message receptions among vehicular encounters as derived from a large deployment of nearly 3000 DSRC-equipped vehicles operating near Ann Arbor, MI. We find that packet losses for many vehicle-to-vehicle (V2V) encounters differ significantly from traditional, static-node networks. Around Ann Arbor,

packet losses exhibit temporal correlations when inter-packet gaps are 400ms or longer, but are mostly uncorrelated for shorter gaps. Third, we evaluate the performance of several existing VCMs and show that the UMTRI large-scale Ann Arbor testbed exhibits significant shadowing and fading effects that traditional VCMs often fail to capture. Fourth, we introduce BUR-GEN, a packet generation algorithm that improves upon other, common models in terms of packet burst pattern generations. Fifth, we propose *SafeRelay*, a safety message dissemination technique that floods geo-addressed safety messages within a nearby flooding zone, and evaluate packet delivery effectiveness using a new metric, *probability of safety awareness*, that combines packet delivery effectiveness with vehicular mobility. Sixth, we conduct a safety assessment that compares BUR-GEN and i.i.d.-based packet loss models to the observations found within the Ann Arbor testbed. We find that our burst-aware packet generation model improves awareness probability for maximum safety tolerance by a factor of 31. Finally, we motivate additional studies of VCMs that avoid the pitfalls we observe within models that are based on i.i.d. assumptions and instead employ bursty packet generator functions. The lessons learned from our studies motivate advances in connected vehicle technologies by improving vehicular channel model accuracy and safety performance measures.

© Copyright 2018 Scott Carpenter

All Rights Reserved

Advancing Connected Vehicle Technologies by Improving Vehicular Channel Model Accuracy and Safety Performance Measures

by
Scott Carpenter

A dissertation submitted to the Graduate Faculty of
North Carolina State University
in partial fulfillment of the
requirements for the degree of
Doctor of Philosophy

Computer Science

Raleigh, North Carolina

2018

APPROVED BY:

_____	_____
Dr. Mihail L. Sichitiu Committee Chair	Dr. David Thuente
_____	_____
Dr. Rudra Dutta	Dr. Raju Vatsavai

DEDICATION

To God, from where all knowledge comes, and to my family.

BIOGRAPHY

The author was born and raised in Wheeling, West Virginia, USA. The author earned his Bachelor of Science (BS) in Computer Engineering from Case Western Reserve University in January 1989, followed by a Master of Science (MS) in Computer Engineering from Case Western Reserve University in May 1993. Prior to joining the doctoral program at the North Carolina State University, the author worked in industry for several years in a variety of software engineering, project management, and managerial roles.

ACKNOWLEDGMENTS

This dissertation is the culmination of roughly 6 years of my mostly part-time education at the North Carolina State University (NCSU). My experiences at NCSU during this wonderful time have played an important part in my growth, intellectually, and as a person. I would like to use this opportunity to thank those who have affected me during this time and assisted me in this growth.

First and foremost, I would like to thank my advisor, Dr. Mihail L. Sichitiu, for his exceptional guidance and support over the course of my time pursuing this degree. At our first meeting, Dr. Sichitiu asked me "Why do you want a Ph.D.?". I don't recall my assuredly pitiful answer. But, I will forever remember Dr. Sichitiu's response, "No, that's not a good reason for a Ph.D.". I quickly realized this was someone who was actually going to make me learn something, not only in an educational sense, but through a journey to learn about myself. I always looked forward to our multitude of meetings, as I came to realize Dr. Sichitiu practices an amazing balance of technical explanation, challenging questions, constructively thorough and helpful comments, humor, and just at the right times, enough silence to allow me to learn. I am forever grateful that he allowed me to be one of his graduate students, and I owe the successful completion of my Ph.D. entirely to Dr. Sichitiu's mentoring. I also believe I owe him several boxes of red pens to replace his supply, but that is another matter altogether.

Over the course of my years in graduate school at NCSU, I have had the benefit of interacting with faculty and staff who have substantially influenced my research with their broad insights and interesting perspectives. I would like to thank the members of my doctoral committee, Dr. David Thuente, Dr. Rudra Dutta, and Dr. Raju Vatsavai for their valuable feedback during the course of my degree. Additionally, I would like to thank the faculty that clarified for me the complexities of many topics and continually challenged me to understand them in ways I would never have otherwise imagined, specifically, Dr. Do Young Eun, Dr. Munidar Singh, Dr. Edgar Lobaton, Dr. Aldo Dagnino, Dr. Douglas Reeves, Dr. George Rouskas, Dr. Laurie Williams, Dr. Wenye Wang, Dr. Khaled Harfoush, Dr. Purush Iyer, and Dr. Javad Taheri. Go Pack!

During my time studying at NCSU, I had the amazing opportunity to work with students and staff as a Computer Science Research Developer, and also as a summer instructor. For the fond memories that I have of these opportunities, I would especially like to thank Dr. R.

Michael Young, Dr. Camille Barot, Dr. Sarah Heckman, Dr. David Sturgill, Carol Allen, Linda Honeycutt, and Terri Martin-Moss. I would also like to thank those Computer Science students that braved the hot, summer months in Raleigh and allowed me the pleasure of teaching them about data structures and operating systems. These classroom interactions were indeed some of my fondest and most rewarding experiences while at NCSU.

I would like to thank the collaborative members of the *ns-3* simulator framework, who guided me in developing much of the code that was eventually contributed, especially Dr. Tom Henderson, Dr. Peter Barnes, Dr. Tomasso Pecorella, Dr. George Riley, and Dr. Konstantinos Katsaros. Additionally, I would like to thank the members of the SAE DSRC Technical Committee, who helped me tremendously in understanding the DSRC operational standards and their intent, especially Dr. Jim Misener and Dr. Sue Bai.

While this body of work was created through many hours spent at home and at libraries, it also resulted in the consumption of what I am sure has been hundreds of gallons of caffeinated beverages, mostly coffee. And much of that consumption was done in the soft, Wi-Fi glow of various coffee shops and fast food establishments. I extend my warmest thanks to all those in the service industry who unknowingly contributed to helping me maintain my focus through copious consumption of caffeinated concoctions while I spent many hours enjoying the fine atmosphere of their establishments.

Most importantly, I would like to thank my family for their love, support and patience. To my mother and father, who encouraged my mathematical and scientific curiosities and accepted my pursuits to be the first generation in my family to attend college, I owe my deepest thanks. To my loving wife, MaryBeth, who, when I asked unexpectedly one day, “What would you think if I got a Ph.D.?”, I eternally offer my love and thanks for answering so supportively and then multiplying that support again and again with each passing accomplishment, no matter how minor. And to my children, Christian, Daniel, and Kaitlyn, who endured my gleaming gladness, when learning about each paper accepted for publication, as well as my times of thoughtful solitude, when the next step along the path seemed unclear, if not impossible to surmount, I offer my thanks for tolerating my many, sleep-deprived moments and for celebrating with me my victories.

To all who touched my life during this process, thank you for making me a better person, for supporting me during this educational period of my life, and for convincing me that anything is possible.

TABLE OF CONTENTS

LIST OF TABLES……. x
LIST OF FIGURES……... xii

1 Chapter 1 Introduction……..…. 1
1.1 Thesis Statement…….. 2
1.2 Contributions……... 5
1.3 Dissertation Outline……..... 7

2 Chapter 2 Related Work……..... 9
2.1 Vehicular Safety…….. 9
2.2 Dedicated Short-Range Communications (DSRC) Standards and Operations……..10
2.3 Radio Propagation Model (RPM) Literature Review…… 15
2.4 Vehicular Channel Models…… 19
2.4.1 Path Loss……19
2.4.2 Probability of Packet Reception……19
2.5 Path Loss Models……...20
2.5.1 Deterministic Path Loss Models…… 20
2.5.2 Probabilistic Path Loss Models……..21
2.6 Obstacle Modeling……26
2.7 Dissemination of Safety Information……28
2.8 Vehicular Mobility Simulation…….. 29
2.9 Vehicular Network Simulation……..... 30
2.10 Safety Assessment and Metrics……... 32
2.11 Evaluations of Vehicular Wi-Fi Networks……...38
2.11.1 Static-node Beaconcasting Wireless Networks…… 38
2.11.2 DSRC FOTs……...38
2.11.3 Safety Pilot Model Deployment (SPMD)……..39
2.11.4 Performance in Ann Arbor……39

3 Chapter 3 An Obstacle Model Implementation for Evaluating Radio Shadowing……...40
3.1 Introduction……40
3.2 Obstacle Shadowing Model……...42
3.2.1 Obstacle Model……..42
3.2.2 Propagation Loss……46
3.3 Experimental Setup and Results…… 47
3.3.1 Experimental Setup……47
3.3.2 Results and Discussion…….. 53
3.3.3 Performance……...59
3.4 Summary……60

4 Chapter 4 Analysis of Packet Loss in a Large-Scale DSRC Field Operational Test…….. 61
4.1 Introduction……62
4.2 SPMD Data Analysis……63
4.2.1 The SPMD Data Environment (DE)……..63

4.2.2 Approach……65
4.3 Results……66
4.3.1 Packet Loss……66
4.3.2 Packet Reception Ratio……67
4.3.3 Inter-Packet Gap (IPG)……68
4.3.4 Time Correlation of IPG Length……71
4.4 Conclusions……74

5 Chapter 5 Evaluating the Accuracy of Vehicular Channel Models in a Large-Scale DSRC Test……75
5.1 Introduction……76
5.2 Background……76
5.2.1 Objective……78
5.2.1 Geometry-Based (GB) Models……78
5.3 Model Evaluation……80
5.4 Results……81
5.4.1 Maximum Likelihood Estimates……81
5.4.2 Packet Reception Ratio (PRR)……82
5.4.3 Inter-Packet Gap (IPG)……83
5.4.4 Consecutive Reception Run-Length (CRRL)……84
5.4.5 Obstacle Shadowing Effects……85
5.4.6 Numerical Results……86
5.5 Conclusions……87

6 Chapter 6 BUR-GEN: Packet Generation for Bursty Vehicular Channel Models……90
6.1 Introduction……91
6.2 Motivation……91
6.3 Problem Statement……92
6.4 Packet Loss / Reception Behaviors in the SPMD……93
6.4.1 Background……93
6.4.2 Field Operations……93
6.4.3 Burstiness of Packet Gaps and Runs……97
6.4.4 Expected PRR……99
6.4.5 Conditional Packet Reception……100
6.4.6 Temporal and Spatial Sensitivity……101
6.5 Packet Loss Models……104
6.5.1 Bernoulli / Memoryless Packet Loss Model……104
6.5.2 Gilbert-Elliott Packet Loss Model……104
6.6 Approach……106
6.7 Packet Generation Model……107
6.7.1 Process Flow……107
6.7.2 Burst Generator (BUR-GEN) Model……108
6.7.3 Packet Reception Rate……109
6.7.4 Packet Generator……113
6.8 Experimental Setup……114
6.9 Results and Discussion……117

6.9.1 Results……..117
6.9.2 Discussion……..…118
6.10 Conclusions……..……118

7 Chapter 7 SafeRelay: Improving Safety in Time-Constrained VANETs with Geo-addressing Relay……...…120
7.1 Introduction……...121
7.2 Motivation……122
7.2.1 Safety Applications……...122
7.2.2 Safety Information Model……122
7.2.3 Channel Pressure……...124
7.2.4 Information Dissemination……...126
7.3 Safety Evaluation……..127
7.3.1 Communications Effectiveness……127
7.3.2 Mobility Effects……128
7.3.3 Safety Awareness Probability……...129
7.4 Evaluation and Results……..130
7.4.1 Simulation Setup……...130
7.4.2 Parameters……131
7.4.3 Results and Discussion……..135
7.5 Conclusions……...140

8 Chapter 8 Assessing the Safety Reliability of Modeling the Bursty Vehicular Channel……..142
8.1 Introduction……...143
8.2 Problem Statement……144
8.3 Approach……...146
8.4 Experimental Setup……...147
8.5 Results and Discussion……..147
8.6 Conclusions……...151

9 Chapter 9 Conclusions and Future Work……..152
9.1 Conclusions…….…… 152
9.2 Future Work……...…153

REFERENCES…… 155

APPENDIX……...162
Appendix A – Abbreviations…….……163

LIST OF TABLES

Table 2.1 DSRC device classes and operating parameters…… 13

Table 2.2 Safety-related vehicle communications applications (adapted from [1]).. 33

Table 2.3 V2V safety communications applications with greatest potential safety benefit…… 35

Table 2.4 Communications requirements for three CAMP/VSCC safety Applications……... 36

Table 3.1 Scenario topology parameters……49

Table 3.2 Network simulation parameters……53

Table 3.3 PDR average and standard deviation for three fading models……...59

Table 4.1 Trip data summary for Safety Pilot Model Deployment Data Environment. Over 22,000 vehicular trips covering 167,000 km in 4,700 hours resulted in more than 48M BSMs that were successfully received…… 65

Table 5.1 Five vehicular channel models for which estimated PRR is compared to the actual large-scale SPMD measurement data…….. 80

Table 5.2 Parametric values for the VCMs. The MLE of each parameter is shown with statistical bias in parentheses and appropriate units in brackets……...…81

Table 5.3 Numerical results for the RSME of three metrics (PRR, IPG, and CRRL) for five VCMs as compared to the Ann Arbor SPMD test data set. As expected, the unit disk model performs poorly in predicting PRR. While all other models better predict PRR, they fail to accurately predict consecutive packet losses (i.e., IPG) and reception (i.e., CRRL). Use of geodata to deterministically estimate path loss through obstacles (i.e., Model *E*) improves CRRL, as compared to a purely stochastic model (i.e., Model *B*) that does not make use of such geodata…….…….. 87

Table 5.4 Summary of five stochastic and/or deterministic VCMs evaluated against the Ann Arbor SPMD data set……. 88

Table 6.1 Expected run lengths and gap lengths for five distance bins. Expected run length increases when distance between transmitting and receiving vehicles decrease. Contrastingly, expected gap *length increases as distances between vehicles increases…….. 99*

Table 6.2 Expected PRR for five distance bins. PRR decreases as distance between transmitting and receiving vehicles increases……..99

Table 6.3 Numerical results of the RSME for three metrics – PRR, IPG, and CRRL – of the combined dual-slope distance-breakpoint model with the BUR-GEN burst distribution function (i.e, Model *F*, compared to five common (i.i.d. only) VCMs (i.e., Models *A*-*E*)…….. 118

Table 7.1 Three message dissemination strategies that are evaluated……. 131

Table 7.2 Four configuration that vary forwarding zone parameters based on different application requirements…….. 134

Table 8.3 Application range and message tolerance for four VSC safety Applications……. 147

Table 8.4 Minimum and maximum safety performance requirements used for evaluation, as a function of distance…… 147

LIST OF FIGURES

Figure 2.1 Total U.S. motor vehicle fatalities per 100,000 population, 1950 – 2012……10

Figure 2.2 DSRC reference model……...12

Figure 2.3 Representative VANET simulation tools. Adapted from: [1]……...31

Figure 3.1 Obstacles in a downtown Raleigh, NC scenario as simulated in SUMO……42

Figure 3.2 Obstacle shadowing model enhancements to the ns-3 reference model…43

Figure 3.3 A subset of buildings data for the downtown Raleigh, NC USA area…...44

Figure 3.4 Pseudo-code for the algorithm that determines the number of obstacle wall intersections and obstructed distance between two points...45

Figure 3.5 Obstacle intersection range……46

Figure 3.6 Process flow for experimental setup……..48

Figure 3.7 View in GoogleEarth™ (above) and visualization in SUMO of Open Street Map (OSM) buildings data (below) for an open highway scenario near Raleigh, NC USA……. 50

Figure 3.8 View in GoogleEarth™ (above) and visualization in SUMO of Open Street Map (OSM) buildings data (below) for a residential neighborhood scenario near Raleigh, NC USA……51

Figure 3.9 View in GoogleEarth™ (above) and visualization in SUMO of Open Street Map (OSM) buildings data (below) for an urban downtown scenario near Raleigh, NC USA……...52

Figure 3.10 Example propagation loss effects near an intersection……..54

Figure 3.11 PDR over time for three fading models……55

Figure 3.12 PDR for the open highway scenario with 250 vehicles, for three different fading models as a function of the distance from the transmitter……...56

Figure 3.14 PDR for the downtown scenario with 250 vehicles, for three different fading models as a function of the distance from the transmitter……..57

Figure 3.13 PDR for the neighborhood scenario with 250 vehicles, for three different fading models as a function of the distance from the transmitter……..57

Figure 3.15 PDR for residential neighborhood scenario with no fading, for 50 – 250 vehicles as a function of the distance from the source of the transmission……. 58

Figure 3.16 CPU-time (minutes) of the sum of times to simulate 2000s of 150 vehicles in the highway, residential, and downtown scenarios for different fading models…… 60

Figure 4.1 Representative coverage area for the Safety Pilot Model Deployment in Ann Arbor, Michigan. Highlights represent the line of sight of over 3 million successful BSM receipts for selected encounters between a receiving vehicle (Rx) and a transmitting vehicle (Tx), as derived from the SPMD DE…….64

Figure 4.2 Packet reception for four example encounters from the SPMD DE. Encounter time can vary significantly. When vehicles are in close proximity to one another, packet reception is more likely, but the correlation to distance is otherwise inconsistent…… 67

Figure 4.3 Packets received (red, below) relative to packets not received (green, above) as a function of the distance between sender and receiver for the SPMD DE. Reception success (i.e., PRR) decreases as distance increases. PRR is greater than 65% only at distances less than 10m and decreases rapidly with distance, with few packets successfully received beyond 400m……...68

Figure 4.4 Average IPG as a function of relative transmitter distance from the receiver as centered at (x=0, y=0). IPG is generally low regardless of senders being directly ahead of or behind the receiver, but increases as distance increases, especially when lateral distances increase and the transmitter is behind the receiver. Numbers indicate the count of IPG values that are averaged for each cell…… 69

Figure 4.5 Log-log plot of the probability distribution of frequency of inter-packet gaps in seconds, out to one minute, within the SPMD DE. A majority (93%) of IPG lengths are less than 200ms (i.e., losses of 0 or 1 packet), while longer IPG lengths plausibly follows a power law distribution model, $p(x)=0.342x^{-2.374}$…… 70

Figure 4.6 Overlapping Allan deviation, $\boldsymbol{\sigma y}(\boldsymbol{\tau})$, of packet loss gaps throughout Ann Arbor, as a function of $\boldsymbol{\tau}$, the averaging factor in seconds. The SPMD DE dataset is split into four quartiles (i.e., $Q_1..Q_4$) by the average gap length for 1950 encounters…….73

Figure 5.1 The receiving vehicle, RX (green trajectory), moves from the top right to the left, while the transmitting vehicle, TX (blue trajectory), moves from the top middle to the bottom middle and enters a parking deck. Multiple packet loss periods (yellow) can be observed

in this encounter. Here, the packet losses do not seem to correspond to building or parking deck obstacles between vehicles. It is possible that the losses are caused by trees, elevation changes, and/or trucks or other vehicles coming between sender and receiver, but there is insufficient data from which to definitively and deterministically derive path loss in this encounter……...78

Figure 5.2 Geodata from Open Street Map (OSM) (a) for a section of the Ann Arbor area, and the equivalent view from Google Earth (b). Maroon areas represent geodata from OSM for various types of buildings, and blue areas represent parking decks, lots, and parks, all of which OSM treats homogenously as 2D outlines. Geodata is missing for many structures present in Ann Arbor and does not account for all obstacles that may occur between vehicles traveling the streets……79

Figure 5.3 PRR for log-scale distance from 5-500m for five VCMs. PRR predictions vary greatly among the models. Stochastic lognormal-based models *B* and *C* favorably predict PRR as does model E that deterministically accounts for obstacle shadowing……...83

Figure 5.4 Log-log scale of the pdf of inter packet gap (IPG) as a function of gap length out to 60s. The results for the i.i.d.-assuming model differ greatly from the power-law fitting test data, indicating that such models do not predict well the packet gap distributions found in the field test data of the SPMD……...84

Figure 5.5 Log-log scale of the pdf of consecutive reception run-length (CRRL) as a function of time out to 60s……85

Figure 5.6 The average number of obstacle walls penetrated (left axis) and the average total distances traveled within them (right axis) as a function of total distance between vehicles, based on the SPMD test data set and geodata available from OSM. As expected, there are few obstacles between vehicles when they are close together, while the average obstacle interior distances traveled is approximately 10% of the total distance between vehicles, up to about 800m……... 86

Figure 6.1 Relative velocity between two vehicles is a function of the individual vector velocities of the vehicles and the angle between them……. 94

Figure 6.2 The pdf of relative velocity of vehicles during V2V communications encounters throughout the Ann Arbor-based Safety Pilot Model Deployment. Over half of the time vehicles move relative to one another less than 5 m/s, indicating that vehicles during encounters are stopped or following one another at similar speeds. The encounter data shows that there are few times when relative velocity is greater than 20 m/s, and there were no incidences of relative velocity of more than 60 m/s……..95

Figure 6.3 The communications pattern of an illustrative V2V encounter within the SPMD test data set of the inter-vehicle distance versus time. Packet receptions within 200m are bursty, and interspersed with inter-packet gaps. Communications is highly asymmetric with respect to distance, as there are no receptions after t=32s, when the vehicles begin to separate away from one another. Prior to the receipt of the first packet, and after the reception of the last packet, there are long gaps of no receptions, even though the vehicles are quite close to one another……...96

Figure 6.4 The log-log scale pdf of IPG and CRRL, respectively, within the SPMD test data set. Both IPG and CRRL follow power-law distributions……97

Figure 6.5 The cdf of IPG and CRRL, respectively, within the SPMD test data set. In both plots, the x-axis is log-scale. A majority of packet gaps are very short, with 95% of all gaps less than 11 packets (i.e., 1.1s). Although the analysis was limited to a maximum gap length of 600 packets (i.e., 60s), approximately 1.5% of all gaps are ≥ 600 packets. Consecutive runs of packet receptions are also typically short, with 95% of all runs being less than 11 packets in length (e.g., 1.1s). Long bursts of consecutively received packets are very rare, with no runs of more than 200 consecutive packets…….98

Figure 6.6 The CPDF of gap and run lengths for the SPMD test data set and a 5PLR estimation model. The probability of a gap ending or a run length continuing are not independent of the previous gap / run length history, indicating that bursty reception and loss behaviors within the environment are not the result of an i.i.d. packet generation phenomenon……... 101

Figure 6.7 5PLR models of the CPDF of gaps < 1.2s and runs < 7.5s, for four distance bins. Conditional probabilities for short gaps and runs (e.g., lengths of 1-2) differ as a function of distance, but are nearly identical for other gap and run lengths, independent of distance bin……. 103

Figure 6.8 5PLR models of the CPDF of gaps < 1.2s and runs < 7.5s, for five different temporal subsets of the SPMD test data set. Conditional probabilities for short gaps and runs (e.g., lengths of 1-2) differ among the temporal data sets, but are nearly identical for other gap and run lengths, independent of the temporal subsets……...103

Figure 6.9 The 2-state Markov chain Gilbert-Elliott Packet Loss Model……. 105

Figure 7.10 Two binary streams, S1 and S2, that illustrate packet generation results with equivalent PRR but different packet gap and consecutive runs……106

Figure 6.11 Architecture and data flow diagram for a packet generation and evaluation model. A Flow Stream Analyzer is used to evaluate the PRR, IPG, and CRRL of the SPMD test data. The resulting distributions are used as inputs into a Burst Generator model that the Packet Generator combines with a path loss model to produce a modeled Flow Stream of alternating gaps and runs of packets. The model results are also analyzed by a Flow Stream Analyzer and the results of the test data and model are compared…… 108

Figure 6.12 The inverse transformation method…… 109

Figure 6.13 Comparison of average PRR and expected PRR. Average PRR (i.e., using the dual-slope distance-breakpoint path loss model derived from the SPMD test data) decreases smoothly as distance increases, while expected PRR drops in a stepwise manner consistent with the distance bins used for their evaluation. Expected PRR is calculated using the subset of data points that occur only during active communications, while the average PRR includes all data points throughout an entire encounter. As expected PRR excludes long periods of leading and trailing packet gaps, the value of expected PRR often exceeds that of the path-loss-modeled average PRR…… 110

Figure 6.14 Sensitivity of $1-\alpha$ as compared to expected gap length. Expected gap length increases as distance increases. However, since leading and trailing long packet gaps are excluded from the calculation of expected gap, the resulting expected PRR is higher than desired average PRR. By injecting long packet gaps into a packet stream with frequency $1-\alpha$, expected PRR can be related to average PRR. The need for such injections is infrequent as short distances, and increases as distance increases…….. 113

Figure 6.15 The BUR-GEN (burst generator) packet stream generator algorithm. The algorithm returns a packet stream S of length L

that consists of alternating gaps and runs that are drawn from gap and run burst distribution functions (i.e., line 15 and 19, respectively). With probability $1-\alpha$,, a long burst of length G of lost packets is injected into the stream……114

Figure 6.16 Simulation parameters. Vehicle mobility is modeled as randomly generated V2V encounters. Path loss is modeled using the dual-slope distance-breakpoint model and using the "best fit" parameters identified in Chapter 5. The i.i.d. packet burst generation Model *C* is evaluated against a model that includes the BUR-GEN algorithm (i.e., Model *F*)……115

Figure 6.17 PRR comparison of the dual-slope distance-breakpoint model (only) and the combined dual-slope distance-breakpoint model with the BUR-GEN burst generation model……117

Figure 7.1 Conceptual view of the safety system in which vehicle *A* desires to target safety messages towards the geocast region (GR) centered at v with radius R_{GR}, requiring messages to be relayed through the entire *forwarding zone* (FZ) that covers the entire area……124

Figure 7.2 An example timing diagram for the beaconcasting VANET……...126

Figure 7.3 Pseudocode (based on [12] for broadcast flooding. Line 1 receives a message, *m*; line 2 decides if *m* should be forwarded; line 3 generates a new message, *m*', by potentially amending the original message, *m*; line 4 determines the time at which the message should be resent; and line 5 schedules the rebroadcast of the amended message m' at some future time, *t*……127

Figure 7.4 Pictorial illustration of geocast regions for four configurations (i.e., *A*, *B*, *C*, and *D*) that represent different application requirements. The vehicle transmitting a BSM is located at the point labeled v and is assumed to be moving left to right at approximately 20 m/s……...133

Figure 7.5 Vehicular density (a) for a subset of the configuration space, where darker-colored regions indicate areas through which more vehicles have traveled, and average BRR (b-e) for two different subsets of the scenario space and two different configurations (*B* and *C*), where darker-colored regions indicate higher BRR. Average BRR between scenarios is localized and may improve (e.g., (c) vs. (b)), or degrade (e.g., (e) vs. (d))…… 136

Figure 7.6 A comparison for four different scenarios of the total number of distinct tagged BSMs that are received, as a function of distance between the vehicle that originates the tagged BSM and receiving vehicles……137

Figure 7.7 A comparison for four different scenarios of the averages of BRR as a function of distance between the vehicle that originally transmits a BSM and vehicles that receive it……... 139

Figure 7.8 A comparison for four different scenarios of the averages of awareness probability as a function of distance between transmitting and receiving vehicles……. 140

Figure 7.9 A comparison for four different scenarios of the averages of safety awareness probabilities as a function of distance between transmitting and receiving vehicles. Application requirements that increase forwarding zone coverage area help receiving vehicles that are likely to come in contact with one another improve their safety awareness of the sending vehicle…….. 140

Figure 8.1 Packet reception for a subset of a V2V encounter derived from the SPMD test data set for inter-vehicle separational distances less than 100m. Successful packet receptions are marked with a red "+", and their absence indicates periods of packet loss. Packet receptions and losses are bursty, and highly asymmetrical……..145

Figure 8.2 Awareness probability as a function of distance between transmitter vehicle and receiving vehicle for maximum safety tolerance requirements……...149

Figure 8.3 Awareness probability as a function of distance between transmitter vehicle and receiving vehicle for minimum safety tolerance requirements……...150

Figure 8.4 Numerical results of the RMSE of awareness probability between the model and the SPMD Test Data, for maximum and minimum safety tolerances……...150

CHAPTER

1

INTRODUCTION

Collisions among moving vehicles lead all causes of traffic fatalities, injuries, and property damage [2]. By exchanging information using wireless communications, vehicles may employ both safety applications (e.g., accident avoidance), and non-safety applications (e.g., traffic congestion alerts) [3]. The US Intelligent Transportation Systems (ITS) Joint Program Office (JPO) suggests that vehicle safety applications and supporting technologies will prevent tens of thousands of automobile crashes every year [4]. The most promising technologies in the U.S. that will enable such a vehicular ad hoc network (VANET) are collectively referred to as Dedicated Short-Range Communications (DSRC).

While prototype testing thus far has been constrained to limited testbed environments, various vehicular and networking simulation tools assist VANET researchers by providing supporting functions from which to model a variety of environmental conditions. Despite the availability of such models, results are inconsistent and often do not accurately predict behaviors observed in real-world situations.

Vehicular channel models (VCMs) are especially challenged in correctly accounting for the many harsh environmental conditions that exist, as they differ significantly from conventional cellular channel models, chiefly in terms of fading statistics due to varying environmental conditions, link types, vehicle types, and objects that result in complex propagation calculations. Significant fading and/or shadowing effects challenge the accuracy

of VCMs and the resulting observations of packet loss behaviors. Furthermore, while many VCMs can predict somewhat accurately the packet loss rates observed in real-world deployments, they over-estimate inter-packet gap lengths greater than 0.2s and under-estimate the likelihood of runs of three or more consecutively and successfully received packets, potentially threatening the accuracy of packet-level performance when multiple safety messages much be received in short time windows.

Aside from the packet loss categorization that VCMs attempt, the notion of safety itself is endangered by the inconsistent data delivery requirements of safety applications. To be effective, different safety applications may each require distinct numbers of safety packets to be successfully received with varying latencies, presenting challenges in determining how to distribute the safety information to other vehicles and making it difficult to quantify the current value of safety. Evaluations that commonly consider information dissemination approaches that use geo-casting and flooding techniques often decline to include mobility considerations and do not focus on assessing safety efficiency in terms of safety application requirements.

This dissertation investigates VCMs and their impact to safety packet delivery and safety performance evaluations within especially challenging, realistic DSRC testbed environments.

1.1 Thesis Statement

By cooperatively communicating using DSRC technologies, a system of connected vehicles can improve situational awareness among drivers with the intent on improving driving safety and reducing automobile-related accidents.

The DSRC collection of standards includes IEEE Std. 802.11-2012 [5], IEEE Std. 1609/WAVE [6] [7] [8] [9] [10], and SAE J2735 Message Set Dictionary [11]. Modifications to the IEEE Std. 802.11-2012 [5] MAC and PHY layers (formerly known as IEEE 802.11p) allow every vehicle to rapidly broadcast information about itself (e.g., location, speed and heading) as a safety beacon (i.e., *beaconcasting*) to make other nearby vehicles aware of it so they can alert drivers of unsafe situations such as pre-crash scenarios.

Safety success requires high probability of safety beacon delivery while considerable movement and environmental variety (e.g., obstacles such as other vehicles, buildings, foliage, etc.) jeopardize safety by impeding radio-wave transmissions. With DSRC standards [12] attempting to handle the high throughput and rapid delivery requirements under high mobility

scenarios, successful packet reception remains particularly challenging when numerous vehicles need to concurrently deliver safety messages in time-limited intervals under extreme environmental conditions. Packet losses in a VANET commonly result from separation distance, obstacles, and multi-path fading effects. Our analysis using an extensive experimental dataset collected from a deployment of approximately 3000 DSRC-capable vehicles operating around Ann Arbor, Michigan reveals that several common assumptions for DSRC (e.g., high packet reception rate for distances smaller than 100m) simply do not hold in real deployments.

Furthermore, accurate modeling of the vehicular channel endures as a challenging task. Vehicle-to-vehicle (V2V) channel attributes vary decidedly from those of traditional cellular channels, especially in terms of complicated propagation by-products from varying link variety, vehicle types, and environmental conditions, such as obstacles, that impact fading outcomes. Our results show that the DSRC deployment near Ann Arbor exhibits considerable shadowing and fading (i.e., sub-Rayleigh) events that challenge traditional VCM accuracy. In fact, while the packet error rates observed near Ann Arbor can be predicted reasonably well by several existing VCMs, the same models fail to accurately predict consecutive runs of successfully received packets and the gaps between them.

Beyond the challenges of packet loss and vehicular channel modeling, safety application requirement inconsistencies challenge data dissemination protocols and threaten the effectiveness of measuring safety. While many data delivery techniques have been proposed for VANETs, such as flooding and geo-casting, evaluations often disregard mobility considerations and fail to measure performance based on safety application requirements. To improve safety in a VANET, we propose *SafeRelay*, a flooding-based safety message distribution technique that disseminates geographically addressed safety messages to nearby neighbors. Simulations show that *SafeRelay* can significantly improve safety awareness using moderately-sized forwarding zones.

Prior work has proposed the application of various wireless channel models to the vehicular environment and analyzed the consequences upon packet loss within the system with the use of different information dissemination techniques. While packet loss is a commonly studied metric in VANETs, few works study the implications of packet loss upon safety measures.

In this dissertation, we study the challenges and opportunities for improved VCMs that more accurately represent the safety packet delivery repercussions observed within the authentic DSRC testbed environment around Ann Arbor, Michigan, and the connections with safety information dissemination and thus safety effectiveness.

From our analysis, we observe that common VCMs may predict well the overall average packet losses but fail to address consecutive runs of received or lost packets and do not handle well the specific environmental conditions such as obstacle shadowing. This observation leads us to the thesis statement of this work, as follows:

Improvements to vehicular channel models for connected vehicle technologies not only advances modeling accuracy in ways that better match real-world observations, but also enhance how vehicular safety measures themselves are assessed.

Evidence for this thesis can be found throughout this dissertation. Our first study contributes to the *ns-3* simulator an implementation of a VCM that supports obstacle shadowing using geodata and provides simulation results that compare its performance to other common VCMs. Our second study details the performance of DSRC safety message receptions among vehicular encounters as derived from a large deployment of nearly 3000 vehicles and shows that longer gaps exhibit temporal correlation tendencies while short-gapped consecutive losses are commonly uncorrelated. Our third study evaluates various existing VCMs and show that the UMTRI large-scale DSRC testbed exhibits significant shadowing and fading effects that traditional VCMs often fail to capture. Our fourth study proposes a bursty packet generation algorithm, BUR-GEN, that improves VCM packet loss and reception probabilities by factors of 6 and 4, respectively, as opposed to common, i.i.d.-base packet generation models, when compared to the SPMD results. Our fifth study proposes *SafeRelay*, a safety message dissemination technique that floods geo-addressed safety messages within the FZ, and evaluates packet delivery effectiveness using a new metric, *probability of safety awareness*, that combines packet delivery effectiveness with node mobility. Our final study assesses safety measures and shows that an improved VCM that includes a bursty packet

generation algorithm (i.e., BUR-GEN) improves awareness probability by factors of 31 and 128, respectively, for maximum and minimum safety tolerances, when compared to the actual awareness probabilities of the SPMD measurement campaign.

Our results motivation future directions in vehicular channel modeling accuracy through the consideration of further DSRC field operation test data analysis, model advancements in micro-level scenarios, and additional simulation studies.

1.2 Contributions

In this dissertation, we make the following contributions:

- *We implement in ns-3 a vehicular channel model that uses geodata to model obstacle and provide simulation results that compare the performance of the model to other common models* [13]. Since obstacles interfere with signal propagation of radio waves by contributing fading and shadowing effects, models must address the presence of obstacles to yield results that reflect truthful topologies and accurately state network performance. An obstacle shadowing model was implemented for the *ns-3* network simulator and tested using obstacle data from Open Street Map (OSM). Results show that deterministic obstacle shadowing improves performance assessment and compares differently than stochastic fading models, such as Nakagami-m.
- *We describe the packet-level performance of safety message exchanges among vehicular encounters, as obtained from the measurement data collected from nearly 3000 DSRC-equipped vehicles operating around Ann Arbor, Michigan, and show that smaller inter-packet gaps are commonly uncorrelated while longer gaps exhibit temporal correlations.* To improve the understanding of authentic operating conditions of the wireless vehicular channel, the characteristics of Packet Reception Ratio (PRR) and Inter-Packet Gap (IPG) behaviors and spatial and temporal correlations are examined. Analysis shows that packet loss from DSRC-based V2V encounters differs significantly from traditional, static-node wireless beaconing networks, due mainly to the vehicles' high mobility and signal obstructions between them. As long runs of consecutively lost safety messages could threaten

vehicle safety awareness, IPG is scrutinized further, finding that short-length IPGs are often uncorrelated while longer gaps are more temporally correlated.

- *We evaluate several existing, common VCMs and show that the UMTRI large-scale DSRC testbed measurement data reveals significant fading (i.e., sub-Rayleigh) and/or shadowing effects that challenge the accuracy of traditional VCMs.* Modeling the vehicular channel accurately remains arduous, since channel characteristics differ decidedly from those of traditional cellular channels, primarily due to environmental variety that impacts fading measurement, resulting in complex propagation outcomes. Existing, common VCMs are evaluated and compared to authentic measurement data from the UMTRI large-scale DSRC testbed. While many existing VCMs estimate appropriately the average packet error rates observed near Ann Arbor, they over-estimate IPG and under-estimate successfully received packet run-lengths. Furthermore, a deterministic obstacle shadowing model that uses OSM geodata does not explain all shadowing by-products. Evaluating VCMs in terms of realistic, large-scale experiments improves the understanding of actual behaviors and supports the development of new and/or improved models that more accurately reflect reality.
- *We present a new bursty packet generator algorithm, BUR-GEN, to address problems with vehicular channel models that fail to address the bursty packet patterns that are observed in large-scale DSRC measurement campaigns*. We show that BUR-GEN improves the accuracy of packet loss and reception probabilities by factors of 6 and 4, respectively, as opposed to common, i.i.d.-base packet generation models, when compared to the SPMD results.
- *We propose SafeRelay, a flooding-based message distribution technique that disseminates geo-addressed safety messages to nearby neighbors and evaluates packet success performance using a new metric, probability of safety awareness, which combines packet delivery effectiveness with node mobility*. While other data dissemination proposals attempt to improve delivery rates in a VANET using techniques based on geo-casting and flooding, the safety application data delivery requirements are often inconsistent and can possibly jeopardize safety itself, especially when evaluations neglect mobility considerations, such as time to

contact (TTC). We evaluate *SafeRelay* using different forwarding policies in terms of several metrics, including safety awareness probability, which combines both communications and mobility performance. Simulation results show that *SafeRelay* can considerably improve safety awareness using targeted, nearby forwarding zones.

- *We present evidence of the improvements to safety measures, such as awareness probability, that an improved VCM that includes a bursty packet generation algorithm (i.e., BUR-GEN) has when evaluating VCMs*. As compared to common, i.i.d.-based packet generation models that often mis-predict safety, we show that BUR-GEN improves awareness probability by factors of 31 and 128, respectively, for maximum and minimum safety tolerances, when results generated using BUR-GEN are compared against those from commonly available VCMs, and compared to the actual awareness probabilities of the SPMD measurement campaign.

1.3 Dissertation Outline

The goal of this dissertation is to investigate VCMs in light of safety performance evaluations and safety packet delivery within especially challenging, faithful DSRC deployments. We now provide a brief outline of the rest of this dissertation.

First, it is noted that Appendix A provides a list of abbreviations used throughout this work.

In Chapter 2, we describe background and related work. Specifically, Chapter 2 provides insights into the related work in seven primary domains: vehicular safety, DSRC standards and operations, vehicular channel models, dissemination of safety information, vehicular mobility simulation, vehicular network simulation, and safety assessment metrics.

Chapter 3 elaborates our work [13] that describes an implementation in *ns-3* of a VCM that uses geodata to evaluate obstacle shadowing and provides simulation results that contrast the effectiveness of other common VCMs to the obstacle shadowing model.

Chapter 4 discusses our work [14] that provides analysis of the characterization of the performance packet reception/loss among V2V exchanges as derived from measurement data of DSRC-equipped vehicles operating around Ann Arbor, Michigan. Consecutive, short-gapped losses are mostly uncorrelated while longer gaps show temporal correlations.

Chapter 5 presents our work [15] that evaluates several commonly used VCMs and indicates that significant shadowing and fading repercussions that challenge VCM accuracy occur throughout the DSRC test environment around Ann Arbor, MI. Although several VCMs estimate accurately the average packet error rates as observed in the test scenario, they tend to over-estimate IPG and under-estimate consecutive packet run-length probabilities.

Chapter 6 presents a new bursty packet generation algorithm, BUR-GEN, that improves upon vehicular channel models that fail to address the bursty packet patterns that are observed in large-scale DSRC measurement campaigns. BUR-GEN improves the accuracy of packet loss and reception probabilities by 83% and 78%, respectively, as opposed to common, i.i.d.-base packet generation models, when compared to the SPMD results.

Chapter 7 covers our work [16] that describes *SafeRelay*, a geographically addressing safety-message forwarding approach, and assesses packet delivery using a new metric, probability of safety awareness, that combines packet delivery effectiveness with mobility measures.

Chapter 8 presents evidence of the improvements to safety measures, such as awareness probability, that an improved VCM that includes a bursty packet generation algorithm (i.e., BUR-GEN) has when evaluating VCMs. As compared to common, i.i.d.-based packet generation models that often mis-predict safety, we show that BUR-GEN improves awareness probability by factors of 31 and 128, respectively, for maximum and minimum safety tolerances, when results generated using BUR-GEN are compared against those from commonly available VCMs, and compared to the actual awareness probabilities of the SPMD measurement campaign.

Finally, Chapter 9 provides conclusions and describes directions for future work.

CHAPTER

2

RELATED WORK

2.1 Vehicular Safety

Vehicular collisions cause the majority of traffic injuries, fatalities, and property damage. According to data from the National Highway Transportation Safety Administration (NHTSA), although approximately 5.3 million vehicle crashes in the US resulted in about 32,000 fatalities in 2011, motor-vehicle fatalities continue to decrease as safety measures, such as seal belts and airbags, have been mandated (see Figure 2.1) [17].

Modern technical advances provide autonomous and connected vehicles the potential to improve driving safety. Yet a relatively few, recent, highly-publicized incidents brings into question the safety effectiveness of these technologies. For example, a series of accidents involving Google's driverless cars caused collateral damage and human injuries [18], and a Tesla on autopilot resulted in a fatality when the car's automatic braking failed to engage as a tractor trailer crossed its path [19]. While autonomous vehicles act independently and therefore have sensors with somewhat limited range, a network of connected vehicles (autonomous or not) can cooperatively share information to improve safety.

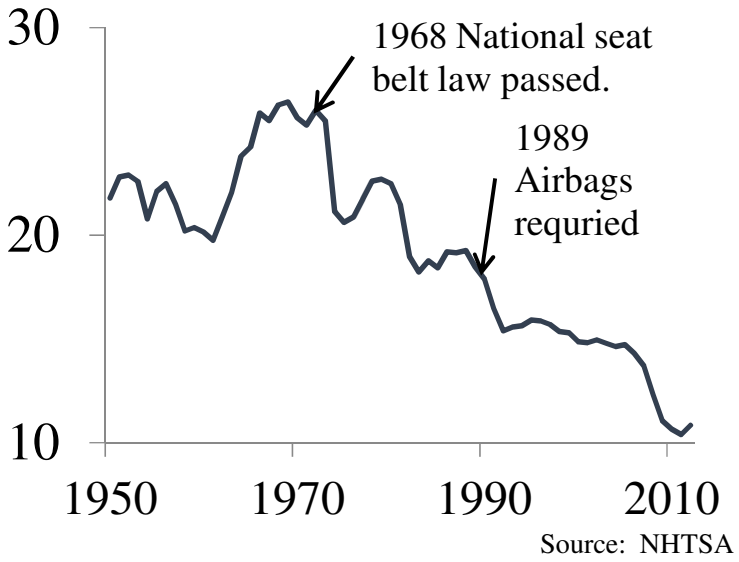

Figure 2.1 Total U.S. motor vehicle fatalities per 100,000 population, 1950 – 2012

Intending to further improve driving safety and reduce traffic-related fatalities, the United States Department of Transportation (USDOT) expects to push for regulations requiring vehicles to communicate cooperatively using DSRC technologies [20].

Using DSRC to interchange information, cars and trucks enable both safety applications, such as accident avoidance, and non-safety applications, such as pre-crash warnings and traffic congestion alerts [3]. Vehicular safety applications are expected to reduce or eliminate annually vast numbers of vehicular accidents [21].

2.2 Dedicated Short-Range Communications (DSRC) Standards and Operations

To make driving safer in a VANET, each vehicle regularly generates pertinent "here I am" information packets about itself (e.g., position, direction, and velocity) that are encapsulated within a Basic Safety Message (BSM) [11] and rapidly broadcast as a safety beacon that alerts other nearby drivers of unsafe conditions (e.g., imminent crash situations). Safety effectiveness requires highly successful packet delivery probabilities of the 200-300 byte messages that are especially challenged by vehicular mobility and environmental issues (e.g., obstacles) that impede radio-wave transmissions, thus potentially jeopardizing safety. While standards [12] intend to address the low latency and high throughput needs in highly mobile conditions, safety message delivery in time-limited intervals under harsh environmental

conditions remains challenging, especially in scenarios with high node densities that result in channel congestion that defeat delivery attempts.

In the U.S., DSRC technologies support wireless communications within a VANET. DSRC-related standards include IEEE Std. 802.11-2012 [5], IEEE Std. 1609/WAVE [6] [7] [8] [9] [10], and SAE J2735 Message Set Dictionary [11]. Figure 2.2 shows the DSRC reference model.

IEEE Std. 802.11-2012 specifies the MAC and PHY layers (formerly known as IEEE 802.11p) of the reference model and provides extensions intended to address the dynamic nature of potentially fast-moving vehicles. A primary enhancement allows a STA that is not a member of a Basic Service Set (BSS) to transmit data frames, allowing the PHY to operate "outside the context of a BSS," (i.e., OCB) and thus defining a new type of 802.11 communications. The PHY layer of DSRC uses Orthogonal Frequency Division Multiplexing (OFDM) at a 10 MHz channel bandwidth to achieve data rates from 3 to 27 Mbps. Applying forward error correction (FEC) reduces the effective bit rate but improves the probability of successful decoding [12]. The majority of DSRC testing in the U.S. has utilized the 6 Mbps configuration (i.e., Quadrature PSK with ½ rate coding), since it seems to balance channel load and signal-to-noise requirements [22].

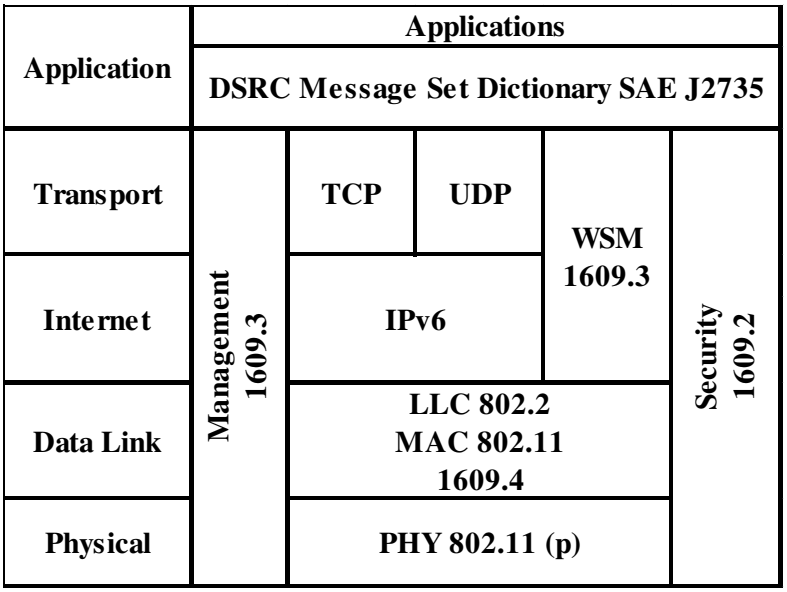

Figure 2.2 DSRC reference model

While the 802.11 family is well-understood, 802.11 unicasting is not well-suited to the VANET environment [23]. The IEEE Std. 802.11 supports safety beacons via broadcast transmissions. Because such broadcasts are unacknowledged, receipt by other nearby vehicles is not guaranteed. Channel availability is performed using Carrier-Sense Multiple Access with Collision Avoidance (CSMA/CA). While sensing of the carrier delays a transmission which would otherwise cause a collision, CSMA/CA does not prevent all such collisions, especially in the hidden node scenario [24] in which one vehicle cannot sense that a transmission would collide with another transmission from a nearby vehicle. When transmitters sense the carrier is busy, they employ a back-off scheme to re-attempt a transmission at a randomly selected future time controlled using the Congestion Window (CW) parameter.

The IEEE 1609/WAVE stack is built on top of the 802.11 MAC and PHY layers and provides further capabilities, such as: channel allocation and multi-channel access, priority queueing and channel routing, congestion control, security and privacy mechanisms, and an application programming interface (API) for messaging. WAVE supports both IPv6-based data transfers and non-IP-based traffic through the WAVE Short Message Protocol (WSMP). IEEE 1609.3 specifies the WAVE Management Entity (WME) and corresponding network services, as well as WSMP. Channel coordination is a collection of enhancements to the IEEE 802.11 MAC, and interacts with the IEEE 802.2 LLC and IEEE 802.11 PHY; IEEE 1609.4

describes multi-channel operations. WAVE security services are specified in IEEE 1609.2. The design of IEEE 1609/WAVE supports a single control channel (CCH) and six service channels (SCH), and it is generally assumed that the CCH will be primarily dedicated to safety applications [12]. Channels are defined in the 5.9 GHz range and typically occupy 10 MHz each, although the potential exists for 5 MHz and/or 20 MHz channels. While the WAVE standard does not preclude multiple channel-dedicated radios for continuous channel access, it also supports three additional options for periodic channel switching, commonly known as alternating, immediate, and extended channel access modes. Sync intervals split the channel at a rate of 10 Hz, which CCH and SCH intervals then typically split equally to support channel switching. A 4ms guard interval separates channel switches, resulting in a CCH interval of (½ x 1/10s) – 4ms = 46ms. Continuous channel access is also supported. Vehicles operate autonomously to synchronize clocks using an external GPS or a WAVE-advertised timing service.

The WAVE standard addresses message priority using four different Access Classes (AC) per (CCH or SCH) channel, AC0 (lowest priority) to AC3 (highest priority), with the MAC layer maintaining separate queues and channel access for each AC [12]. The WAVE contention mechanism is similar to the one used in conventional Wireless Local Area Network (WLAN) and the IEEE 802.11e Enhanced Distributed Channel Access (EDCA) Quality of Service (QoS) enhancements [25]. During packet transmission selection, the four ACs first contend internally with the winning packet then contending for the channel externally using its contention parameters. Each AC specifies a number of Arbitration Inter-Frame Spacing (AIFS) and CW slots and each AC waits at least its AIFS slots, plus additional slots determined by the selected CW value.

Built upon the SAE J2735 DSRC Message Set Dictionary [11], the VANET applications are over the 1609/WAVE stack. Data elements that enable many safety applications are

Table 2.1 DSRC device classes and operating parameters

RSU Class	Maximum output power (dBm)	Communications zone (meters)
A	0	15
B	10	100
C	20	400
D	28.8	1000

described in the most important message in the J2935 standard [12], the BSM, which every vehicle broadcasts at a nominal rate of 10 Hz. The BSM is divided into i) Part I mandatory elements such as position, motion, braking status, and vehicle size and ii) Part II optional elements such as vehicle events, path history and path prediction. Additionally, SAE J2735 defines non-safety messages, such as for toll collection, and provides guidelines on message prioritization among different message types. Applications may involve strictly V2V messaging using an On-Board Unit (OBU), or may also involve the use of Roadside Units (RSUs) to support vehicle-to-infrastructure (V2I) communications. The Federal Communications Commission (FCC) defines four classes for DSRC device operations with desired communications zones ranging from 15 to 1000 meters, as shown in Table 2.1 [26] [12]. The most commonly-expected operations category is Class C with a transmitter power of 20 dBm and an expected range of approximately 400m. While vehicles and infrastructure expect to communicate reliably over these ranges, radio-blocking obstacles and other interference that prevent message delivery challenge the safety effectiveness of all applications.

To successfully reduce injuries and fatalities, vehicle safety applications require high penetration rates of DSRC-enabled vehicles that successfully deliver safety information to nearby vehicles with low loss rates. To quickly alert users, safety applications often define performance requirements in terms of metrics such as: BSM transmission rate, Packet Error Rate (PER), IPG, latency (i.e., age of the data in the outgoing BSM [27]), and time to alert (i.e., time from BSM generation until the user is notified).

Devices within 1-300m of a transmission should receive them with a maximum PER of 10%, assuming measurements of the radio transmission pattern are done in an open field with "no man-made or natural structures that would reflect 5.9 GHz radiation within 2.5 kilometers (km) of the test vehicle(s)" [27].

Requirements for such "ideal" conditions do not necessarily portray lifelike conditions, thus making the evaluation in actual environments important in properly characterizing the true performance of the vehicular channel. For example, in their technology readiness assessment, NHTSA cautions that anticipated non-optimal performance can occur in "urban canyons," tunnels, and under foliage [28]. Additionally, potential channel congestion in high

vehicular density scenarios remains a potential issue that may impact the effectiveness of DSRC and supported safety applications [28].

2.3 Radio Propagation Model (RPM) Literature Review

A radio propagation model (RPM) describes the expected coverage area of a node (e.g., a transmitting vehicle) by characterizing the propagation of radio waves through space, typically as a function of frequency, distance, and/or other parameters. Models typically predict the amount of path loss, or reduction in power density (i.e., attenuation) along the links from the transmitter to each potential receiver. A RPM also often accounts for signal power changes due to the consequences of fading and/or shadowing. Vehicular channel characteristics differ from traditional mobile models in that they are highly dependent upon the existence of LOS paths. Measurement campaigns show that the variety of the types of objects impacts LOS conditions differently, thus making non-line of sight (NLOS) (i.e., LOS blockage from objects) a key factor in modeling V2V propagation channels [29].

Vehicular channel path loss models are based on RPMs and often account for power reductions, or fading, resulting from independent effects often classified as i) large-scale fading, ii) and small-scale fading. Large-scale fading, also called shadow fading, models power losses as varying from one transmitter-receiver link to another, changing slowly as distances between vehicles vary (e.g., over distances that are large compared to a wavelength), depending on the physical environment (e.g., urban, rural, suburban). Large-scale fading models often depict variations as random processes, although some models [30] [31] [13] treat signal fading deterministically based on obstructing obstacles between vehicles. Contrastingly, small-scale fading varies over space in a seemingly random way [32] and changes rapidly, i.e., over travel distances of a wavelength or less, accounting for the results of multi-path fading, power delay profiles, and the Doppler spectrum. Large- and small-scale fading are also sometimes referred to as slow and fast fading, respectively.

A RPM thus collectively models the impacts of signal attenuation due to distance, multipath signal fading due to reflectors, and shadowing as radio waves move through free space and obstacles, such as buildings and potentially other vehicles. Many different RPMs have been proposed for VANET, ranging in their design complexity from simpler models such as unit-disk up through more complex ones that specifically address the attenuation caused by

obstacles. The authors of [29] survey VCMs, comparing geodata availability and the usability of models at link or system levels, providing guidelines for the selection of suitable channel models. Models are classified based on their implementation approach (i.e., deterministic (D) or stochastic (S)) and geodata availability (i.e., geometry-based (GB), or non-geometry-based (NG)).

Vehicular scenario differences are sometimes classified and studied in terms of environmental commonality, such as: highway, rural street, suburban neighborhood, urban street, and urban intersection [29] [33]. However, measurements studies are quite rare for specific environments such as: multilevel highways, tunnels, parking garages, bridges, and roundabouts [29]. Additionally, vehicular differences extend beyond the myriad of passenger car shapes, including scooters and public and commercial transportation vehicles, making the propagation characteristics for one vehicle type not readily applicable to other types [29].

The simplest model, often used in VANET simulation, is the unit-disk model, in which vehicles can communicate with each other if they are within a threshold distance and cannot communicate otherwise [34]. The authors of [35] conclude that "a complex shadow fading environment is well approximated by a simpler and more tractable unit-disk model."

The free space model, also known as the Friis model after its author, models a single, unobstructed communication path [36]. When all V2V links are symmetrical with identical communications limits, then the free space model essentially behaves as the unit disk model.

Another commonly simulated RPM in VANET is the two-ray ground model, which takes into account signal reflection from the road surface and captures additional path loss as in IVC [37]. Because signals between road-based vehicles are assumed present in at least direct LOS and ground reflection, the two-ray ground model seems more appropriate for VANET than the free-space model.

The authors of [34] conclude that the commonly used unit disc model fails to realistically model a communication channel, while parameters of simplistic models like lognormal can be adjusted to match the corresponding system metrics of more complex and hard to implement obstacle based models. For (small-scale) fast fading models, various stochastic distributions have been proposed, including Rice, Rayleigh, Nakagami-m, lognormal, and Weibull distributions [34]. The authors of [38] report that the large-scale fading in radio propagation channels at 5.3 GHz was found to be lognormally distributed, whereas the small-scale fading

was characterized by the Weibull distribution. A special case of the general gamma distribution, the Nakagami-m fading model determines signal power reception probabilistically dependent on model parameters that simulate fading levels and may be described as:

$$f_{Nakagami-m}(r; m, \Omega) = \frac{2m^m r^{2m-1}}{\Omega^m \Gamma(m)} e^{-\frac{mr^2}{\Omega}}, \quad 2\text{-}1$$

where m is the Nakagami parameter (i.e., shape parameter), $\Gamma(m)$ is the gamma function, and Ω is the average power of multipath scatter field, which controls the distribution spread.

Stochastic models determine the physical parameters of the vehicular channel in a completely probabilistically way without recognizing fundamental geometry [34]. Stochastic communications modeling could therefore differ dangerously from real behavior, negatively impacting simulations of transmission-critical safety applications [31].

To reduce the randomness of stochastic models, geometry-based deterministic (GBD) models [29] estimate additional path loss using geodata that describes environmental conditions such as the locations of potentially radio wave inhibiting buildings. Examples include CORNER [30] and [31] [13] that deterministically model signal fading in the presence of obstacles that obstruct V2V line of sight (LOS).

To avoid environmental generalities, experiments that capture signal behavior from actual devices operated by typical drivers in realistic environments best serve the need to realistically characterize wireless vehicular channels [29]. However, numerous measurement studies report highly variable and often contradicting results for the same environments in path loss exponents [29] [33] delay spread, and Doppler spread [33], further supporting the thesis that environmental differences significantly prevent an easy characterization of the vehicular channel. For example, crowded highways were found to exhibit large path loss variations [33]. Additionally, the authors of [39] found that the shorter critical distance may be caused by more densely distributed objects like vehicles and pedestrians on the road, creating reflections from points higher than the ground. If measurements for a specific environment are not available, then NG models provide inconsistent results [29].

Obstacles play a part in radio signal propagation, with various modeling approaches being undertaken. Both Radio Propagation Model with Obstacles (RPMO) [40] and the Mahajan Model [41] behave similar to a two-ray ground model, adding the influence of obstacles and distance attenuation [42]. The impact of surrounding vehicles as obstacles is considered

lognormally by [34] and using a multiple knife-edge model by [43]. The authors of [44] assert that obstruction by a large building does not involve a pure shadowing but heavily reduces the received power.

A progressive series of models combining distance-based attenuation with building modeling has been proposed by the authors in [42] [45] [46]

The authors of [47] propose a hybrid solution that differentiates between LOS conditions using one set of settings for LOS conditions, and another for Around the Corner (ATC) settings, based on experimental measurements. The authors of [48] propose a similar approach, with different settings for LOS vs. NLOS, using a multi-ray propagation model and including the "foliage" effect in both NLOS and LOS models. Similarly, the authors of [30] classify vehicle communications potential into one of three cases: LOS, NLOS1 (NLOS with one corner along the path) and NLOS2 (NLOS with two corners along the path). The authors of [44] also use two classifications of NLOS, but simulate only in a Manhattan grid scenario.

Because radio waves can physically penetrate one or more buildings, models based on direct LOS alone are insufficient, leading the authors of [31] to collect empirical results showing the outcomes of building shadowing in urban environments. Gathering measurements using IEEE 802.11p devices, the authors of [31] present a realistic, yet computationally inexpensive path loss simulation model that uses the number of obstacle walls and distances intersected between them to estimate the effect that buildings and other obstacles have on the radio communications. However, in later work, the authors of [49] point out that "simulating path loss in (sub)urban environments to capture predictable shadowing effects seems to require more complex models than attenuation per wall or attenuation per meter of penetration approaches" while noting that the computational complexity of the resulting required ray-tracing approaches makes this prohibitive. Similarly, the authors of [30] propose CORNER, "a low computational cost yet accurate urban propagation model for mobile networks" that uses information from urban digital maps to estimate building and obstacle presence along the signal path between two vehicles, classifying the propagation environment between them.

The most accurate models are fully deterministic that use ray-tracing approaches that require extensive environmental knowledge and are computationally expensive [29]. Applying sophisticated methods like ray-tracing achieves realistic representation of signal

propagation but remains impractical for evaluating typically large-scale VANETs [47] since it requires site-specific propagation details [34] and does not account for mobile obstacles.

2.4 Vehicular Channel Models

A **vehicular channel model** (VCM) is an RPM that describes a transmitting vehicle's expected coverage area. VCM measurement campaigns indicate that variation in signal attenuation arising from the static and dynamic physical world features is strongly correlated over both time and space (i.e., temporally and spatially, respectively) [29]. Thus, the non-stationarity of the channel makes Wide Sense Stationary Uncorrelated Scattering (WSSUS) assumptions non-applicable and most importantly distinguishes the characteristics of V2V channels from the behaviors of conventional cellular networks [33].

2.4.1 Path Loss

Path loss represents the attenuation that results from the propagation of signals originating from a transmitter, T, and is measured as the net change between the transmitter power and the Receiver Signal Strength (RSS) (in dBm), adjusted for antenna gains:

$$PL(d)[dB] = P_T[dBm] - P_R(d)[dBm] + G_T[dB] + G_R[dB], \quad (2\text{-}2)$$

where $PL(d)$ is the total path loss in decibels (dB) along d, the distance between the receiver and the transmitter, P_T is the transmitter power (e.g., 20 dBm), $P_R(d)$ is the received power, and G_T and G_R are the antenna gain levels in dB of the transmitter and receiver, respectively.

2.4.2 Probability of Packet Reception

We model successful packet reception by considering a receiver sensitivity threshold, P_{TH}: if the received power, $P_R(d)$, is larger than P_{TH}, we assume that the packet is successfully received. PRR is assumed equal to the probability of successfully receiving a signal at the receiver. Ideally, the PRR of short links should be 100% and the PRR of long links should be close to 0%. PRR can be estimated using the link's projected path loss ((2-2) as:

$$PRR(d) = \Pr[P_{TH} \leq P_R(d)] = \Pr[PL(d) < PL_{TH}], \quad (2\text{-}3)$$

where the path loss threshold, $PL_{TH} = P_T - P_{TH} + G_T + G_R$.

As $\Pr[X \leq x] = F_X(x)$, where $F_X(x)$ is the cumulative distribution function (cdf) of X, the probabilities in (2-3 may be re written in terms of their cdfs:

$$PRR(d) = F_{P_{TH}}\big(P_R(d)\big) = 1 - F_{PL_{TH}}\big(PL(d)\big). \quad (2\text{-}4)$$

In effect, the probability of packet reception can be derived from the distribution functions that describe path loss:

$$PRR(d) = \bar{F}_{PL}(PL(d)), \tag{2-5}$$

where $\bar{F}_{PL}(PL(d))$ is the complementary cumulative distribution function (ccdf) of the path loss function.

2.5 Path Loss Models

In this section, we present several widely used path loss models that we will evaluate in Section 5.5 against field operational test data.

2.5.1 Deterministic Path Loss Models

2.5.1.1 Unit Disk Path Loss

Perhaps the simplest conceptual model of path loss is the unit disk path loss model that ignores fading effects altogether and assumes only that those receivers within a limited communications range (i.e., unit) of senders successfully receive signals stronger than the receiver sensitivity threshold (and thus successfully receive packets), while those outside of the range do not. Path loss is given as:

$$PL_{UC}(d) = \begin{cases} 0, & d \le d_{lim} \\ \infty \ge PL_{TH}, & d > d_{lim} \end{cases}, \tag{2-6}$$

where d_{lim} is the distance that limits reception. Thus, PRR for unit disk path loss is:

$$\begin{aligned} PRR_{UC}(d) &= \Pr[PL_{UC}(d) \le PL_{TH}] \\ &= \begin{cases} 1, d \le d_{lim} \\ 0, d > d_{lim} \end{cases}. \end{aligned} \tag{2-7}$$

While failing to accurately reflect waveform propagation effects that are observed in nature, the model is often useful conceptually to address simple node behaviors.

2.5.1.2 Free Space Model

The free space model (i.e., the Friis model), models a single, unblocked communication link where the receiver power, $P_R(d)$, in ((2-2) deterministically depends only on the transmitted power, antenna gains, and distance between nodes, and is [36]:

$$P_R(d)[W] = \frac{P_T[W] G_T G_R \lambda^2}{(4\pi d)^2}, \tag{2-8}$$

where G_T and G_R are the gains of the transmitter and receiver, respectively, and $\lambda = \frac{f}{c}$ is the wavelength of the signal, where f is the signal frequency and c is the speed of light.

Assuming for the DSRC environment symmetrically matched antennas (i.e., setting G_t, and G_r to 1), converting between Watts and dBm by $P[W] = 10^{(\frac{P[dBm]}{10})}/1000$, and substituting ((2-8) into ((2-2), we can rewrite free space path loss (FSPL) in dB as:

$$PL_{FSPL}(d)[dB] = 20log_{10}\left(\frac{4\pi d}{\lambda}\right). \quad (2\text{-}9)$$

When the communications parameters in the vehicular environment in ((2-8) are homogenous with symmetrically limited communications distances, (i.e., some value of d_{lim} in ((2-6) applies to d in ((2-9)), then the free space model essentially becomes the unit disk model.

2.5.2 Probabilistic Path Loss Models

2.5.2.1 Lognormal Path Loss

A large-scale fading model commonly used to model the vehicular channel [39] [29] is the **lognormal path loss model** that relies on two key parameters to model path loss:

i) γ, the path loss exponent that accounts for average large-scale variations as a function of distance and

ii) ii) σ, the standard deviation of the scatter of received power about the average that reflects minor variations that follow a zero mean normal distribution (i.e., $X_\sigma \sim N(0, \sigma)$).

Thus, received signal strengths at locations equally distant from the transmitter are considered i.i.d. random variables, with lognormal path loss as:

$$PL_{LN}(d)[dB] = PL(d_0) + 10\gamma log_{10}\left(\frac{d}{d_0}\right) + X_\sigma, \quad (2\text{-}10)$$

where $PL(d_0)$ is the path loss at the reference distance d_0 (e.g., typically < 10m), d is the distance between sender and receiver, γ is the path loss exponent, and X_σ models the path loss variation across all locations at distance d.

PRR can be estimated for lognormally distributed path loss by combining ((2-3), ((2-5), and ((2-10):

$$
\begin{aligned}
PRR_{LN}(d) &= \Pr[PL_{LN}(d) \le PL_{TH}] \\
&= \Pr\left[PL(d_0) + 10\gamma log_{10}\left(\frac{d}{d_0}\right) + X_\sigma \le PL_{TH}\right] \\
&= \Pr\left[10\gamma log_{10}\left(\frac{d}{d_0}\right) + X_\sigma \le PL_C\right],
\end{aligned}
\tag{2-11}
$$

where $PL_C = PL_{TH} - PL(d_0)$ is a simplifying constant.

Considering the distribution of X_σ, ((2-11) can be expressed as [39]:

$$
\begin{aligned}
PRR_{LN}(d) &= \frac{1}{\sqrt{2\pi}\sigma}\int_{-\infty}^{\xi(d,\gamma)} \exp\left(-\frac{t^2}{2\sigma^2}\right) dt \\
&= \frac{1}{2} + \frac{1}{2}\mathrm{erf}\left(\frac{\xi(d,\gamma)}{\sqrt{2}\sigma}\right),
\end{aligned}
\tag{2-12}
$$

where the error function is $\mathrm{erf}(x) = \frac{2}{\sqrt{\pi}}\int_o^x e^{-t^2}\, dt$, $\xi(d,\gamma) = 10\gamma log_{10}\left(\frac{d_{lim}}{d}\right)$, and d_{lim} is the limiting distance at which $P_R(d) \ge P_{TH}$ (i.e., equivalently, $PL(d) \le PL_{TH}$) in the absence of small-scale fading ($\sigma = 0$), i.e., $d_{lim} = 10^{\frac{PL_C}{10\gamma}}$.

2.5.2.2 Dual-slope Distance-breakpoint Path Loss Model

Vehicular channel studies [39] [50] find that the single path-loss exponent from (9) may not sufficiently reflect environments in which differing channel behaviors occur at different distances. Thus, a dual-slope distance-breakpoint model, in which the path loss exponent changes at breakpoint distance(s), more accurately characterizes measurements in practice. Specifically, a dual-slope distance-breakpoint model characterizes path loss with one path loss exponent γ_1 and a standard deviation σ_1 within a critical breakpoint-distance, d_b, and beyond which the signal falls off with another path loss exponent γ_2 and a standard deviation σ_2. In effect, the dual-slope distance-breakpoint model varies path loss exponent and signal variation parameters of the lognormal path loss model, as a function of distance, by separating the model into two piece-wise linear segments at a single breakpoint distance. The formula for the model is [39]:

$$PL_{BP}(d) = PL(d_0) + \begin{cases} 10\gamma_1 log_{10}\left(\frac{d}{d_0}\right) + X_{\sigma_1}, & d_0 \le d \le d_b \\ 10\gamma_1 log_{10}\left(\frac{d_b}{d_0}\right) + 10\gamma_2 log_{10}\left(\frac{d}{d_b}\right) + X_{\sigma_2}, & d > d_b \end{cases}, \quad (2\text{-}13)$$

In conventional direct LOS models, d_b is the Fresnel distance to the point where the first Fresnel zone touches the ground, which can be calculated as $d_b = \frac{4h_T h_R}{\lambda}$, where h_T and h_R are antenna heights of the transmitter and receiver, respectively, and λ is the wavelength [39]. For example, when the height of the transceiver antennas on the vehicles are $h_T = h_{R=} = 1.5\text{m}$ and the wavelength $\lambda \approx 0.0508\text{m}$, then $d_b \approx 177\text{m}$ in the vehicular environment. However, for our model analysis, we allow d_b to be adjustable.

PRR can be estimated for the dual-slope distance breakpoint model by considering each case in ((2-13) separately. Turning first to the case that $d_0 \le d \le d_b$, the packet receipt likelihood is [50]:

$$\begin{aligned} PRR_{BP}(d) &= [PL_{BP}(d) \le PL_{TH}],\ d_0 \le d \le d_b \\ &= \Pr\left[10\gamma_1 log_{10}\left(\frac{d}{d_0}\right) + X_{\sigma_1} \le PL_C\right] \\ &= \frac{1}{2} + \frac{1}{2}\text{erf}\left(\frac{\xi_1(d,\gamma_1)}{\sqrt{2}\sigma_1}\right). \end{aligned} \quad (2\text{-}14)$$

where $\xi_1(d,\gamma_1) = 10\gamma_1 log_{10}\left(\frac{d_1}{d}\right)$, $d_1 = 10^{\frac{PL_C}{10\gamma_2}}$.

Similarly, when $d > d_b$, then PRR in this case is [50]:

$$\begin{aligned} PRR_{BP}(d) &= \Pr[PL(d) \le PL_{TH}], d > d_b \\ &= \Pr\left[\alpha_1 + 10\gamma_2 log_{10}\left(\frac{d}{d_b}\right) + X_{\sigma_2} \le PL_C\right] \\ &= \frac{1}{2} + \frac{1}{2}\text{erf}\left(\frac{\xi_2(d,\gamma_2)}{\sqrt{2}\sigma_2}\right). \end{aligned} \quad (2\text{-}15)$$

where $\xi_2(d,\gamma_2) = 10\gamma_2 log_{10}\left(\frac{d_b d_2}{d}\right)$, $d_2 = 10^{\frac{PL_C - \alpha_1}{10\gamma_2}}$, and $\alpha_1 = 10\gamma_1 log_{10}(d_b)$.

2.5.2.3 Nakagami-m Small-scale Fading

The Nakagami-m distribution [51] (i.e., $Nk \sim Nak(m, \Omega)$), can represent a variety of fading models, such as Rician and Rayleigh fading, that vary with changes in scatterer density [39]. The parameters are $m \ge 1/2$, commonly known as the shape parameter, and $\Omega > 0$, that controls the spread of the distribution. Analysis shows that in some measurement studies, m

varies with distance, providing insight into environmental changes in the fading channel. For example, in [52], m indicates a change from Rician fading ($m > 1$) at shorter distances with stronger LOS possibilities to Rayleigh fading ($m = 1$) as distance increases and dense scatterers dominate.

The probability distribution function (pdf) of the Nakagami-m power envelope R is [51]:

$$f_R(x; m, \Omega) = \frac{2m^m x^{2m-1}}{\Gamma(m)\Omega^m} \exp\left(-\frac{m}{\Omega}x^2\right), \tag{2-16}$$

where $\Omega = \overline{R^2}$ is the time average of the square of intensity R, and $\Gamma(x) = \int_0^\infty x^{z-1}e^{-x}dx = (x-1)!$ is the gamma function.

By combining ((2-2) and ((2-16), the path loss of the Nakagami-m path loss model is:

$$PL_{Nk}(d) = P_T - f_R(P_r(d)\,[W]; m, \Omega). \tag{2-17}$$

The corresponding cdf of ((2-16), $F_R(x; m, \Omega)$, is [52] [53]:

$$F_d(x; m, \Omega) = \int_0^x f_R(z; m, \Omega)dz. \tag{2-18}$$

$$= \frac{m^m}{\Gamma(m)\Omega^m}\int_0^x z^{m-1}e^{-(m/\Omega)z}\,dz. \tag{2-19}$$

From the form of ((2-19),

$$F_d(x; m, \Omega) = P\left(m, \frac{m}{\Omega}x^2\right), \tag{2-20}$$

where $P(s, x) = \frac{\gamma(s,x)}{\Gamma(s)}$ is the regularized incomplete gamma function, and $\gamma(s, x)$ is the lower incomplete gamma function.

The probability of packet reception for Nakagami-m distributed fading is determined by combining ((2-3) and ((2-20):

$$\begin{aligned} PRR_{Nk}(d) &= \Pr[P_{TH} \le P_R(d)] \\ &= F_d(x; m, \Omega) \\ &= P\left(m, \frac{m}{\Omega}x^2\right). \end{aligned} \tag{2-21}$$

2.5.2.1 Normally-distributed Small-scale Fading

When power fluctuations about the mean include both small-scale fading such as multi-path fading with distribution $N(0, \sigma_{mp})$ and shadow fading with distribution $N(0, \sigma_{sf})$, then the standard deviation in ((2-10) and ((2-13) can be computed as [32]:

$$\sigma = \sqrt{\left(\sigma_{mp}\right)^2 + \left(\sigma_{sf}\right)^2}. \tag{2-22}$$

2.5.2.1 Generalized Gamma (GG) Shadowed Fading Model

Vehicular channels may experience effects of fading and shadowing simultaneously on the received signal. For example, the fading effects of the Nakagami-m model in ((2-15) do not represent shadowing, while the combined fading and shadowing in ((2-22) is assumed Gaussian, which may not be the case. Models that reflect these combined effects of both fading and shadowing are called shadowed fading models [54] and the literature indicates that path loss variation in vehicular channels can effectively make use of the general gamma (GG) distribution [54] [55], from which several distributions can be derived, including the Nakagami-m distribution ((2-20). The pdf of the signal power under the GG shadowed fading model is ([54] Eq. (4.89)):

$$f_{GG}\left(p; m, P_g, s\right) = \frac{sp^{ms-1}}{(P_g)^m \Gamma(m)} exp^{-\frac{p^s}{P_g}}, \tag{2-23}$$

where the average power in the GG channel, $\langle P \rangle$, is related to P_g as ([54] Eq. (4.55)):

$$P_g = \left[\langle P \rangle \frac{\Gamma(m)}{\Gamma\left(m + \left(\frac{1}{s}\right)\right)} \right]^s. \tag{2-24}$$

Thus, the power distribution of the GG shadowed fading model ((2-23) is controlled by three parameters: the scaling parameter, m, and power-scaling parameter, P_g (respectively identical to m and Ω in ((2-15), and a shape parameter, s. Note that while in ((2-16), $m \geq 1/2$ always, this restriction is not the case in ((2-23), making the GG shadowed fading model useful in modeling channels with severe fading conditions. Distribution special cases of ((2-23) include Nakagami-m ($s = 1$), Weibull ($m = 1$), and Rayleigh ($s = m = 1$).

The shape parameter s is typically restricted to $0 < s \leq 1$ in the GG shadowed fading model of ((2-23) [54], where ($s = 1$) implies no shadowing (i.e., $\sigma_{dB} = 0$) and ($s \to 0$) implies extreme shadowing (i.e., $\sigma_{dB} \to \infty$). Relaxing the upper bound on s transforms ((2-23) into the generalized gamma, or generalized Nakagami fading channel in which the lognormal distribution is a limiting case ($m \to \infty, s \to \infty$) [54] [51].

The cdf of ((2-23) is ([54] Eq. 4.54):

$$F_{GG}(p; m, P_g, \mathrm{s}) = P\left(m, \frac{p^s}{P_g}\right). \tag{2-25}$$

The probability of packet reception for GG shadowed fading model is determined by combining ((2-3) and ((2-25):

$$\begin{aligned} PRR_{GG}(d) &= \Pr[P_{TH} \leq P_R(d)] \\ &= F_{GG}(p; m, P_g, \mathrm{s}) \\ &= P\left(m, \frac{p^s}{P_g}\right). \end{aligned} \tag{2-26}$$

2.6 Obstacle Modeling

Modeling improves when a visibility scheme describes the topology as a configuration space and supports obstacle detection. Most visibility schemes divide the configuration space into sub-areas by some criteria. For example, although uncommon in real scenarios [45], the Manhattan grid model assumes that all vehicles move only in streets arranged as a Manhattan-style grid and treats non-street areas as buildings. However, Manhattan layouts are uncommon in real scenarios [45]. The authors of [30] extend the areas of each roadway segment to include a proximity area to include locations within half the width of the roadway.

The authors of [45] propose Visibility Scheme for Real Maps, designed to be used in scenarios where streets are irregular. However, the model assumes a divide of the configuration space into only streets and non-streets, with vehicles only traveling along street centerlines, resulting in an assumption that communications are only possible between vehicles mutually visible within streets. Open communication areas often extend beyond street edges in real urban scenarios, limiting the model's realism.

The authors of [56] propose Topology-Based Visibility model, which extends their previous work of Building and Distance Attenuation Model (BDAM) [42] to take into account "realistic road topologies, such as roundabouts, angled roads, merged-and-split roads, etc., that are not considered by other schemes." The approach converts the roadmap into an undirected graph where junctions are vertices and streets which connect them are edges. The resulting polygonal areas create realistic city profiles [56] as some of the polygons formed using the streets as sides are considered clear areas with little interference in the signal propagation (obstacle-free areas such as roundabouts, gardens, etc.), and the rest of map is regarded as a set of buildings. In this scheme, radio signals can propagate through streets and clear areas but

not buildings. While the model determines the presence of obstacles along the line connecting two vehicles, the results are only valid for the current time instance and cannot be used, for example, to evaluate communications potential using future vehicle position estimates. Additionally, in certain situations, vehicles close to junctions are able to receive enough power to obtain the messages in non-line-of-sight (NLOS) conditions [56]. As such, the model accounts for message receipt potential for vehicles within 20 meters of a junction.

Current approaches to detect obstacles within a configuration space [45] [56] [42] employ different algorithms with varying complexity. Many come from computational geometry techniques including intersection problems [43] [31] and binary space partitions (BSP) [31] that are applied to model vehicles and/or buildings as obstacles.

Models that fail to consider realistic road topologies and the presence of obstacles [56] lead to inconsistent results [57]. Especially in certain simulation scenarios, such as VANET, accurate environmental representation of obstacles is absolutely required in urban scenarios because obstacles not only constrain vehicular movement but also interfere with radio transmissions [58]. Signal propagation varies especially between direct LOS and obstructed-line-of-sight (OLOS) [47] and when radio waves propagate "Around-the-Corner" (ATC) [31].

Radio wave attenuation is often modeled deterministically based mainly on inter-vehicular LOS distance, while stochastic modeling improves upon this by accounting for radio wave shadowing. Recent research deterministically models shadowing by addressing radio wave propagation through buildings [31] [56] [30].

Geometric intersection problems deal with pairwise intersections between line segments in n-dimensional space [43]. In their study, the authors of [43] restrict their line segments of interest to LOS rays between vehicles and lines composing a bounding rectangle representing the vehicle, further restricting the class of intersection problems to so-called "red-blue" intersections. The problem is thus stated: Given a set of red line segments r and a set of blue line segments b, with a total of $N = r + b$ segments, the goal is to report all K intersections between red and blue segments. The authors of [43] report that Agarwal presented an efficient algorithm with time-complexity using the randomized approach of $O(N^{4/3} \log N + K)$, where K is the number of red-blue intersections, and with space complexity of $O(N^{4/3})$.

The authors of [59] find V2V obstacle intersections using a BSP algorithm, but only apply the approach to a Manhattan-style grid scenario with uniformly quadratic building sizes with

edge length of 480 m. Obstacle edges are stored in a BSP structure. Using a bounding box derived from the LOS path between two vehicles, the potential obstructing buildings between them are identified. Lastly, obstacle edges are tested for intersection with the LOS path.

The calculation of intersection between all lines of sight and all buildings is an expensive step [31]. However, finding the intersections can be done in $O(n^2 \log n)$ using caching and binary space partitioning approaches [59].

2.7 Dissemination of Safety Information

While current standards [11] restrict the effective range of each BSM to the single hop transmission limits of each vehicle, every vehicle that receives the BSM becomes situationally aware of the sending vehicle. Effective safety information dissemination requires the rapid distribution effects of flooding techniques, constrained to short distances that are limited to regions nearby the emitting vehicles but beyond the single hop transmission limits.

While numerous VANET routing protocols have been proposed for message dissemination [60] [61], they may not be especially effective for safety application requirements. For example, the probability evaluations that select forwarding nodes may cause intolerable delay that ultimately makes safety messages obsolete. While georouting protocols [62] reference distant geocast regions and intend to limit communications overhead by targeting specific nodes, reducing message frequency, and/or increasing IPG, these typical approaches are often counter to the safety needs of the beaconcasting VANET.

In Chapter 6, we explore a means of relaying safety information throughout a VANET using geographic addressing (i.e., geo-addressing). Several works similar to ours study the dissemination of safety packets using varying means to extend information beyond one-hop nearby neighbors (e.g., [63], [64], [65], [66]). The authors of [63] propose OB-VAN that uses opportunistic routing in a broadcast VANET to dynamically select a relay node from all nodes that successfully receive a packet. OB-VAN is a modified MAC-layer protocol that requires acknowledgement of a modified broadcast packet that is not time-constrained. In [63], the authors also assume message forwarding without time constraints while considering both geo-constrained and un-constrained message propagation in a highway setting assuming Poisson vehicle arrivals. The authors of [65] consider a relay selection scheme that selects the longest life time and best quality of signal route through the maximization of predicted link lifetime,

received signal strength indicator (RSSI), and minimization of signal-to-interference-plus-noise ratio (SINR). The approach relies on route discovery using a hybrid gateway technique and assumes a maximum forwarding delay of 3.75 seconds, significantly longer than the safety message lifetime expectancy of 100ms. In [66], the authors propose Zero-Coordination Opportunistic Routing (ZCOR), a solution most related to ours. ZCOR avoids pre-condition processing and the overhead of low-rate heartbeat packets and uses opportunism in relaying safety messages by using an R-ALOHA style channel/slot reservation system that uses CSMA back-offs that differ between the original and relayed safety messages. However, ZCOR uses heartbeats, assumes the use of several individual zones to exploit spatial diversity, assumes a time-synchronized, switching safety channel with a 30 ms safety channel access, and does not divulge the latency threshold parameters, after which a safety packet will expire.

Other studies do not quantify impact using a metric that specifically includes a safety measure, and often only compare results to packet delivery probabilities [63], [64], [65], [66].

Our model in Chapter 6 differs from other works by using a message-forwarding approach that addresses the safety-based, time-constrained VANET characteristics and limits the impact to delivery of primary BSMs by using deferred rebroadcast prior to expiration, in which retransmissions of primary BSMs are only attempted after all primary BSMs have been successfully sent and if the retransmission can be completed before the current STI ends. This approach does not require additional communications coordination, and it attempts to minimize the impact to the channel. Furthermore, we evaluate the impact of the approach using a new safety-inclusive metric that combines mobility and communications effectiveness, safety awareness probability.

2.8 Vehicular Mobility Simulation

Vehicular movements are modelled using mobility simulators, which often support various mobility models, such as random waypoint (RWP), random direction (RD), and Manhattan grid. The Simulator for Urban Mobility (SUMO) [67] is an open source macroscopic traffic simulation package [68] that represents traffic demands throughout road networks with the capability to produce vehicular movement trace files in a number of formats. SUMO can import road network data from various sources including TIGER, OSM, RoboCup, and openDRIVE. Trips (i.e., routes) can be explicitly defined or generated randomly from

pathways within the road network. SUMO supports vehicle variety in which vehicles behave as expected according to laws of physics, and can use car-following models, such as the Krauss model [69]. Lane-changing models may be employed. Vehicles obey traffic light signaling and other traffic laws. SUMO integrates with several network simulation tools, and provides a "real-time" interactive control interface, TRaCI.

2.9 Vehicular Network Simulation

Numerous available simulation frameworks assist VANET researchers by providing toolsets with supporting models from which a rich set of environmental scenarios are simulated. Often treated as separate architectural modules, simulators address mobility, networking, and radio propagation [58], while some tight coupling among these primary modules may be found in some over-arching VANET simulators [57]. For a good review of VANET simulator toolsets and models, see [57]. However, despite the availability of such tools, results are inconsistent. For example, when simulating the same environment and protocol, one investigation of VANET mobility generators shows performance deviations among them, making simulation results "unconvincing and inconclusive [57]." Indeed, the simulation requirements of VANET environments presents numerous challenges to the VANET researcher, such as "constrained road topology, multi-path fading and roadside obstacles, traffic flow models, trip models, varying vehicular speed and mobility, traffic lights, traffic congestion, drivers' behavior, etc. [57]" The level of capability for addressing these challenges varies among current simulators. Most concerning to environmental accuracy, VANET simulations often fail to examine accurate roadway networks and the proximity of obstacles [56]. Figure 2.3 shows a classification of representative mobility generators and VANET and network simulators.

Because obstacles not only limit vehicular movement but also interfere with radio-wave propagations, urban scenarios require precise representation of obstacles to benefit VANET simulation, although less critical in highway scenarios [58]. Previous simulation and experimental research studies the impact of radio obstacles, with obstacle classes (i.e., buildings or vehicles) often studied separately. For example, the authors of [70] investigate OLSR in simulation environment with and without large buildings and conclude that the presence of buildings creates communication holes resulting in disconnections. The authors

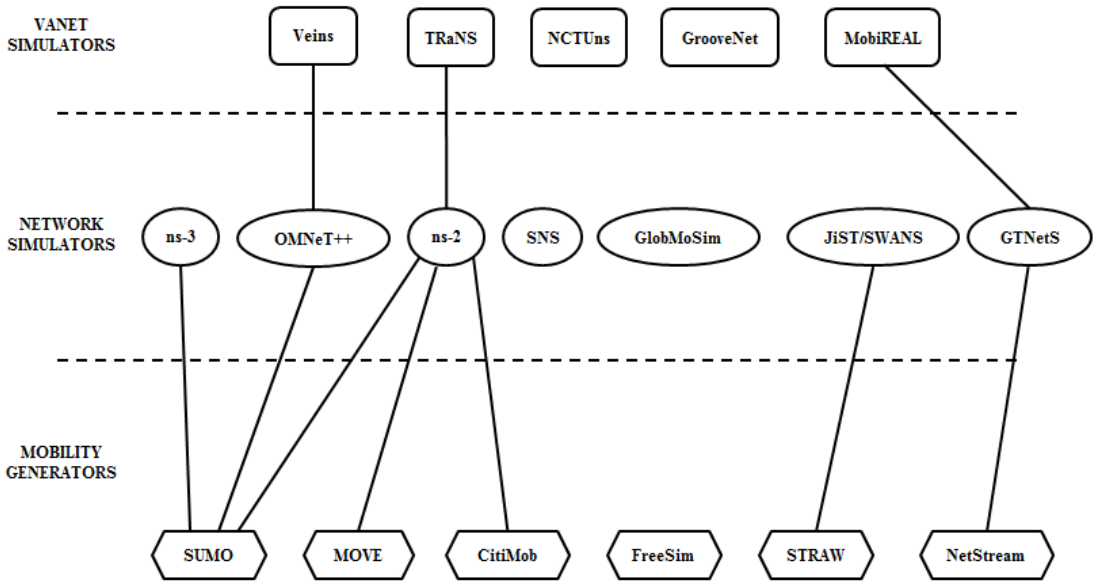

Figure 2.3 Representative VANET simulation tools. Adapted from: [1].

of [71] use GloMoSim to evaluate under street environments the impact routing protocols using a Manhattan-style grid environment and assuming all non-street areas are large buildings. The authors of [72] use VanetMobiSim and ns-2 to investigate the effects of four kinds of radio signal features (including one in which the signal can be diffracted up to 15° at the edge of obstacles), while assuming uniformly large rectangular buildings on 4 block x 4 block streets. Instrumenting vehicles to characterize IEEE 802.11b signal propagation between them in a variety of urban and suburban settings, the authors of [47] found that signal propagation varies especially between LOS and obstructed-line-of-sight (OLOS) . The authors of [31] found similar effects occur when radio waves propagate "Around-the-Corner" (ATC).

Due to the costs of vehicles, communications equipment, and road systems access and control, establishing a VANET test environment remains mostly cost-prohibitive in academic research, although collaborative organizations have developed some limited connected-vehicle test beds [73]. While simulation tools thus remain a highly useful toolset to the VANET modeler, realism continues to present challenges within the environmental models including: vehicular mobility, city-scape (e.g., open highway versus urban settings), and radio wave propagation loss and shadowing. Recent models allow shadowing to be modeled more deterministically when interference includes radio wave propagation through buildings [31] [56] [30]. However, availability remains limited for such models within non-proprietary

network simulation tools. For example, within OMNeT++ [74], the Simple Obstacle Model [31] is only available through Veins [75], making it useful only to vehicular network modeling. Within *ns-3* [76], a buildings model exists, but limits buildings to cubes with linearly placed *x*- and *y*-coordinates and is implemented mainly for LTE modeling only. None of these models generically supports realistic building footprints for shadowing effects that are available to all simulation models (e.g., LTE, WiFi, Bluetooth, Zigbee, etc.).

2.10 Safety Assessment and Metrics

Many VANET applications have been proposed. The Crash Avoidance Metrics Partnership (CAMP) put forth a comprehensive list for the Vehicle Safety Communications Consortium (VSCC) [77] that was subsequently used within SAE J2735. Examples of purely V2V safety applications that assist with impending crash notifications include: Approaching Emergency Vehicle Warning, Wrong Way Driver Warning, Cooperative Forward Collision Warning (CFCW), Emergency Electronic Brake Lights (EEBL), Lane Change Warning, Blind Spot Warning, Highway Merge Assist, Cooperative Collision Warning, and Pre-Crash Sensing

Table 2.2 Safety-related vehicle communications applications (adapted from [1])

Category	Safety Application
Intersection Collision Avoidance	Traffic Signal Violation Warning Stop Sign Violation Warning Left Turn Assistant Stop Sign Movement Assistant Intersection Collision Warning Blind Merge Warning Pedestrian Crossing Information Warning
Public Safety	Approaching Emergency Vehicle Warning Emergency Vehicle Signal Preemption SOS Services Post-Crash Warning
Sign Extension	In-Vehicle Signage Warning Curve Speed Warning Low Parking Structure Warning Wrong Way Driver Warning Low Bridge Warning Work Zone Warning In-Vehicle Amber Alert Warning
Information from Other Vehicles	Cooperative Forward Collision Warning Road Condition Warning Emergency Electronic Brake Lights Lane Change Warning Blind Spot Warning Highway Merge Assistant Visibility Enhancer Cooperative Collision Warning Cooperative Vehicle-Highway Automation System (Platoon) Cooperative Adaptive Cruise Control Road Condition Warning Pre-Crash Sensing Highway/Railroad Collision Warning Vehicle-to-Vehicle Road Feature Notification Cooperative Glare Reduction Adaptive Headlamp Aiming

(PCS). Table 2.2 categorizes several safety-related vehicle communications applications that are potentially enabled or improved by V2V communications (adapted from [1]).

The plethora of envisioned safety applications creates confusion when attempting to evaluate and compare their performance. For instance, what is the difference between Cooperative Forward Collision Warning, Emergency Electronic Brake Lights, and Pre-Crash Sensing? VANET applications differ by their communications requirements, which include

[1]: Transmission Mode, Update Rate, Allowable Latency, Data to be Transmitted and/or Received, Maximum Required Range of Communications. For example, Table 2.4 summarizes the data frequency (i.e., update rate), latency, and range communications requirements for CFCW, EEBL, and PCS and shows that CFCW and EEBL have similar performance criteria, except that EEBL functions over a longer communication range (~300m) than CFCW (~150m). Furthermore, PCS requires the highest update rate, the least latency, and the shortest communications range. Intuitively, we might say that PCS has stricter operational characteristics and thus may have a greater safety meaning to the driver. The Vehicle Safety Communications (VSC) project evaluated vehicle safety applications enabled or enhanced by V2V communications. Table 2.3 lists the preliminary application communications requirements for the V2V safety applications with the greatest potential for safety benefit as identified by the VSC project team (adapted from [1]).

Table 2.3 V2V safety communications applications with greatest potential safety benefit.

Application	Latency [ms]	Primary Data Elements	Maximum Required Communications Distance [m]
Emergency Electronic Brake Lights (EEBL)	~100	Position Heading Velocity Deceleration Bank Road surface condition	~300
Pre-Crash Sensing (PCS)	~20	Vehicle Type Position Velocity Acceleration Heading Yaw Rate	~50
Cooperative Forward Collision Warning (CCFW)	~100	Position Velocity Acceleration Heading Yaw Rate	~150
Lane Change Warning (LCW)	~100	Position Heading Velocity Acceleration Turn signal status	~150

Driving condition safety improvements from VANET technologies remain difficult to assess. Foremost, while numerous safety applications have been proposed, none are standardized [12]. Furthermore, large-scale system deployments have been limited to test-bed environments where DSRC adoption rates have been relatively low, and even if comprehensive testing results were available, significant legal hurdles remain regarding risks and liabilities that could jeopardize successful deployment [78]. Put bluntly, if injuries still occur in operational conditions involving safety-certified VANET applications, then who is responsible?

How, then, do we assess application safety in a VANET? The WAVE protocol stack of Figure 2.2 shows a five-layer model top-down from Application to Physical layers and various metrics are used to assess the performance of each layer. Indeed, researchers [25] [79] [80] have studied in depth the physical layer performance of IEEE Std. 802.11 / WAVE VANETs, commonly using throughput, end-to-end delay, and collision probability as comparative metrics. While network performance is often assessed using throughput, end-to-end delay, and packet loss to quantify Quality of Service (QoS), these metrics generally express the Routing, Link and MAC layer effectiveness. In a VANET, information dissemination of safety packets is critical, requiring a need to evaluate network-layer routing and delivery [81]; for accurate packet delivery we have to consider the packet delivery ratio (PDR) [82] and packet drop rate [83]. Additionally, routing overhead (i.e., number of routing bytes required by the routing protocol to construct and maintain its route [84]) and hop count from source to destination help assess routing performance [83]. While network layer metrics are commonly evaluated in many different types of networks, the safety-enabled VANET demands unique application requirements.

Potential safety benefits of VANET applications can be assessed based on the estimated effectiveness of the application in terms of reduction of "crash-related factors" (e.g., functional years lost, vehicles crashed, and direct costs) [1]. While network level metrics have been historically important to the understanding and tuning of traditional Internet and Mobile Ad hoc Networking (MANET) communities [81], application performance depends instead on reliability metrics [81] [85] [82]. Performance measurements considered are often network- (or packet-) level metrics (e.g., PDR and Average Per-Packet Latency) and/or application-level reliability metrics (e.g., Application-level T-Window Reliability [81]).

Packet Delivery Ratio, $PDR_{net}(d)$, is the percentage of broadcast packets that are successfully received by all vehicles within each transmitting vehicle's coverage range, d [81]

Table 2.4 Communications requirements for three CAMP/VSCC safety applications

Application	Cooperative Forward Collision Warning (FCW)	Emergency Electronic Brake Lights (EEBL)	Pre-Crash Sensing
Update Rate	~10 Hz	~10 Hz	~50 Hz
Latency	~100 ms	~100 ms	~20 ms
Range	~150 m	~300 m	~50 m

[82]. Receipt failures degrade PDR due to concurrent transmissions, hidden terminal problems and the impact from channel fading [82].

Application-level T-window reliability (TWR), $P_{app}(d)$, is the probability of receiving at least one packet out of multiple packets from a broadcasting vehicle at distances smaller than or equal to d, within a time interval, T. $P_{app}(d)$ describes the application-level reliability for safety applications, whereas $PDR_{net}(d)$ commonly represents an i.i.d. packet-level metric that describes the wireless communications reliability [81]. Application-level reliability can be expressed in terms of network-level reliability as [81]:

$$P_{app}(d) = 1 - (1 - PDR_{net}(d))^{\frac{T}{\tau}}, \tag{2-27}$$

where t is the beaconcasting interval and τ is the tolerance time window.

Generalizing, the awareness probability, $P_A(x, n, T_{Tol})$, is the probability at distance x of receiving at least n packets in the tolerance time window, T_{Tol} [82] [85], where $P_s(x) = PDR_{net}(x)$; awareness probability equals application-level T-window reliability when $n = 1$.

$$P_A(x, n, T_{Tol}) = \sum_{k=n}^{\left\lfloor \frac{T_{Tol}}{\tau} \right\rfloor} \binom{\left\lfloor \frac{T_{Tol}}{\tau} \right\rfloor}{k} P_s(x)^k (1 - P_s(x))^{\left\lfloor \frac{T_{Tol}}{\tau} \right\rfloor - k}, \tag{2-28}$$

By considering the number of packets and time tolerance windows, awareness probability can be applied to different safety applications in order to assess application reliability. We can, in fact, assess the effectiveness of CFCW and EEBL, both of which, according to Table 2.4, generate safety messages at the update rate of 10 messages per second. However, although an awareness probability can be calculated analytically using network-level PDR, confusion remains over how to best use this application-level metric to evaluate application performance, as there are no standards that define suitable numbers for messages received or time tolerance windows and the requirements are hard to capture. For example, do we need to receive 1 message every 0.1 seconds? Or 5 messages every half a second? Or ten messages in one second? What if we receive 9 messages in one second, or 99 messages in 10 seconds – would that be "safe"?

The authors of [85] provide a methodology that extends the use of awareness probability to instead determine the awareness range, $R_A(P_A)=d$, which is the maximum distance, d, at which a threshold awareness probability, P_A, is met or exceeded. By first fixing an awareness probability threshold (i.e., P_A = 90%, 95%, 99.99%), the network-level PDR necessary to

achieve P_A can be determined and the effective awareness range of the PDR can further be calculated. The awareness range can then be compared to the vehicular operating conditions (e.g., braking distance, expected communications range, etc.) to determine if such conditions can be met. Intuitively, awareness range describes whether or not there is sufficient distance and time for a safety application to support user responses that maintain safe operating conditions. As such, this is conceptually much closer to a suitable measure of application-level performance. Nonetheless, the authors of [85] strongly caution that even they have failed to answer the general, open question, "How much safety can be achieved by Intelligent Transportation Systems?".

2.11 Evaluations of Vehicular Wi-Fi Networks

2.11.1 Static-node Beaconcasting Wireless Networks

Packet loss causes in an urban setting were analyzed in the measurement study of Roofnet [86], a static 38-node 802.11b multi-hop network covering six square kilometers of Cambridge, Massachusetts, in which nodes emit packets at regularly timed intervals. Loss rates between nodes were found to be relatively uniform and distance-independent. Most link loss rates remained generally stable and temporally independent, although a small minority exhibited bursty losses. Intermediate link loss rates are more likely due to multi-path fading rather than attenuation or interference. SINR and distance were found to have little correlation to loss rate predictability.

2.11.2 DSRC FOTs

Empirical measurements from realistic, DSRC-based driving environments were analyzed in [87] to investigate the temporal, spatial, and symmetric communications correlation characteristics. Intermediate loss rates were found to be a dominating feature, with propagation environment being a major contributing factor, whereas Doppler effects, RSSI value, and transmission power did not significantly affect performance. Bursty effects were found to be common, implying a weak temporal correlation, although the environmental variation surrounding a vehicle can have a high impact to temporal-dependence (e.g., in environments with large numbers of moving vehicles, mobile scatterers dominate, increasing volatility of the vehicular channel).

2.11.3 Safety Pilot Model Deployment (SPMD)

The SPMD was conducted in Ann Arbor, Michigan, from August 2012 to February, 2014 [28], and represents the first large-scale test [88] of V2V technology in a real-world multimodal operating environment [89] [88].

As the model for (US) national deployment of connected vehicle technology, over 75 miles (121 km) [28] of urban, suburban, and rural roadways around Ann Arbor served as the "sandbox" for 2,787 cars, 19 commercial vehicles, and three passenger buses [88] [90] that sent and/or received SAE J2735 BSMs and other information wirelessly to/from each other (i.e., V2V) and 25 RSEs (i.e., roadside equipment for V2I). Participation from eight different auto [88] and four DSRC equipment manufacturers [28] allowed significant interoperability to be tested. Of the study vehicles, 2,397 (86%) [88] were equipped with devices that only emitted safety messages but could not receive them, while 382 vehicles (14%) [88] [90] were instrumented with either integrated or retrofit/aftermarket devices [88] that could both send and receive safety messages [88]. While the low number of vehicles that cannot both transmit and receive limits the amount of data for bidirectional analysis, it does not otherwise invalidate our results, and future FOTs will expand the available data by increasing the total number of inter-communicating vehicles.

Expanding upon the SPMD, the University of Michigan envisions its Mobility Transformation Center (MTC) supporting a major deployment of 9,000 vehicles in Ann Arbor and infrastructure in southeast Michigan to support 20,000 connected vehicles [89].

2.11.4 Performance in Ann Arbor

Results collected from eight trucks equipped with DSRC-retrofit kits and logging over 60,880 encounters with other SPMD vehicles are reported in [91]. Less than 10% of BSMs broadcast by vehicles between 20m behind and 60m ahead of the truck were not received (i.e., PER < 10%). Higher losses to the left and right sides the truck were attributed to the likelihood that buildings or trees existed between the vehicles. Packet loss gaps in 98% of the encounters were less than 300ms. While PER was low at short range, the results show that at distances of 300m, PER is above 70%, with better performance ahead of the truck than behind, implying that characteristics of the truck (e.g., length, materials, and antenna placement) and environmental constraints (e.g., obstacles such as buildings, trees, and other vehicles) significantly impact PER.

CHAPTER

3

AN OBSTACLE MODEL IMPLEMENTATION FOR EVALUATING RADIO SHADOWING

Obstacles, such as buildings and trees, interfere with radio wave signal propagation by contributing fading and shadowing effects. To produce results that accurately reflect authentic topologies, models must capture the radio-interfering conditions that obstacles present. Failing to account for the effects of obstacles can therefore inaccurately overstate network performance. An obstacle shadowing model was implemented for the *ns-3* network simulation toolset and tested using an *ns-3* script for wireless VANET scenarios and obstacle-based geodata from OSM. Results show that deterministic obstacle shadowing compares differently than stochastic Nakagami-m fading. The obstacle shadowing model algorithm can be executed in time complexity similar to other simpler models. Including realistic obstacle shadowing in simulation modeling improves performance assessment.

3.1 Introduction

Outdoor obstacles, such as buildings, buses, and trees, challenge network researchers to produce accurate and consistent results [56] because obstacles interfere with radio signal

propagation by contributing fading and shadowing effects, especially in a VANET [58]. To improve simulation results, models must accurately reflect the natural topology and their impact to the energy of signals traveling through it. While deterministic radio wave attenuation models are often supplemented with stochastic models that reflect fading effects, the stochastic nature of such intended model improvements determine the physical parameters of channel transmissions in a completely probabilistic manner without considering underlying geometry [34] and could therefore deviate severely from realistic behavior, negatively impacting performance assessments [31].

This research presents an accurate, deterministic obstacle shadowing model for *ns-3* that follows the model introduced in [31] and discusses how it impacts network performance assessment. The following research questions (RQ) guide our investigations:

RQ1: Can fast fading and shadowing effects of obstacles, such as buildings, vehicles and trees, be modeled and efficiently simulated in *ns-3*[76]?

Because model realism improves simulation results, a deterministically real fast fading and shadowing model that accounts for radio wave propagation through obstacles will improve the usefulness of existing detailed network simulation tools, such as *ns-3*.

RQ2: How does performance in a VANET compare between the deterministic obstacle shadowing model and other stochastic fading and shadowing models?

By implementing a deterministic obstacle shadowing model and quantifiably comparing simulation results to other stochastic fading models, a performance characterization of the obstacle shadowing model can be made.

Our primary contributions include:

1. Following the model introduced in [31], an efficient implementation of an obstacle model based on computational geometry techniques was developed and offered to the *ns-3* network simulator community[1].
2. Simulation results using obstacles compare quantitatively the effects of i) deterministic obstacle shadowing to ii) stochastic Nakagami-m fast fading and iii) no fading.

[1] https://codereview.appspot.com/201200043

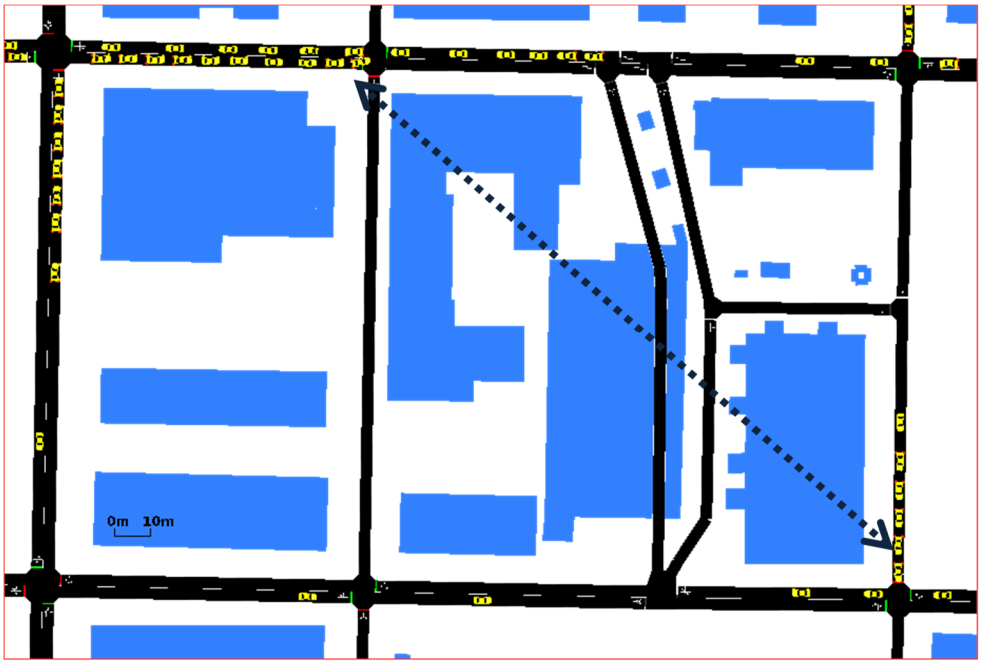

Figure 3.1 Obstacles in a downtown Raleigh, NC scenario as simulated in SUMO

3.2 Obstacle Shadowing Model

3.2.1 Obstacle Model

VCMs that could address transmissions in unobstructed conditions should account for the effects of radio waves as they travel through obstacles. To deterministically evaluate for *ns-3* the effects of obstacles, an obstacle model is implemented in which two-dimensional polygons represent obstacle boundaries. Figure 3.1 shows an example urban downtown scenario (Raleigh, NC, USA) using buildings data from OSM [92] and simulated in the SUMO open source traffic simulation package [67] [68]. As shown in the example, the OLOS between two vehicles may pass at oblique angles through multiple walls and interior distances among several buildings.

Using the obstacle model, an obstacle-aware shadowing model leverages the Computational Geometry Algorithms Library (CGAL) to count the number of walls as obstacle intersections, calculate the distance traveled through obstacles as interior intersection lengths and implement deterministically the shadowing effects of wireless transmissions for OLOS pathways.

<table>
<tr><th colspan="5">Source code modules</th><th>Usage and examples</th></tr>
<tr><td colspan="5">test</td><td></td></tr>
<tr><td colspan="5">helper</td><td>High-level wrappers for everything else
Aimed at scripting</td></tr>
<tr><td>protocols</td><td>applications</td><td>devices</td><td>propagation</td><td>…</td><td>obstacle shadowing propagaion loss</td></tr>
<tr><td colspan="3">internet</td><td colspan="2">mobility</td><td>Mobility modules (static, random walk, etc.)</td></tr>
<tr><td colspan="5">network</td><td>Packets, Packet tags, Packet headers, Pcap/ASCII file writing
Node class, NetDevice, Address types (IPv4, MAC, etc.), Queues, Sockets</td></tr>
<tr><td colspan="5">core</td><td>Smart pointers, Dynamic type system, Attributes, Callbacks, Tracing, Logging, Random variables, Events, Schedulers, Time arithmetic, obstacles and topology management</td></tr>
</table>

Figure 3.2 Obstacle shadowing model enhancements to the *ns-3* reference model

To implement the model, propagation and core modules of the *ns-3* reference model were enhanced, as shown and identified in Figure 3.2.

Three classes comprise the obstacle model: `Obstacle` retains the geometric elements to represent an obstacle, `Topology` uses it to load obstacle data points into a managed collection, and `ObstacleShadowingPropagationLossModel` uses both to implement the obstacle shadowing propagation loss model. All classes are initially placed in a new *ns-3* module, `obstacle`.

The `Obstacle` class represents an obstacle using a CGAL `Polygon_2` object, and retains parameters that determine the fading effects through obstacle walls and interior space.

The `Topology` class loads buildings data from a file in the format as available through OSM [92] and processed using SUMO's Polyconvert utility. A user obtains from OSM the buildings data file for the region of interest (e.g., a city area), processes it with Polyconvert, and loads the resulting buildings data into the `Topology` object via the LoadBuildings() method. A subset from an example buildings file is shown in Figure 3.3. A single topology instance to handle all buildings is assumed. Furthermore, the Topology object can be used to determine the obstructed loss between two points by use of the GetObstructedLossBetween() method, which implements the algorithm that determines for two vehicles (i.e., points) the number of walls penetrated and total distance traveled through obstacles, for which the pseudo-code is given in Figure 3.4.

```
<?xml version="1.0" encoding="UTF-8"?>
<!-- generated on 06/12/14 16:58:30 by SUMO polyconvert Version 0.19.0 <?xml version="1.0" encoding="UTF-8"?
xsi:noNamespaceSchemaLocation="http://sumo-sim.org/xsd/polyconvertConfiguration.xsd"> <input> <net-file valu
full-type value="true"/> </input> <output> <output-file value="Raleigh_Downtown.buildings.xml"/> </output> </
<shapes>
    <poly shape="1690.05,2341.48 1691.34,2469.30 1672.88,2470.03 1669.79,2356.91 1645.53,2356.81
        id="135692669"/>
    <poly shape="1141.90,2293.97 1123.01,2271.05 1132.43,2263.06 1151.78,2286.49 1141.90,2293.97"
    <poly shape="1211.96,2467.63 1136.69,2469.68 1137.13,2451.33 1155.11,2450.32 1153.83,2402.94
        id="135692671"/>
    <poly shape="1087.61,2331.80 1122.56,2331.20 1139.74,2322.91 1151.75,2326.82 1168.21,2329.87
        1199.30,2207.43 1199.39,2203.57 1118.24,2205.87 1111.22,2216.65 1085.03,2217.23 1087.61,2
    <poly shape="1239.12,2327.23 1234.83,2202.97 1349.83,2202.35 1352.50,2212.33 1346.72,2231.03
        1333.62,2291.34 1339.34,2291.48 1338.69,2282.28 1348.88,2282.53 1348.25,2308.37 1333.67,2
        type="building.yes" id="135692673"/>
    <poly shape="1019.60,2868.35 1075.08,2868.50 1074.10,2801.30 982.60,2802.73 983.76,2862.68 10
        id="135693009"/>
    <poly shape="1071.46,2927.09 1071.60,2923.98 1074.85,2918.98 1077.83,2919.02 1076.76,2892.91
        997.10,2926.50 1001.39,2926.38 1000.84,2929.51 1022.44,2928.83 1022.57,2926.39 1030.09,29
        1071.46,2927.09" layer="-1.00" fill="1" color="51,128,255" type="building.yes" id="135693010"/>
    <poly shape="1252.66,3131.91 1253.62,3182.63 1249.57,3182.71 1249.81,3195.32 1253.86,3195.25
        1296.21,3210.64 1295.94,3196.89 1298.23,3196.84 1297.00,3131.09 1252.66,3131.91" layer="-1
    <poly shape="1357.01,3226.29 1374.84,3225.93 1374.44,3194.39 1354.83,3194.44 1355.06,3197.52
        1357.01,3226.29" layer="-1.00" fill="1" color="51,128,255" type="building.yes" id="148163971"/>
    <poly shape="1258.27,3211.34 1258.64,3231.27 1258.72,3235.40 1258.88,3244.07 1343.88,3242.36
        1356.89,3235.04 1354.89,3231.23 1352.24,3228.32 1356.07,3228.11 1355.47,3210.23 1303.20,3
        type="building.yes" id="148163972"/>
```

Figure 3.3 A subset of buildings data for the downtown Raleigh, NC USA area

When considering obstructions between two vehicles, only obstacles that lie less than 500m between the vehicles are included, as obstacles at greater distances tend to entirely block residual radio wave energy. Figure 3.5 further illustrates an example where two vehicles (i.e., V1 and V2) are shown with the OLOS between them as a dashed line. Shaded around each vehicle is a circle of 500m radius that represents the region of potential obstructing obstacles (i.e., corresponding to step 4 is the algorithm of Figure 3.4). For performance optimizations, potential obstacles are found by searching a BSP of obstacle centerpoints (i.e., the midpoint of an obstacle's bounding box). An example centerpoint, P, is labeled in Figure 3.5, within the region surrounding vehicle V1. All buildings with centerpoints within the shaded regions are each tested for intersections along the OLOS path between the two vehicles. For each obstacle that meets the intersection test, the total number of intersection edges (i.e., walls) and distances within the obstacle interiors are determined and the ensuing sum total is returned. As an additional optimization, inter-vehicle obstacle obstructions are cached by assuming that each

Algorithm GETOBSTRUCTEDDISTANCEBETWEEN (p_1, p_2, B)

Input. Locations, p_1 and p_2, of two vehicles and a pre-determined binary search partition (BSP), B, of obstacles.

Output. The total obstructed distance, m_o, and the number of obstacle edge intersections, n.

1. $m_o \leftarrow 0$; $n \leftarrow 0$
2. Initialize a maximum range, r, the distance from either point p_1 or p_2 to an obstacle center-point, that is used to filter the set of obstacles to the subset which are sufficiently nearby for calculation purposes (i.e., for optimization, exclude far-away obstacles).
3. Create a bounding box, b, for p_1 and p_2 and extend in all directions by r.
4. Get the set of potential obstacles, O. $O \leftarrow$ the range search of b within B.
5. For every obstacle $o \in O$, do:
6. if the distance from p_1 or $p2$ to the obstacle center is within range, r, then
7. for each edge $s \in o$,
8. if s intersects a ray from p_1 to p_2
9. $n \leftarrow n + 1$
10. save the min. and max. distances from $\{p_1, p_2\}$ to the intersection pt.
11. $m_o \leftarrow m_o$ + distance between min., max. values in step 10 (i.e., obstructed distance)
12. return m_o and n

Figure 3.4 Pseudo-code for the algorithm that determines the number of obstacle wall intersections and obstructed distance between two points

pair of vehicles that have not both changed position by more than 0.1m retain the same obstructed-distance results.

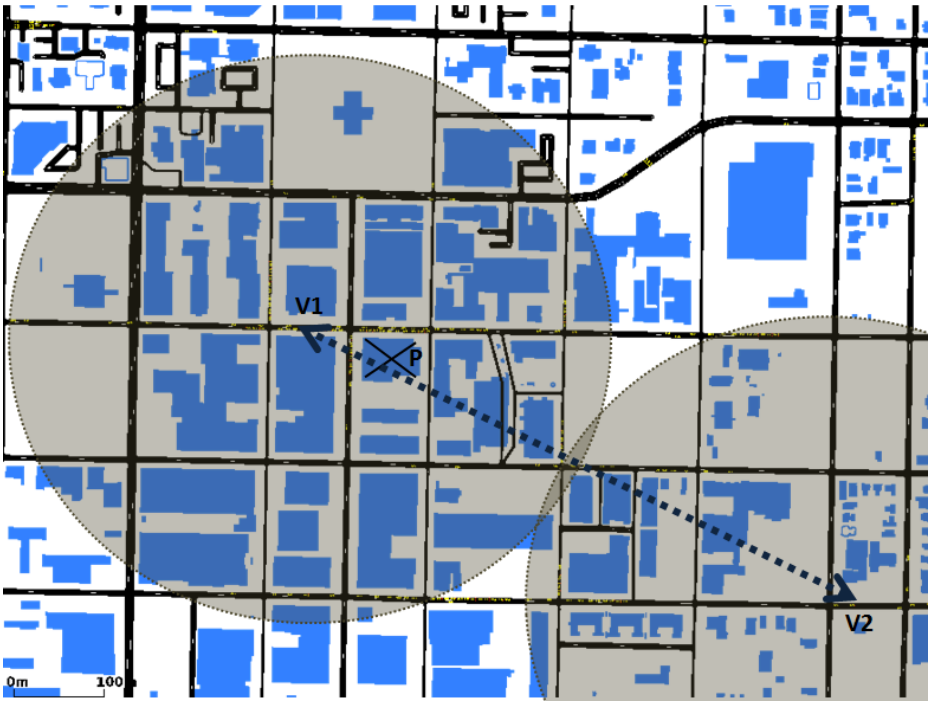

Figure 3.5 Obstacle intersection range

3.2.2 Propagation Loss

Following the model introduced in [31], an obstacle shadowing model was developed for the *ns-3* network simulation toolset using computational geometry techniques to determine OLOS distances traversed and number of segment intersections (i.e., walls penetrated) in roadway scenarios using building footprint information from OSM.

Slow fading shadowing effects of obstacles are modeled using the Simple Obstacle model of [31], in which obstacle shadowing path loss, $L_{s,o}$, is dependent on both per-wall-attenuation and per-meter-attenuation as:

$$L_{s,o} = \alpha n + \beta d_o, \tag{3-1}$$

where α is the attenuation per wall, in dB, n is the number of walls penetrated, β is the attenuation per meter, in dB, and d_o is the distance, in meters, traveled through obstacles. Default values as per [31] of α = 9 dBm and β = 0.9 dB / m are used. However, the implementation supports configuration of these values per obstacle, so that radio wave propagation effects can be modeled for obstacles composed of different types of construction

materials (e.g., "brick and mortar" buildings versus wooden-framed houses, garages, sheds, etc.).

To implement the model, class `ObstacleShadowingPropagationLossModel` derives from `PropagationLossModel` and can thus be used in *ns-3* for propagation loss chaining. For example, a user could set up a simulation to use the Two-Ray Ground or Friis propagation loss model, and additionally chain Nakagami-m fading and obstacle shadowing (or other supported propagation loss models).

As an example calculation, consider a scenario (e.g., as in Figure 3.5) where the line between two vehicles passes through n=10 walls and an interior distance of $d_o = 125$m. Substituting into ((2-2) yields $L_{s,o}$=9×10+0.9×125=202.5 dB. With the cumulative losses for this example, it is unlikely that a transmission from one vehicle would have sufficient power to be received by the other, as obstacle shadowing causes significant propagation loss.

3.3 Experimental Setup and Results

3.3.1 Experimental Setup

Several steps are necessary to set up an experiment that uses the obstacle shadowing model, as shown in Figure 3.6. First, buildings data is obtained from OSM and fed through SUMO's Polycovert utility and also optionally included in SUMO's Netconvert utility if obstacles are to be shown in SUMO's vehicular simulation. Next, SUMO combines road network and simulation criteria to produce a vehicular trace file that is converted to *ns-2* format using the traceExporter2.py python script. Lastly, the buildings data is loaded into *ns-3* (i.e., via the `Topology` class) and the *ns-2* vehicle trace file is played back using `Ns2MobilityHelper` while the network configuration is simulated.

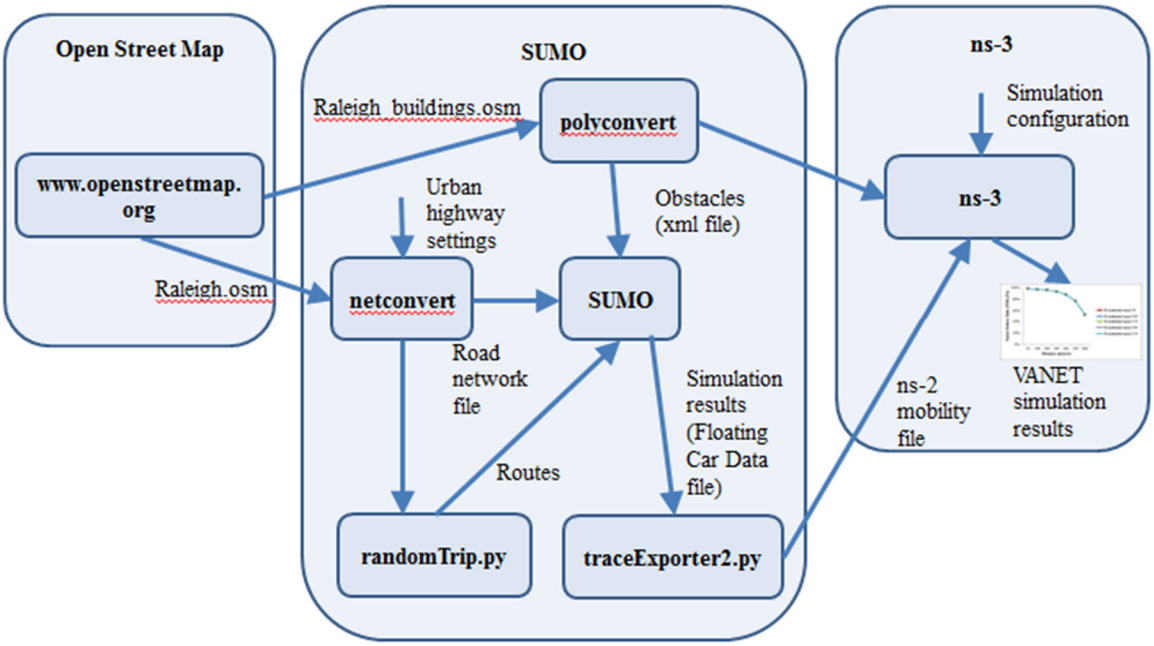

Figure 3.6 Process flow for experimental setup

To answer RQ1 the obstacle shadowing model was implemented for the *ns-3* network simulation toolset and to answer RQ2 it was tested using the (*ns-3* WAVE) *vanet-routing-compare* script that enabled BSM traffic only (i.e., disabled routing protocol traffic) and was extended to support scenarios with obstacles.

To test the obstacle shadowing model, scenarios with numerous interestingly-shaped buildings were sought in which many nodes would generate wireless traffic frequently and by movement would change their orientation among the set of buildings. Wireless VANET scenarios in open highway, residential neighborhood, and urban downtown settings were ultimately selected, with topology parameters as shown in Table 3.1 and depicted in Figure 3.7, Figure 3.8, and Figure 3.9.

Network simulation uses the mobility trace files produced by SUMO simulations (i.e., *ns-2* trace files) played back for 2000 seconds (i.e., 33.3 minutes) of network simulation time in *ns-3* during which every vehicle emits a BSM 10 times per second. Network simulation parameters are summarized in Table 3.2 with example command line arguments for the *vanet-routing-compare* script that users can modify to evaluate different VANET simulation scenarios. Propagation loss is calculated for each transmission between sender and other nearby potential receiving vehicles.

Table 3.1 Scenario topology parameters

		Scenario		
		Open highway	**Residential neighborhood**	**Urban downtown**
Latitude	**N**	35.8855	35.8758	35.7828
	S	35.8420	35.8650	35.7714
Longitude	**W**	-78.8858	-78.6770	-78.6506
	E	-78.7785	-78.6502	-78.6237
Approx. Area (sq. mi.)		39.17	1.68	2.01
Buildings		348	1440	1776
Traffic lights		7	5	75
Vehicles, routes		50-250	50-250	50-250
Car-following model		Krauss	Krauss	Krauss

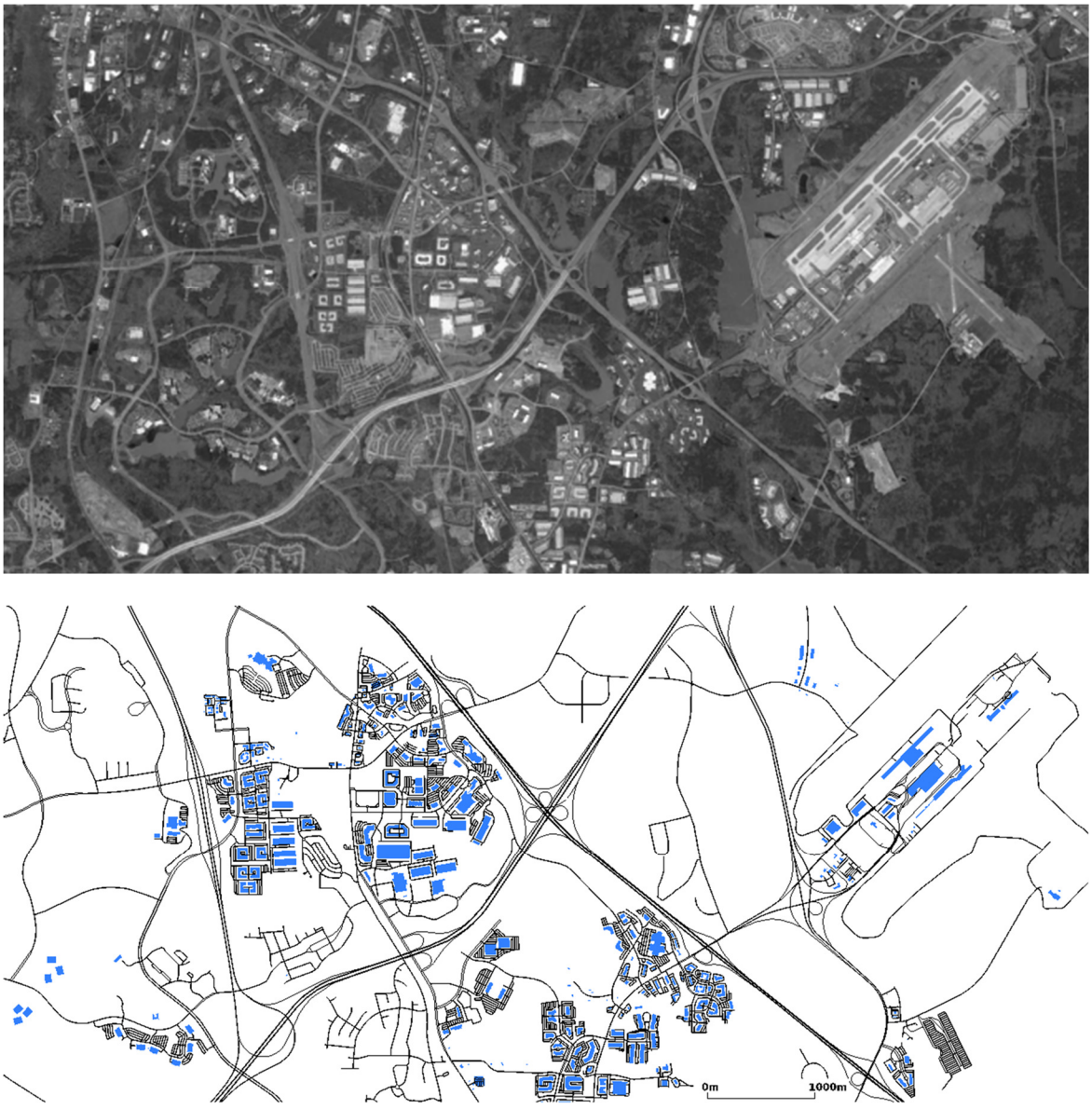

Figure 3.7 View in GoogleEarth™ (above) and visualization in SUMO of Open Street Map (OSM) buildings data (below) for an open highway scenario near Raleigh, NC USA

Figure 3.8 View in GoogleEarth™ (above) and visualization in SUMO of Open Street Map (OSM) buildings data (below) for a residential neighborhood scenario near Raleigh, NC USA

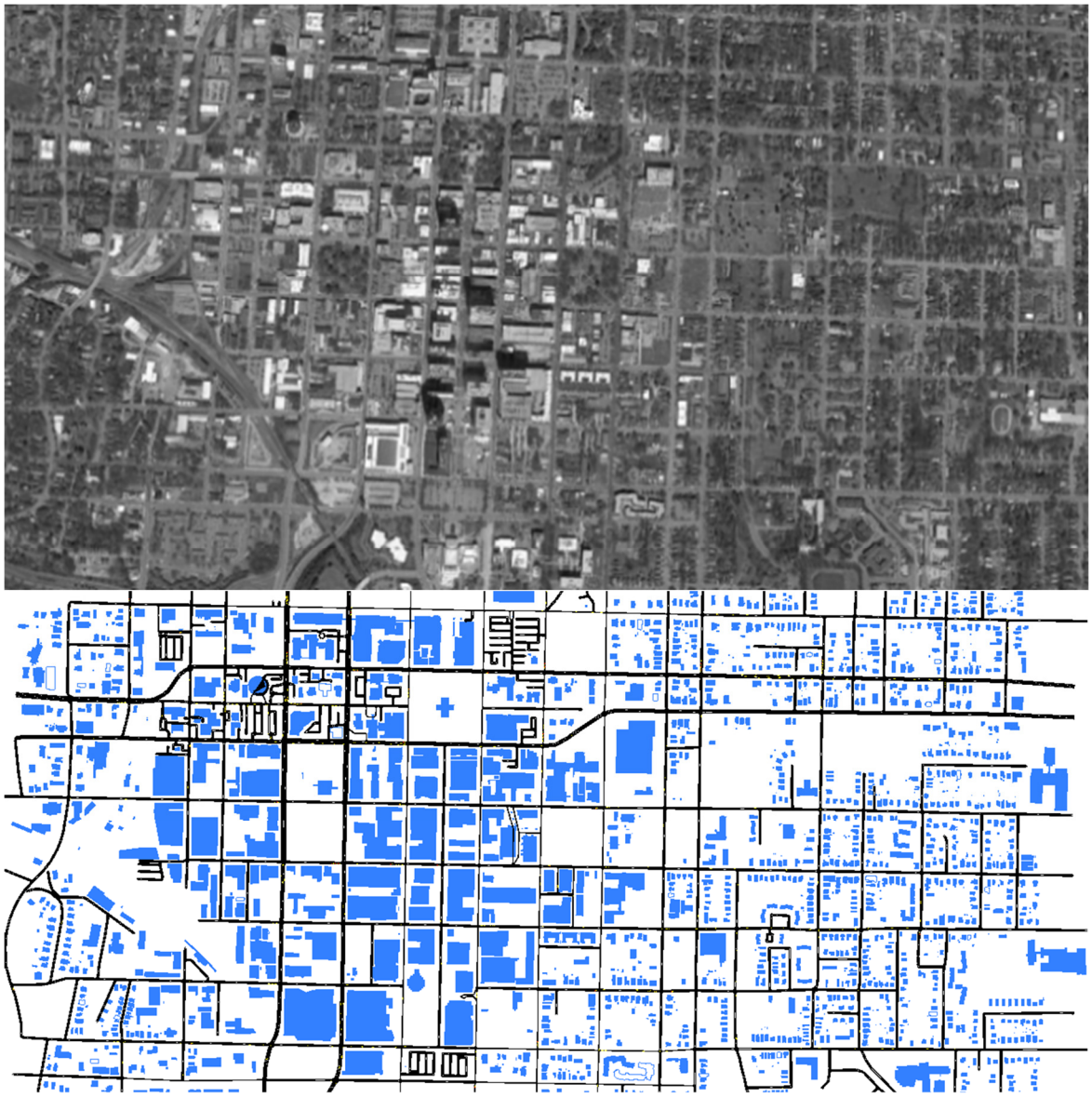

Figure 3.9 View in GoogleEarth™ (above) and visualization in SUMO of Open Street Map (OSM) buildings data (below) for an urban downtown scenario near Raleigh, NC USA

Table 3.2 Network simulation parameters

Parameter	Value	*ns-3* commnd line argument
BSM size	200 bytes	`--bsm=200`
BSM rate	10 Hz	`--interval=0.1`
Transmit power	20 dBm	`--txp=20`
Frequency	5.9 GHz	`(N/A - value hard-coded)`
Channel bandwidth	10 MHz	`--phyMode=OfdmRate6MbpsBW10MHz`
Channel access	802.11p OCB	`--80211Mode=1`
Tx range	50 - 2000 m	`--txdist[n]=[d]`
Sync time accuracy	1-10 μs (uniform)	`--gpsaccuracy=10000`
Encoding	OFDM	`--phyMode=OfdmRate6MbpsBW10MHz`
Rate	6 Mbps	`--phyMode=OfdmRate6MbpsBW10MHz`
Propagation loss model	Two-ray ground	`--lossModel=3`
Simulation time	2000 s	`--totaltime=2000`
Fading Model	Obstacle Shadowing	`--buildings=1`

To compare the effects of obstacle shadowing, identical experiments are repeated and results compared using different propagation loss models for:

i) two-ray ground propagation loss only,

ii) two-ray ground propagation loss and stochastic Nakagami-m fast fading, and

iii) two-ray ground propagation loss and deterministic obstacle shadowing.

Performance is evaluated by comparing the PDR (i.e., the ratio of actually received packets to expected packets) among different path loss models for a given coverage radius from the transmitter.

3.3.2 Results and Discussion

Using *ns-3*, simulations evaluate path loss between vehicles using the two-ray ground propagation loss model, with additional fast fading effects modeled using the obstacle shadowing model of this research and compared to the stochastic Nakagami-m fading model as well as results without any fading effects.

The varying effects of propagation loss models can be explained by example of a downtown intersection, as shown in Figure 3.10. Here, traffic signaling causes vehicles to

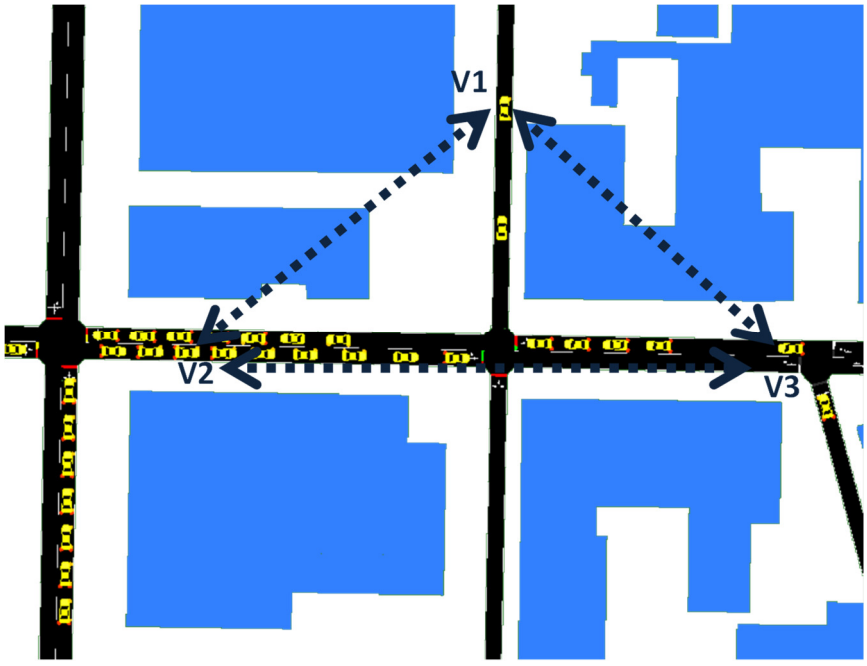

Figure 3.10 Example propagation loss effects near an intersection

gather often at intersections. When obstacle shadowing is ignored, the propagation loss effects of the buildings is unaccounted for between vehicles V1 and V2 and also V1 and V3, leading to an overstatement of the likelihood of packet reception. However, if stochastic fading models are used, then the fading potentials between vehicles V2 and V3 are equally probable as between V1 and V2 or V1 and V3, resulting in an understatement of the communications potential between the unobstructed vehicles V2 and V3.

The increased path loss from fading effects decreases PDR, as does increased shadowing path loss from higher obstacle density. Figure 3.11 compares the PDR at a range of 500m over time for an urban downtown scenario with 250 vehicles for the different propagation loss models. Earlier results (e.g., prior to 500s) show more variability before the randomization of vehicle trip and traffic light signaling leads to more steady-state behavior of vehicle flows. The PDR for “no fading” is the highest, as no additional fading and shadowing losses are taken

into account. Repeating the same scenario and including stochastic Nakagami-m fading effects results in the lowest PDR, as additional fading is probabilistically considered for every vehicle transmission potential. Results for obstacle shadowing lie between the "no fading" and stochastic fading results, implying that a deterministic evaluation of obstacle shadowing shows a fading effect that is not as severe as evaluating propagation loss stochastically for every transmission, as achieved using Nakagami-m fading.

Figure 3.12, Figure 3.14, and Figure 3.13 show that PDR decreases as transmission range increases and is further affected by fading. In the open highway scenario (i.e., Figure 3.12), the tendency for PDR towards limited fading effects (i.e., 200-600m) is explained by more frequent unimpeded communications that do not exhibit fading effects along the open highway road segments resulting in the higher chance of successful safety message exchanges. In both the residential and downtown scenarios (i.e., Figure 3.14 and Figure 3.13), PDR drops off rapidly for short (i.e., < 100m) ranges for both the no fading and Nakagami-m fading models. This is because higher intersection densities of vehicles simultaneously emitting safety messages can saturate the channel with resulting transmission collisions degrading PDR. However, if obstacles sufficiently reduce power such that some messages are blocked from receipt, then the lower localized amount of background noise increases the SINR and improves the chance of reception for those unobstructed signals that receivers can sense.

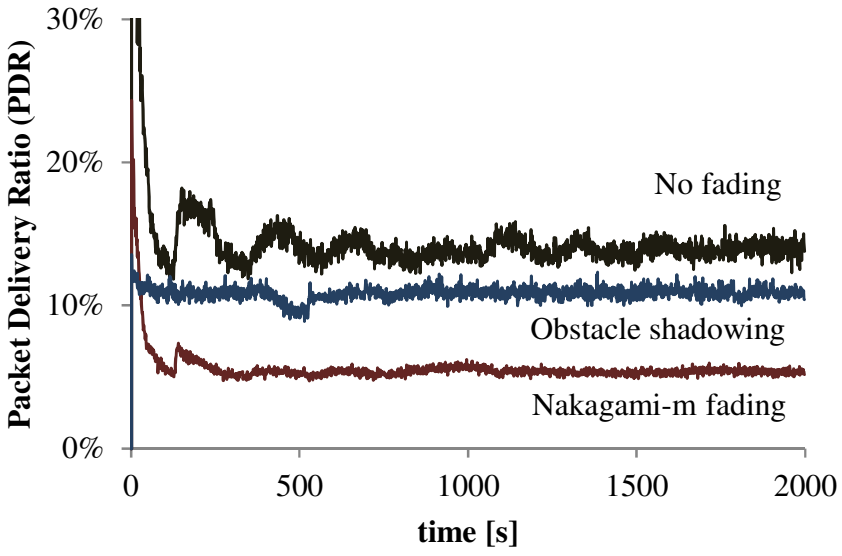

Figure 3.11 PDR over time for three fading models

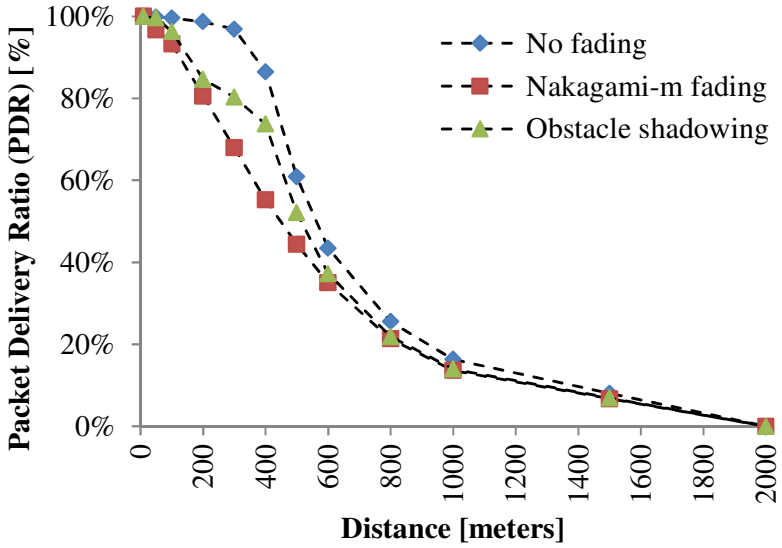

Figure 3.12 PDR for the open highway scenario with 250 vehicles, for three different fading models as a function of the distance from the transmitter

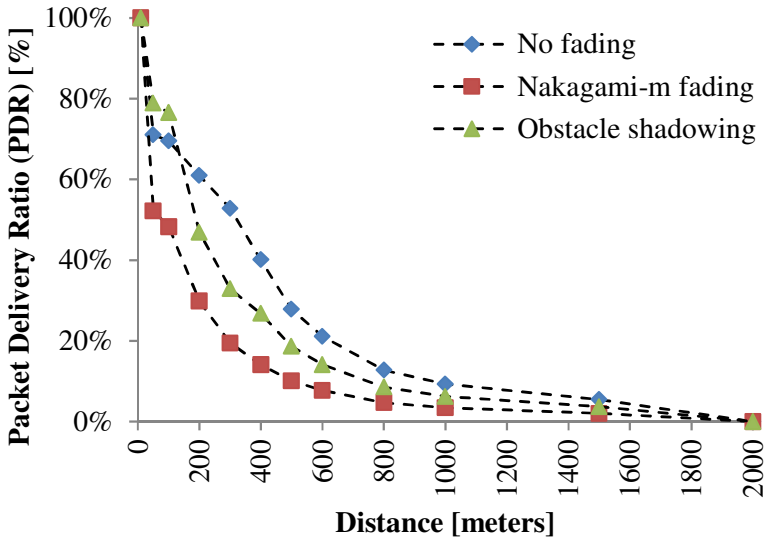

Figure 3.14 PDR for the neighborhood scenario with 250 vehicles, for three different fading models as a function of the distance from the transmitter.

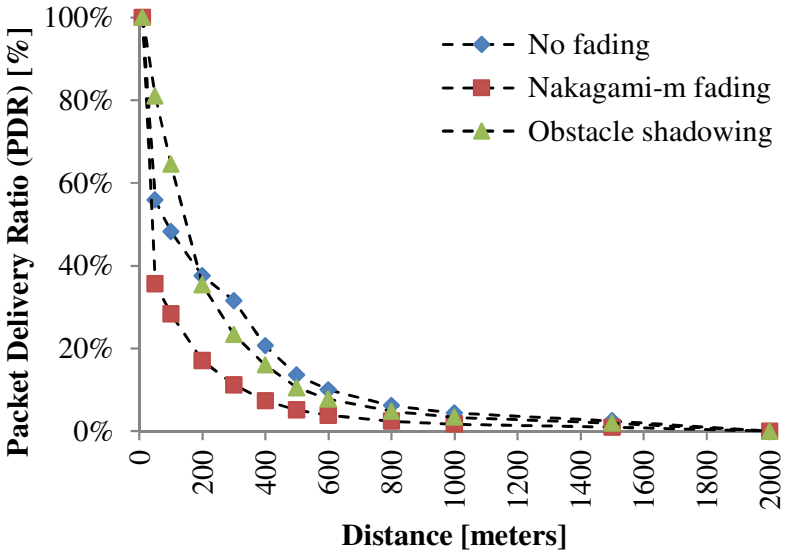

Figure 3.13 PDR for the downtown scenario with 250 vehicles, for three different fading models as a function of the distance from the transmitter.

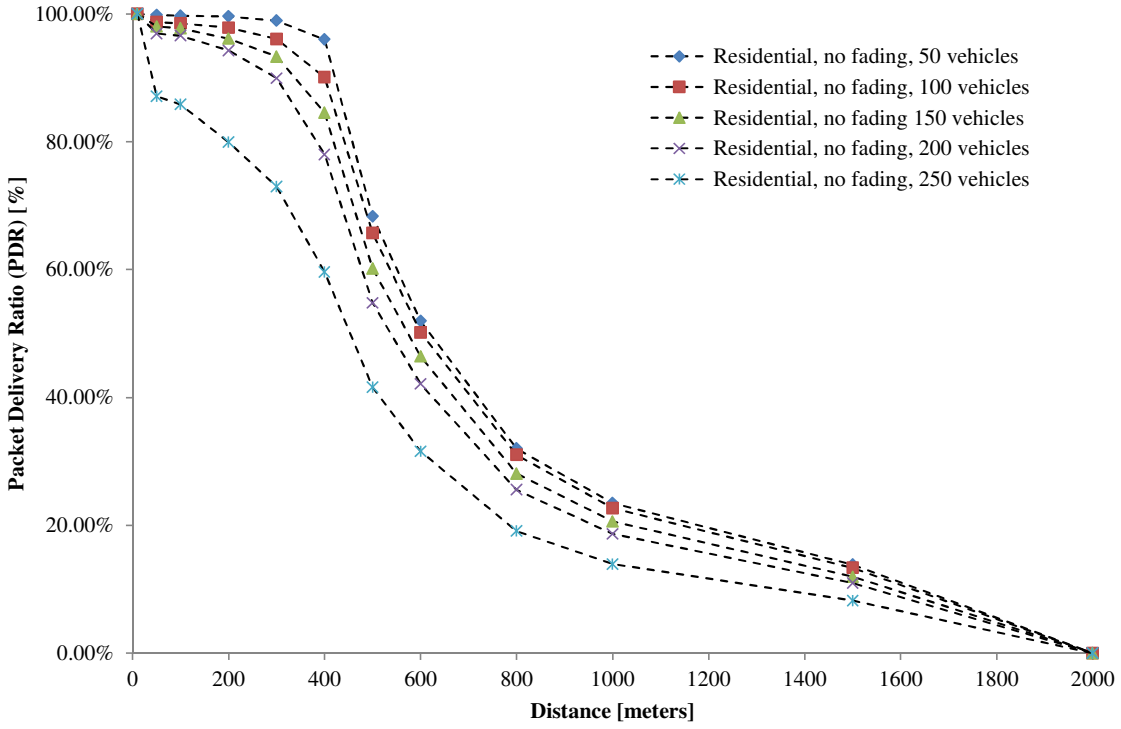

Figure 3.15 PDR for residential neighborhood scenario with no fading, for 50 – 250 vehicles as a function of the distance from the source of the transmission.

Figure 3.15 charts PDR for the residential neighborhood scenario with no fading effects, and shows that PDR decreases as transmission range and/or vehicle density increase.

Lastly, the PDR average and one standard deviation (i.e., σ) are shown in Table 3.3. For the same scenario repeated with only changing the fading model, obstacle shadowing shows the least variation over time.

The results of Figure 3.12, Figure 3.14, Figure 3.13 and Table 3.3 are explained by the obstacle shadowing effects in scenarios with high obstacle densities tending to bifurcate results into those that are entirely unobstructed and so allow successful delivery and those that encounter sufficient radio wave blockage that prevents delivery. In effect, obstacles increase spatial reuse. Similar to the effects experienced by party guests that relocate to more quiet places to continue conversation, often placing walls between themselves and other, louder side-conversations, so too do obstacles such as buildings block inter-vehicle communications thus improving localized PDR, an effect that we call *The Dinner Party Effect*. However, while

Table 3.3 PDR average and standard deviation for three fading models

Model	Mean	σ
No fading	14.38%	2.48%
Nakagami-m fading	5.60%	1.35%
Obstacle shadowing	10.85%	0.56%

obstacle shadowing can therefore improve PDR, there is also a downside in that messages that are prevented from reaching recipients could jeopardize safety.

3.3.3 Performance

Scenarios were simulated for 30 trials each with 50-750 vehicles moving in highway, residential, or downtown areas via *ns-2* trace files and each node transmitting 10 BSMs per second, for 2000s of simulation time. Each trial was repeated to evaluate three different fading models: no fading, stochastic Nakagami-m fading, and deterministic obstacle shadowing. Simulations were conducted using the equipment from the High-Performance Computing services at North Carolina State University, with the longest scenario taking up to six wall-clock days to complete. As shown in Figure 3.16, although the average times indicate that the expected overhead of using the deterministic obstacle shadowing model is greater than the stochastic Nakgami-m fading model, the confidence intervals imply that the simulation performance of the obstacle shadowing model in on the time complexity order of using the Nakagami-m fading model.

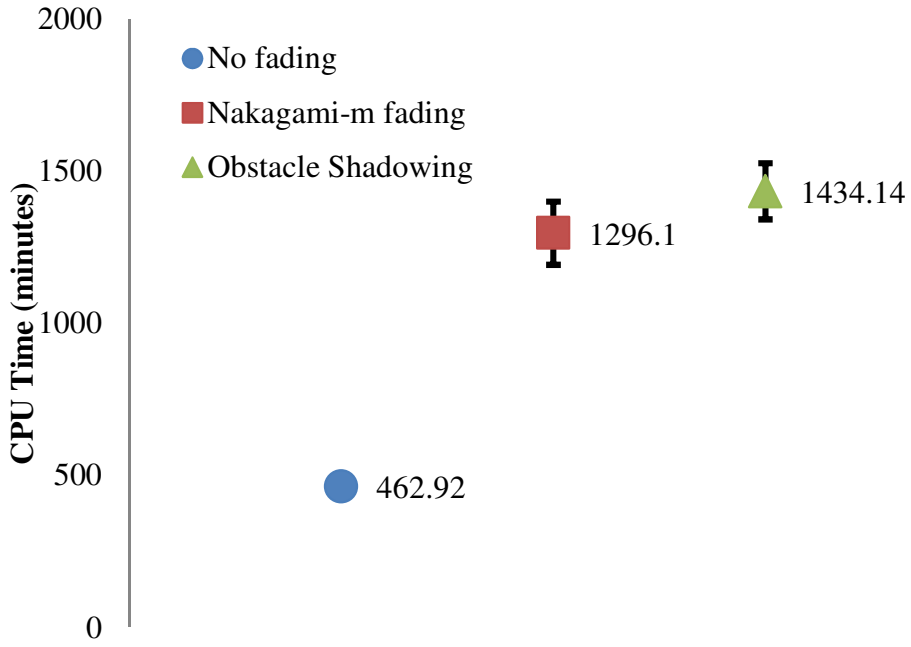

Figure 3.16 CPU-time (minutes) of the sum of times to simulate 2000s of 150 vehicles in the highway, residential, and downtown scenarios for different fading models

3.4 Summary

Performance assessments improve when models accurately reflect environmental conditions such as the fading effects of radio wave propagation through buildings and other obstacles. Results based on stochastic Nakagami-m fading fail to realistically differentiate between highway, residential, and urban settings and differ from the deterministic results obtained using the obstacle shadowing model.

An obstacle model and a fading model that uses it has been implemented and offered to the open source *ns-3* network simulator community. The models are shown to execute efficiently with simulation overhead on the time complexity order of the stochastic Nakagami-m fading model. Results generated from simulation experiments that use these models show that deterministic obstacle shadowing can greatly degrade PDR and compares differently than stochastic Nakagami-m fading. Failing to account for the effects of obstacles can therefore inaccurately or even greatly overstate the performance of VANET scenarios. Including realistic obstacle shadowing in VANET simulation modeling improves VANET assessment.

CHAPTER

4

ANALYIS OF PACKET LOSS IN A LARGE-SCALE DSRC FIELD OPERATIONAL TEST

DSRC intends to improve transportation safety by using wireless technology to allow vehicles to exchange safety-awareness message between them. Using a large empirical dataset collected from a field operational test of nearly 3000 vehicles operating around Ann Arbor, Michigan, we characterize the packet-level performance of safety messages exchanged among vehicular encounters. Specifically, to better understand the real-world operating conditions of the vehicular wireless channel, the characteristics of PRR and IPG behaviors and temporal and spatial correlations are examined. Analysis of vehicle-pair encounters shows DSRC packet losses differing from other, static-node wireless beaconing networks, due mainly to the vehicles' high mobility and the possibilities of signal scatterers and/or obstructers that may come between them. As long bursts of consecutively lost packets could jeopardize vehicle safety awareness, IPG is explored further, with short-gapped consecutive losses commonly uncorrelated and longer gaps exhibiting temporal correlation tendencies. The findings of this chapter can be used to inform channel models for DSRC systems, which in turn can produce meaningful simulation results.

4.1 Introduction

This chapter analyzes packet loss of the nearly 3000 vehicle large-scale wireless V2V field operational test (FOT), commonly called the Safety Pilot Model Deployment (SPMD) [88] [28]. SPMD nodes are cars, trucks, and buses equipped with DSRC devices that move throughout Ann Arbor, MI and surrounding areas using roof-mounted antennas that transmit and/or receive vehicular safety messages wirelessly between them [93].

In the SPMD, all vehicles emit safety messages as beacons at regular intervals that other vehicles can receive (i.e., beaconcasting). Yet, perfect packet reception is not the norm in a VANET [87], with packet losses commonly resulting from separation distance, obstacles, and multi-path fading effects [87]. Understanding packet loss in authentic scenarios requires data from large numbers of vehicles operating within varying scenarios. However, the high costs of such deployments often lead researchers to limit the field range and/or number of vehicles in DSRC beaconing network FOT studies [86] [91] [87]. Thus, the analysis of safety packet losses in large-scale FOTs is important towards an improved understanding of packet-level performance under real-world operating conditions.

The main contribution of this chapter is an analysis of the performance of safety packet receipt and loss within the SPMD, as derived from two months of operational data [94]. The analysis reveals that several common assumptions for DSRC (e.g., high packet reception rate for distances smaller than 100m) simply do not hold in real deployment. The results can be used to develop more accurate wireless propagation models for DSRC systems, which can subsequently improve the performance evaluation of these systems.

The rest of this chapter is organized as follows: Section 4.2 further elaborates the operations around Ann Arbor, MI. Section 4.3 presents analysis and results and shows that DSRC packet loss within Ann Arbor follows a power law distribution with roughly half of gap losses being short-length and uncorrelated, while the remaining average gap losses greater than 400ms exhibit temporal correlation and/or non-stationarity tendencies. Section 4.4 concludes the chapter.

4.2 SPMD Data Analysis

4.2.1 The SPMD Data Environment (DE)

Goals of the SPMD data collection include assisting NHTSA in its V2V safety system decisions and for eventual wide-spread dissemination of the data to a variety of researchers [95] to better understand the safety benefits of a larger scale real-life deployment [93]. The data collected for the SPMD includes almost 4 million trips in nearly 900,000 hours [88] and covering 27 million miles on the road [90] that generated approximately 47 TB [90] of data representing over 84 billion safety messages [96].

To help researchers better understand the performance of connected vehicle technologies, the USDOT makes several connected vehicle research data environments accessible through the Research Data Exchange (RDE) [94], including the SPMD Data Environment (DE) corresponding to a sanitized subset of SPMD data including BSM and other data elements that were generated during October, 2012 and April, 2013 from over 2,700 vehicles, equipped with

Figure 4.1 Representative coverage area for the Safety Pilot Model Deployment in Ann Arbor, Michigan. Highlights represent the line of sight of over 3 million successful BSM receipts for selected encounters between a receiving vehicle (Rx) and a transmitting vehicle (Tx), as derived from the SPMD DE.

V2V wireless technologies, traversing Ann Arbor, MI. Figure 4.1 shows the area around Ann Arbor covered by selected vehicular encounters within the two months of operational data as provided by the SPMD DE.

The 107 GB SPMD DE includes eight datasets for driving data (i.e., for two different vehicle sets, DAS1, and DAS2), BSM captures, roadside equipment (RSE) interactions, and four contextual data sets (i.e., Network, Weather, Schedule, and Road-Work Activity) [97]. Data is organized conceptually for each trip that a vehicle makes. A trip occurs when the ignition is turned on in a DSRC-equipped vehicle, and ends when the ignition is turned off. Trip data for two vehicle data sets, DAS1 and DAS2, was analyzed. Data set DAS1 provided 8,230 unique trips, representing data collected from a majority of the participating vehicles that used the Data Acquisition System (DAS) developed by UMTRI, and data set DAS2 provided 14,315 unique trips representing the data collected by CAMP's 64 vehicles. Trip

Table 4.1 Trip data summary for Safety Pilot Model Deployment Data Environment. Over 22,000 vehicular trips covering 167,000 km in 4,700 hours resulted in more than 48M BSMs that were successfully received.

Dataset	Time Period	Trips	Time (hr)	Distance traveled (km)	Unique Vehicles	BSMs received
DAS1	October, 2012	269	201	4,831	13	502,894
DAS2	October, 2012	7,422	1,360	N/A	64	12,613,845
DAS1	April, 2013	7,961	2,092	95,604	96	12,582,217
DAS2	April, 2013	6,893	1,118	56,664	63	22,551,427
Total		22,545	4,771	157,098		48,250,383

data is not available for vehicles that only emit BSMs but cannot receive them (i.e., the largest number of vehicles participating in the SPMD).

4.2.2 Approach

Data for each trip was time synchronized with BSM reception data. No messages were successfully received when vehicles were separated by 1.2km or more. An encounter between two vehicles exists when they remain within 1.2 km of one another and the interval between successively received BSMs does not exceed 60s. The Packet Loss Burst Length (PLBL), measured as the time gap between successfully received BSMs, defines the IPG. IPG longer than 60s implies significant communications difficulties (e.g., vehicles separated by long distances for long periods of time, or out of range of one another due to obstructions).

A total of 44,482 unique encounters was extracted from the DAS1 data set for April, 2013. Because a majority of the DSRC-equipped vehicles in Ann Arbor only emit but do not receive BSMs, a majority of these encounters represent only unidirectional communications from transmitting vehicle (Tx) to receiving vehicle (Rx). However, a further subset of 1,950 encounters were isolated that represent symmetric communications between Tx and Rx. Table 4.1 summarizes the trip data for the DAS1 and DAS2 data sets.

4.3 Results

4.3.1 Packet Loss

For each encounter, Tx emits BSMs 10 times per second that Rx could receive. Thus, a packet sent by Tx that is not received by Rx during a 100ms interval is considered a lost packet.

For receiver-centric safety packet performance, PER captures the BSM packet loss rate as a ratio, in percent, of the number of packets sent that are not successfully received by other nodes within range over a given time interval. PER for transmitting node *i*, receiving node *j*, and time interval *t*, is defined as:

$$PER(i,j,t) = 1 - \frac{N_{Rx}(i,j,t)}{N_{Tx}(i,\ t)}, \tag{4-1}$$

where $N_{Rx}(i,j,t)$ is the number of BSMs transmitted by *i* that are successfully received by *j* in interval t, and $N_{Tx}(i,\ t)$ is the number of BSMs that *i* transmitted in interval *t*.

Whereas PER characterizes packet loss, its counterpart, PRR, captures the BSM packet receipt success rate.

$$PRR(i,j,t) = 1 - PER(i,j,t). \tag{4-2}$$

Figure 4.2 shows example encounters between four vehicle pairs. Lines show the time vs. distance path of the pair's encounter. Markers denote successful packet reception events and their absence indicates packet loss. Encounters A, B, and C represent vehicle passing scenarios, while encounter D shows a car-following example. While the encounters selected are illustrative and not necessarily representative of typical passing / following scenarios, they show that the length of encounter times can vary significantly. Furthermore, reception is more likely when vehicles are close, but the relation to distance is otherwise inconsistent for the selected encounters. However, in certain encounters, such as the car-following example D,

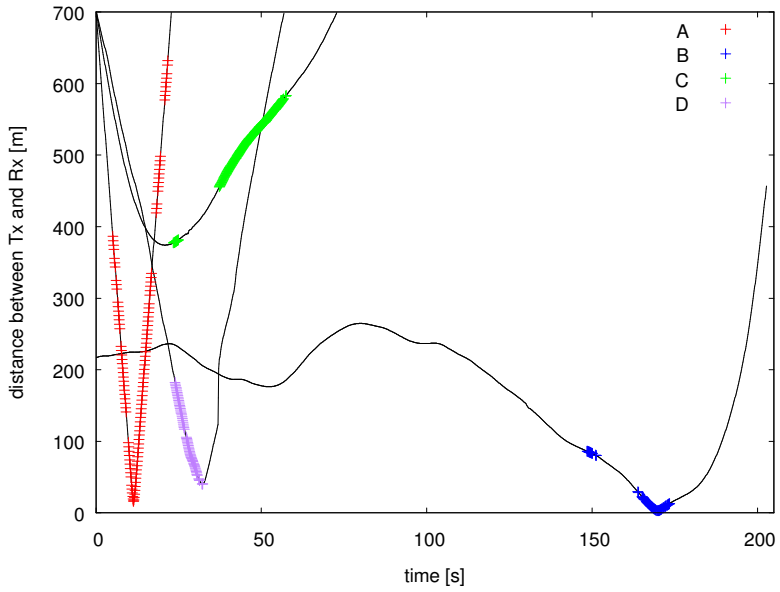

Figure 4.2 Packet reception for four example encounters from the SPMD DE. Encounter time can vary significantly. When vehicles are in close proximity to one another, packet reception is more likely, but the correlation to distance is otherwise inconsistent.

radio-interfering obstacles (i.e., hills, buildings, trucks, etc.) often block the path between vehicles, despite their close proximity.

4.3.2 Packet Reception Ratio

Figure 4.3 compares the total sent and successfully received packets out to 1.2km for the DAS1 encounters. The distribution of BSMs transmitted within range of receivers is nearly uniform, but slightly more frequent in the 400-600m range. Packets are more likely to be received at shorter distances, with half of the total successfully received packets occurring at inter-vehicle distances less than approximately 125m. The low reception rates at longer distances alludes to the effects of obstacles and scatterers in the operating environments.

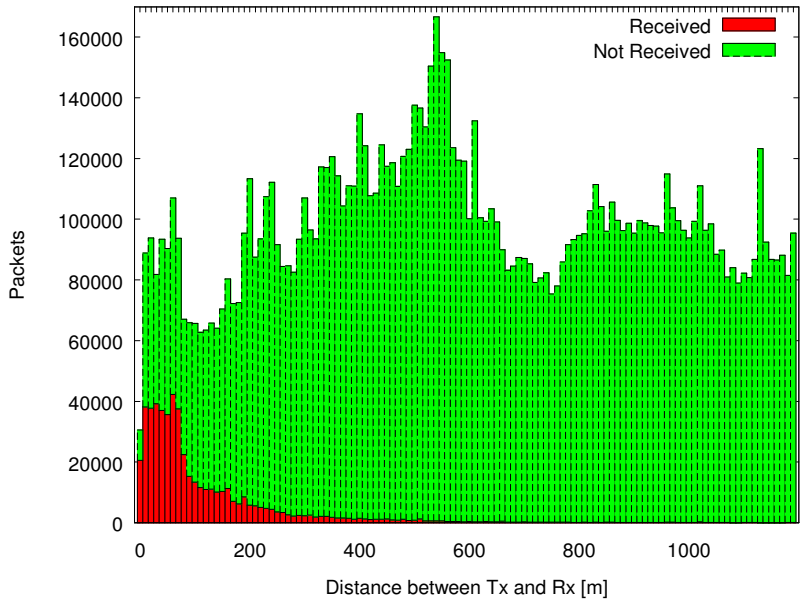

Figure 4.3 Packets received (red, below) relative to packets not received (green, above) as a function of the distance between sender and receiver for the SPMD DE. Reception success (i.e., PRR) decreases as distance increases. PRR is greater than 65% only at distances less than 10m and decreases rapidly with distance, with few packets successfully received beyond 400m.

4.3.3 Inter-Packet Gap (IPG)

Time between successfully received packets indicates periods of packet loss and occurs with varying IPG length, as seen by examining the intervals between markers in Figure 4.2. To properly understand the behavior of the vehicular channel, packet loss patterns and their potential temporal dependencies in consecutive losses must be explored.

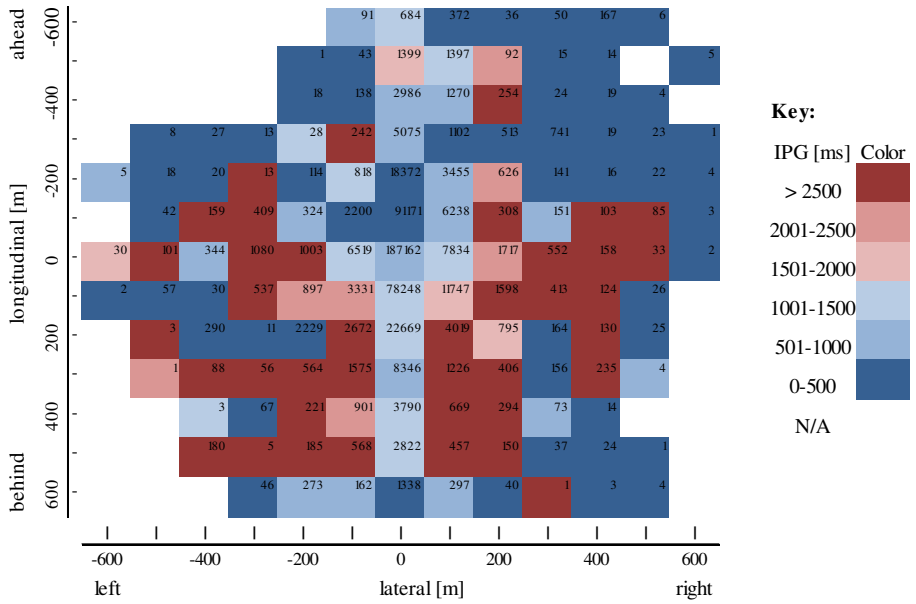

Figure 4.4 Average IPG as a function of relative transmitter distance from the receiver as centered at (x=0, y=0). IPG is generally low regardless of senders being directly ahead of or behind the receiver, but increases as distance increases, especially when lateral distances increase and the transmitter is behind the receiver. Numbers indicate the count of IPG values that are averaged for each cell.

The average IPG lengths are plotted in Figure 4.4 as a function of the relative position of the transmitting vehicle with respect to the receiving vehicle. By translating receiving vehicles to be centered at (x=0, y=0), IPG can be seen to be low when transmitters are near the vehicle, and is generally low regardless of senders being directly ahead of or behind the receiver, over the full range of reception. IPG is slightly asymmetrical for longitudinally positioned transmitters, being lower for senders that are ahead of the receiver, as compared to vehicles that are behind.

To characterize IPG lengths, Figure 4.5 plots (log-log scale) the normalized probability distribution of the frequency of consecutive lost packets (i.e., "gaps") out to one minute. At a transmission rate of 10Hz, the expected IPG is 100ms. From the SPMD DE encounters, the IPG was found to be below 300ms 95% of the time, consistent with other Ann Arbor studies

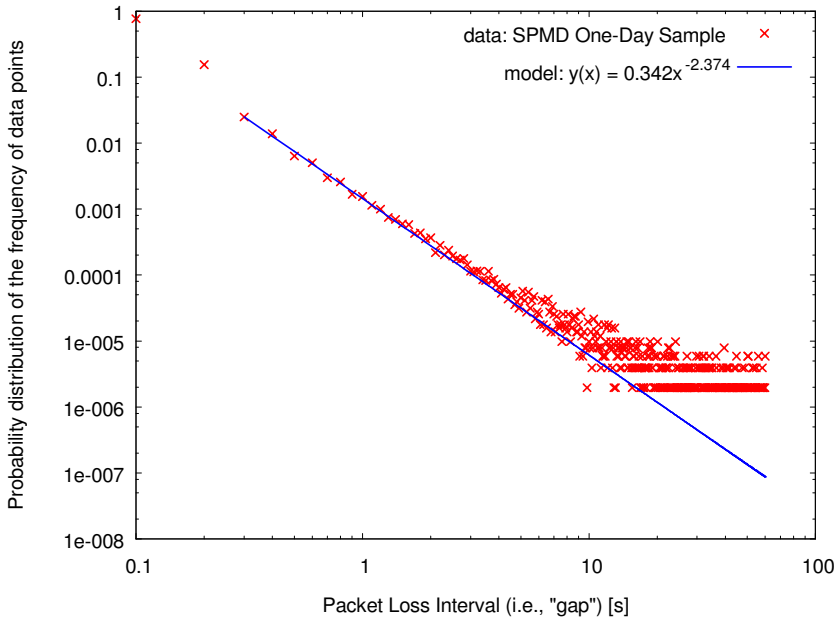

Figure 4.5 Log-log plot of the probability distribution of frequency of inter-packet gaps in seconds, out to one minute, within the SPMD DE. A majority (93%) of IPG lengths are less than 200ms (i.e., losses of 0 or 1 packet), while longer IPG lengths plausibly follows a power law distribution model, $p(x)=0.342x^{-2.374}$.

[91]. Although infrequent, gaps longer than 300ms represent increasingly longer periods of lost communications. Such losses are important to properly characterize and model, as they capture the periods during which safety messages were not successfully exchanged, thus potentially threatening safety application effectiveness.

Several long-gap packet losses indicate a long-tailed power law distribution. Following the approach in [98], a power law distribution (i.e., $p(x)=Cx^{-\alpha}$) was fit from the empirical data, with C=0.342 and α=2.374. This hypothesis was tested for goodness-of-fit using the Kolmogorow-Smirnov (KS) statistic (i.e., KS test) [98] from which the probability of match (i.e., p-value = 0.8 > 0.1) indicates that the power law model is a plausible fit for the distribution. Additional distribution models (e.g., exponential, lognormal, and Poisson) were also considered for data fit plausibility by applying to each distribution model the KS test which rejected the null hypothesis for each alternative model.

4.3.4 Time Correlation of IPG Length

Previous analysis of packet loss in DSRC communications [87] found that bursty effects are generally common, indicative of weak temporal correlations in vehicular networks, with environment significantly effecting temporal correlation, as fewer signal scatterers lead to reduced channel volatility. Contrastingly, analysis of packet loss in Roofnet [86], a constantly beaconing, static 38-node 802.11b multi-hop network in an urban setting, shows that packet loss behaves as if it were independent for short time intervals while for longer intervals, some of the links show bursty losses, and some do not.

Unlike Roofnet, where all nodes remain stationary with few (if any) changing influences of radio blocking obstacles between them, the dynamicism brought about by the high mobility of vehicles in the Ann Arbor environment leads to significant changes in obstacles (i.e., signs, buildings, other cars and trucks) blocking LOS conditions between them. Furthermore, in some cases, such LOS interruptions may be short-lived (e.g., when cars moving in opposite highway directions briefly have a truck between their LOS path). In other cases, obstacles can block V2V signals for longer terms (e.g., when slow moving vehicles and/or those stopped at an intersection have buildings or other large vehicles between them). Such spatial differences within the environment help explain the temporal gap length variations shown in Figure 4.5.

By analyzing the SPMD DE for packet reception / loss at the expected frequency of one message every 100ms, we can investigate packet loss to see if losses occur randomly or otherwise correlate to temporal and/or spatial dimensions.

The time variation of packet loss rate of beaconing nodes has been examined in both static-node networks (e.g., Roofnet [86]) and mobile-node conditions (e.g., DSRC communication environments [87]) to determine if there exists a time-dependent correlation to IPG length, using the Allan deviation (ADEV) [99] [100], which describes frequency stability and is sometimes used to evaluate the potential sensitivity to time fluctuations within other time series [101]. Allan deviation relies on the difference between successive samples instead of the difference between each measure and the long-term average, as computed by the standard deviation. Several different frequency stability measures exist that differ in their time lag and autocorrelation methods, resulting in measures that vary in convergence properties and abilities to handle drift and different types of noise (e.g., see [102] for a detailed explanation). For example, the original Allan deviation, as used by [86] in analyzing Roofnet, has been widely

superseded by the Overlapping Allan deviation, which provides higher confidence and better convergence [102].

The formula for the Overlapping Allan deviation of a sequence of samples y_i, where $|y| = M$, is [102]:

$$\sigma_y(\tau) = \sqrt{\frac{1}{2m^2(M-2m+1)} \sum_{j=1}^{M-2m+1} \left[\sum_{i=j}^{j+m-1} (y_{i+m} - y_i) \right]^2}, \quad (4\text{-}3)$$

where m is the *averaging factor*, or distance between the two terms in the series (i.e., m=1 uses immediately neighboring pairs, m=2 uses the 1st and 3rd terms in the series, 2nd and 4th, etc.). Allan deviations are commonly presented as log-log plots comparing $\sigma_y(\tau)$ to τ (i.e., sigma-tau plots [99] [100] [102]) where $\tau = m\tau_0$ for some value τ_0 that represents the sampling time of the series.

The SPMD DE data was split into four equally-sized quartiles based on the average gap length for encounters that lasted at least one second. The Modified Allan deviation, $\sigma_y(\tau)$, for $\tau_0 = 0.1s$, with 95% confidence intervals is shown in Figure 4.6 for each of the four quartiles (i.e., Q_1, .., Q_4). Additionally, a line with slope = -0.5 is shown, which corresponds to a series

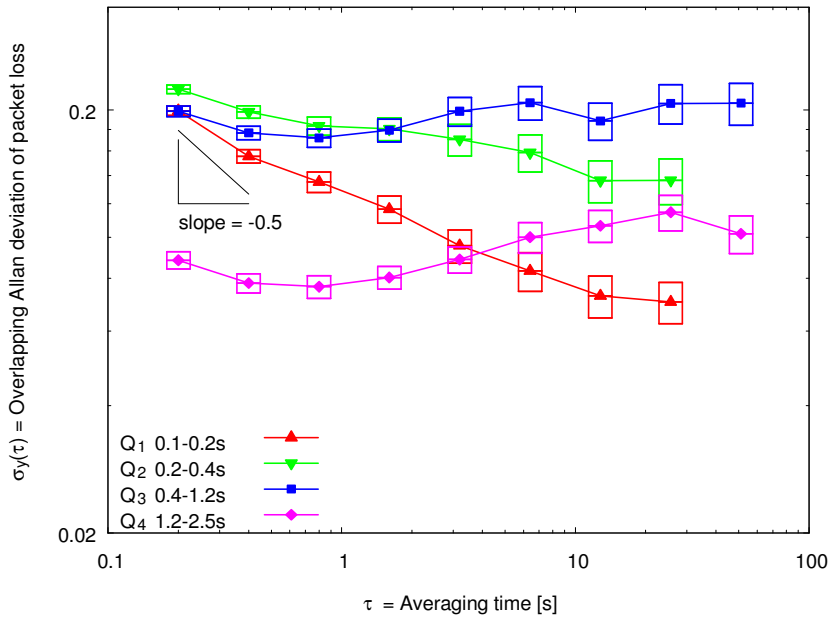

Figure 4.6 Overlapping Allan deviation, $\boldsymbol{\sigma_y(\tau)}$, of packet loss gaps throughout Ann Arbor, as a function of $\boldsymbol{\tau}$, the averaging factor in seconds. The SPMD DE dataset is split into four quartiles (i.e., $Q_1..Q_4$) by the average gap length for 1950 encounters.

with independent, identically Gaussian distributed (i.i.d.) fluctuations in frequency stability [99] [100] [101].

The results for the first quartile, Q_1, exhibit a behavior that generally follows the expected behavior for uncorrelated data (i.e., a linear decrease in the log-log plot of $\sigma_y(\tau)$ vs. τ with slope = -0.5). The trend is also present, but to a lesser extent for Q_2. However, as packet loss gap length increases, $\sigma_y(\tau)$ shows a significantly different behavior. The increasing trends (i.e., flattening slopes) exhibited by Q_3 and Q_4 suggest the presence of packet-loss correlations in the encounters and/or the presence of non-stationary features in the series [101]. Thus, the first two quartiles (i.e., 50%) with average packet loss gaps below 400ms are commonly independent loss events, while the remaining half exhibit correlated packet losses and/or non-stationarity. The correlation tendencies for longer packet gaps require further study to understand how the losses relate to spatial and/or temporal environmental conditions.

4.4 Conclusions

Over 2000 V2V encounters were isolated from the SPMD DE, in which safety messages were successfully exchanged during the largest on-road test to date of connected vehicle technology. DSRC IPG was less than 300 ms in 95% of encounters, consistent with other Ann Arbor studies [91], and found to follow a long-tailed power law probability distribution, $p(x) = 0.342x^{-2.374}$. As reported in [87], bursty effects are common, which differs from the static-node Roofnet study [86], in which bursty losses were rare and link loss rates remained generally temporally independent. In Ann Arbor, however, packet loss by quartiles shows a significantly different behavior, given the average packet loss gap length of an encounter. Roughly half of gap losses are short-length (i.e., less than 400ms) and commonly uncorrelated, while the remaining average gap losses that are greater than 400ms exhibit temporal correlation and/or non-stationarity tendencies that could benefit from further examination of their relation to environmental conditions.

Characterizing DSRC packet loss behaviors in large-scale field operations tests, in terms of loss probability functions and IPG length correlations, provides insights into vehicular channel volatility. The findings can be used to improve existing DSRC channel models, thus leading to improved tools for evaluating the performance of these systems.

CHAPTER

5

EVALUATING THE ACCURACY OF VEHICULAR CHANNEL MODELS IN A LARGE-SCALE DSRC TEST

Vehicle-to-vehicle channel characteristics differ significantly from those of conventional cellular channels, principally in terms of fading statistics due to varying environmental conditions, link types, vehicle types, and objects that result in complex propagation effects. Accurate modeling of the vehicular channel remains a complex challenge. In this chapter, existing, common VCMs are evaluated and compared to measurement data from the UMTRI large-scale DSRC testbed involving nearly 3000 vehicles and conducted over several months around Ann Arbor, MI. While many VCMs can predict reasonably well the frequent packet error rates observed near Ann Arbor, they over-estimate IPG and under-estimate the likelihood of runs of consecutively and successfully received packets. The testbed environment shows significant fading (i.e., sub-Rayleigh) and/or shadowing effects that challenge the accuracy of traditional VCMs. Furthermore, despite 60% of the inter-vehicle paths being obstructed by items available using OSM geodata, a deterministic obstacle shadowing model that makes use of such geodata does not account for all shadowing effects. Evaluating VCMs in terms of realistic, large-scale experiments helps researchers

better understand actual behaviors and allows for the development of new and/or improved models that more accurately reflect reality.

5.1 Introduction

This chapter analyzes commonly referenced wireless VCMs and compares them to truthful FOT measurement data of a large-scale wireless V2V testbed, commonly called the Safety Pilot Model Deployment (SPMD) [28], [88]. The approximately 3000 SPMD nodes consist of cars, trucks, and buses equipped with DSRC devices that move in and around Ann Arbor, MI using roof-mounted antennas that transmit at regular, 100ms intervals and/or receive vehicular BSMs wirelessly between them [93] (see [14], [28], [88] for details on the SPMD environment).

The successful safety performance in the DSRC network requires PRR with high probabilities, longer consecutive reception run-length (CRRL), and short IPG. For example, in the presence of an imminent crash scenario, the need for highly successful and rapid data exchanges over short periods of times is imperative, with analysis of long-term packet reception behaviors being insufficient when evaluated in such short time-windows.

An analysis of the packet-level receptions of the dataset [14] indicates packet errors occur frequently in this environment, with transmission packet losses commonly resulting from separation distance, obstacles, and multi-path fading effects [87], while collisions of transmissions are rare due to the scarcity of encounters between vehicles. Furthermore, unlike static-node networks, the consecutive packet losses, or IPG, for many V2V encounters in the SPMD exhibit temporal correlations and/or non-stationarity tendencies [14]. Evaluating VCMs in terms of representative, large-scale experiments helps researchers better understand actual behaviors and allows improved models to more accurately reflect reality.

Furthermore, for the many researchers that propose protocols and applications relying on DSRC, we provide realistic parameters for several VCMs suitable for realistic error rates, while cautioning about their drawbacks related to IPGs.

5.2 Background

Connected vehicle networks promise communications capabilities intended to improve vehicular safety while simultaneously supporting driver infotainment applications. Yet V2V

channel characteristics differ significantly from those of conventional cellular channels, particularly in terms of fading statistics and their associated time and frequency selectivity [33], differing environmental conditions, link types, vehicle types, and objects that result in complex propagation effects. With potential for wireless signal reflection and scattering brought about by varying vehicle sizes and shapes, material differences in road surfaces, building construction materials, foliage densities, and antenna-to-antenna slope differences from terrain and road design [33], accurate modeling of the vehicular channel remains a very complex challenge [29]. Indeed, two different trips from home to store, school, or work will not yield exactly the same channel behaviors due often to the subtle changes in environment between trips.

Figure 5.1 plots results from SPMD data for an encounter between two vehicles (one transmitter and one receiver). Orange lines represent inter-vehicle LOS paths for successfully received packets and are interspersed with periods of packet loss events (yellow) of varying lengths. Reception is inconsistent and packet losses do not necessarily correspond to visible environmental elements, such as buildings.

Analysis of safety packet reception within the SPMD shows low reception rates with significant variations among different V2V encounters. Roughly half of the encounters exhibit short-length average IPG in which consecutive packet losses are uncorrelated, while the remainder show temporal correlation and/or non-stationarity tendencies [14]. While results show that typical VCMs can accurately predict long-term average packet reception rates, they do not predict well the per-packet behaviors and bursty patterns that are found in the SPMD test data.

Figure 5.1 The receiving vehicle, RX (green trajectory), moves from the top right to the left, while the transmitting vehicle, TX (blue trajectory), moves from the top middle to the bottom middle and enters a parking deck. Multiple packet loss periods (yellow) can be observed in this encounter. Here, the packet losses do not seem to correspond to building or parking deck obstacles between vehicles. It is possible that the losses are caused by trees, elevation changes, and/or trucks or other vehicles coming between sender and receiver, but there is insufficient data from which to definitively and deterministically derive path loss in this encounter.

5.2.1 Objective

While many measurement studies enact highly-controlled scenarios that focus on limited environmental conditions, such as a relatively short stretch of highway or a specific intersection or campus area, it is crucial to assess model applicability in terms of large-scale operational field tests. To do so, we model packet reception/loss as a function of differing fading/shadowing components that we then evaluate to find parameters that best-fit the Ann Arbor SPMD test environment. We then statistically analyze the accuracy of several common, existing VCMs against the actual FOT measurement data (i.e., the SPMD dataset provides only packet reception/loss indicators, and does not provide actual RSSI data).

5.2.1 Geometry-Based (GB) Models

To reduce the randomness of stochastic models as in ((2-10), ((2-13), and ((2-26), geometry-based deterministic (GBD) models [29] estimate additional path loss using geodata

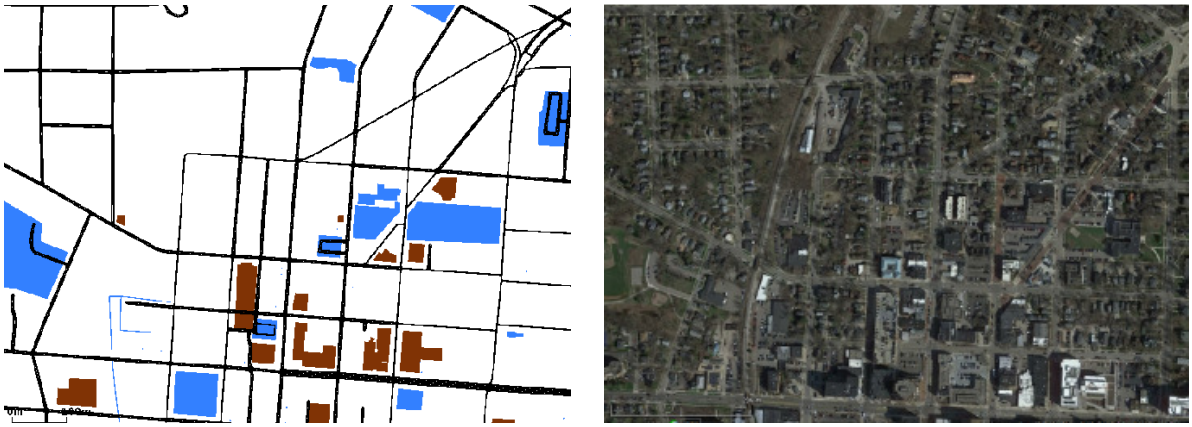

Figure 5.2 Geodata from Open Street Map (OSM) (a) for a section of the Ann Arbor area, and the equivalent view from Google Earth (b). Maroon areas represent geodata from OSM for various types of buildings, and blue areas represent parking decks, lots, and parks, all of which OSM treats homogenously as 2D outlines. Geodata is missing for many structures present in Ann Arbor and does not account for all obstacles that may occur between vehicles traveling the streets.

that describes environmental conditions such as the locations of potentially radio wave inhibiting buildings.

The existence of geodata sources is a vital requirement of GBD models. In fact, the authors of [29] claim that, if geodata is not readily available, suitable VCMs do not exist for studies involving safety-critical applications and/or location-dependent statistics.

Geodata from OSM for a small region in the Ann Arbor area is plotted using SUMO in Figure 5.2 and compared to satellite imagery from Google Earth. Although some building information is available, it is incomplete and has insufficient information to account for all radio-blocking obstacles that could occur as vehicles travel the streets.

An example GBD model [31] deterministically models path loss by combining

i) the free space model ((2-9) with

ii) ii) a shadowing path loss model based on the number of walls intersected and interior distances through buildings.

To instead retain a stochastic contribution to path loss, we model obstacle shadowing path loss, $PL_{OBS}(d)$, by combining the shadowing path loss model in [31] with lognormal fading ((2-10), as:

$$PL_{OBS}(d) = PL(d_0) + 10\gamma log_{10}\left(\frac{d - d_{obs}}{d_0}\right) + X_\sigma + \alpha n + \beta d_{obs}, \tag{5-1}$$

where α is the attenuation per wall, in dB, n is the number of walls penetrated, β is the attenuation per meter, in dB, and d_{obs} is the distance, in meters, traveled through obstacles.

5.3 Model Evaluation

Five different VCMs (see Table 5.1) are analytically compared to the measurement data from the large-scale SPMD data set [14], including the GG shadowed fading model (25) that more generically represents several other models, such as Nakagami-m (20), Weibull, Rayleigh, and Rician. The maximum likelihood estimate (MLE) for each of the VCM parameters are found by minimizing the root-mean-square-error (RMSE), $rmse$, between the PRR of the model, $PRR_m(d)$ and test data, $PRR_t(d)$, where $rmse$ is:

$$rmse = \sqrt{\sum_d \left(PRR_m(d) - PRR_t(d)\right)^2}. \tag{5-2}$$

To compare models, the results are evaluated for spatial relationships as a function of distance between vehicles using PRR. Additionally, temporal relations are evaluated for consecutive packet loss *gaps* (i.e., IPGs) and consecutive packet reception *runs* (i.e., *consecutive reception run-length*, CRRL).

To evaluate the accuracy of each model, the SPMD data set is first partitioned into $k = 5$ samples for validation using the *k*-Fold Cross Validation (KFCV) technique (also: *V*-Fold Cross Validation, VFCV) [103], in which *k* experiments each produce model estimators by using $k - 1$ subsamples as training data. The statistical biases, which quantify the amount of

Table 5.1 Five vehicular channel models for which estimated PRR is compared to the actual large-scale SPMD measurement data.

	Model	**Equations**
A	Unit disk	(6)
B	Lognormal	(11)
C	Dual-slope lognormal	(13), (14)
D	Generalized gamma shadowed fading	(25)
E	Lognormal fading with obstacle shadowing	(26)

subsample deviations from that of the full data set, are determined (see Table 5.2) and indicate how sensitive the model estimates are to the diversity of V2V encounters within the test data. For each of the k training data sets, the best-fit parameters are applied to the corresponding validation data sets and the results of the RSME for each metric evaluated (i.e., PRR, IPG, CRRL) are averaged and compared to the SPMD test data set (see Table 5.3).

5.4 Results

5.4.1 Maximum Likelihood Estimates

The MLE model parameters are summarily shown in Table 5.2. The unit disk model performs with a highly unrealistic average limiting distance of 10.59 m. Path loss exponents of $\gamma = 4.13$ for *B*, $\gamma_1 = 4.30$ for *C* at shorter distances, and $\gamma = 4.53$ for *E* indicate strong fading effects that increase to $\gamma_2 = 7.10$ in *C* beyond the breakpoint distance of 100m. These large path loss exponents that exceed the expected $\gamma = 2$ of the FSPL and the large standard deviations of signal variations (i.e., $29.14 \leq \sigma \leq 64.50$) reflect the strongly varying and inconsistent influence upon signal receipt capabilities brought about by the environmental variety throughout Ann Arbor. The GG shadowed fading model *D* indicates severe sub-

Table 5.2 Parametric values for the VCMs. The MLE of each parameter is shown with statistical bias in parentheses and appropriate units in brackets.

	Model	MLE (bias)
A	Unit disk	d_{lim} = 10.60 (11.33) [m]
B	Lognormal	γ = 4.17 (0.03) σ = 29.14 (-0.62) [dB]
C	Dual-slope lognormal	γ_1 = 4.30 (0.57) σ_1 = 63.70 (8.33) [dB] γ_2 = 7.10 (-0.04) σ_2 = 34.90 (2.98) dB
D	Generalized gamma shadowed fading	m = 0.44 (0.07) s = 0.90 (-0.03)
E	Lognormal fading with obstacle shadowing	γ = 4.53 (-0.10) σ = 64.50 (-5.13) [dB] α = 39.00 (-6.64) [dB / wall] β = 1.20 (0.21) [dB / m]

Rayleigh fading (i.e., $m \leq 1/2$) combined with a shadowing effect (i.e., $s < 1$) that implies the channel is not an empirical fit with the Nakagami-m model. The deterministic obstacle shadowing parameters (i.e., α and β in model E) do not account for all fading effects, as the lognormal model fading parameter, σ, remains large. The statistical bias of all parameters for all models is relatively large (i.e., non-zero), implying strong environmental variety among different V2V encounters within the SPMD test data.

5.4.2 Packet Reception Ratio (PRR)

Packet reception in the Ann Arbor environment drops quickly as vehicular separation increases [14], thus challenging VCM accuracy, with PRR varying greatly among models and differing from the SPMD measurement data, as Figure 5.3 shows. In fact, PRR throughout Ann Arbor fluctuates in the 10-100m range, further indicating the strong impact that environmental variety throughout Ann Arbor has on PRR. For example, the unit disk model *A* is the worst predictor of actual PRR behavior in Ann Arbor, implying that the environment is far from a purely deterministic one based on inter-vehicle distance alone. Lognormally-behaving models *B* and *C* compare favorably, with the dual-slope model *C* better matching the PRR of the test data set. The GG shadowed fading model *D* tends to over-estimate PRR at shorter distances and under-estimate it at longer distances. By deterministically accounting for obstacle shadowing, the lognormal fading model *E* fits well the PRR of the test data.

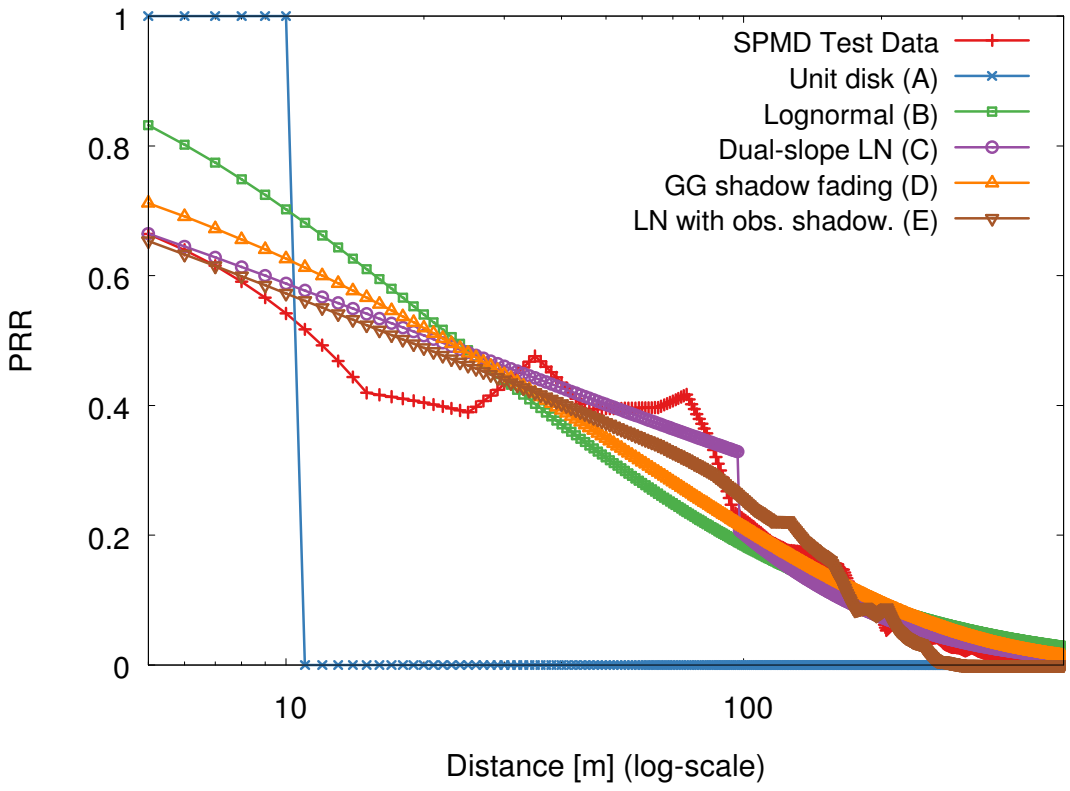

Figure 5.3 PRR for log-scale distance from 5-500m for five VCMs. PRR predictions vary greatly among the models. Stochastic lognormal-based models *B* and *C* favorably predict PRR as does model *E* that deterministically accounts for obstacle shadowing.

5.4.3 Inter-Packet Gap (IPG)

After receiving a packet, the amount of time until the next packet is successfully received defines the IPG. Since BSMs are regularly emitted at the rate of 10 Hz, a safety packet is expected every 100ms from every other vehicle within communications range. When the average PRR is prr, then the probability of a gap of n consecutively missed packets, $p_{gap}(n)$, of length $t[s] = n/10$, in an uncorrelated channel is:

$$p_{gap}(n) = (1 - prr)^n. \tag{5-3}$$

The distribution of IPG in the Ann Arbor environment follows a power-law distribution and exhibits correlation tendencies for many V2V encounters [14]. The log-log scale plots of the pdfs of IPG out to 60s are compared in Figure 5.4. The unit disk model *A* poorly predicts IPG of any lengths, as the model's short limiting distance predicts lost packets at most

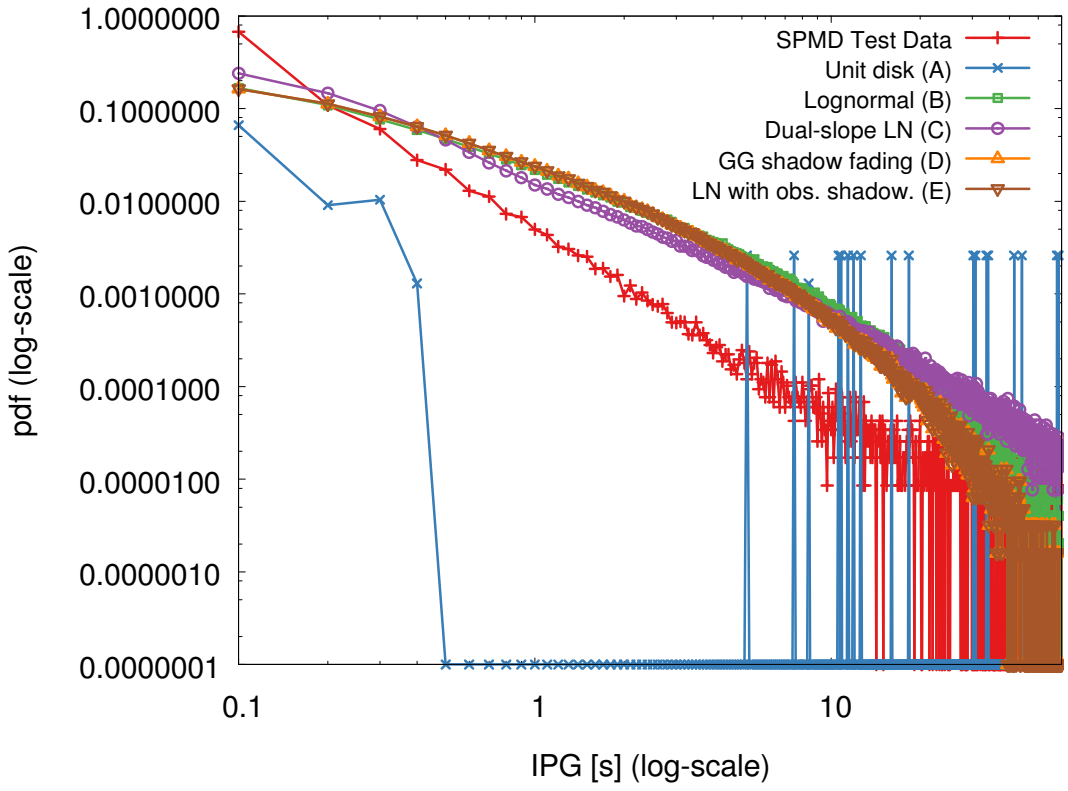

Figure 5.4 Log-log scale of the pdf of inter packet gap (IPG) as a function of gap length out to 60s. The results for the i.i.d.-assuming model differ greatly from the power-law fitting test data, indicating that such models do not predict well the packet gap distributions found in the field test data of the SPMD.

distances. All the other models that better predict PRR do not accurately estimate IPG, overshooting the likelihood of packet gaps between 0.2s and 20s.

5.4.4 Consecutive Reception Run-Length (CRRL)

While IPG reflects the likelihood of a run of consecutively lost packets, the effects of consecutively and successfully received packets may also be examined. We define the *consecutive reception run-length* (CRRL) to be the number of successive packets received following the end of a packet loss gap. In an uncorrelated channel, the probability of a run of n consecutively received packets, $p_{run}(n)$ is:

$$p_{run}(n) = prr^n. \tag{5-4}$$

The log-log scale plots of the pdfs of CCRL out to 60s are compared in Figure 5.5. As with IPG, the unit disk model *A* performs poorly. All other models under-estimate the

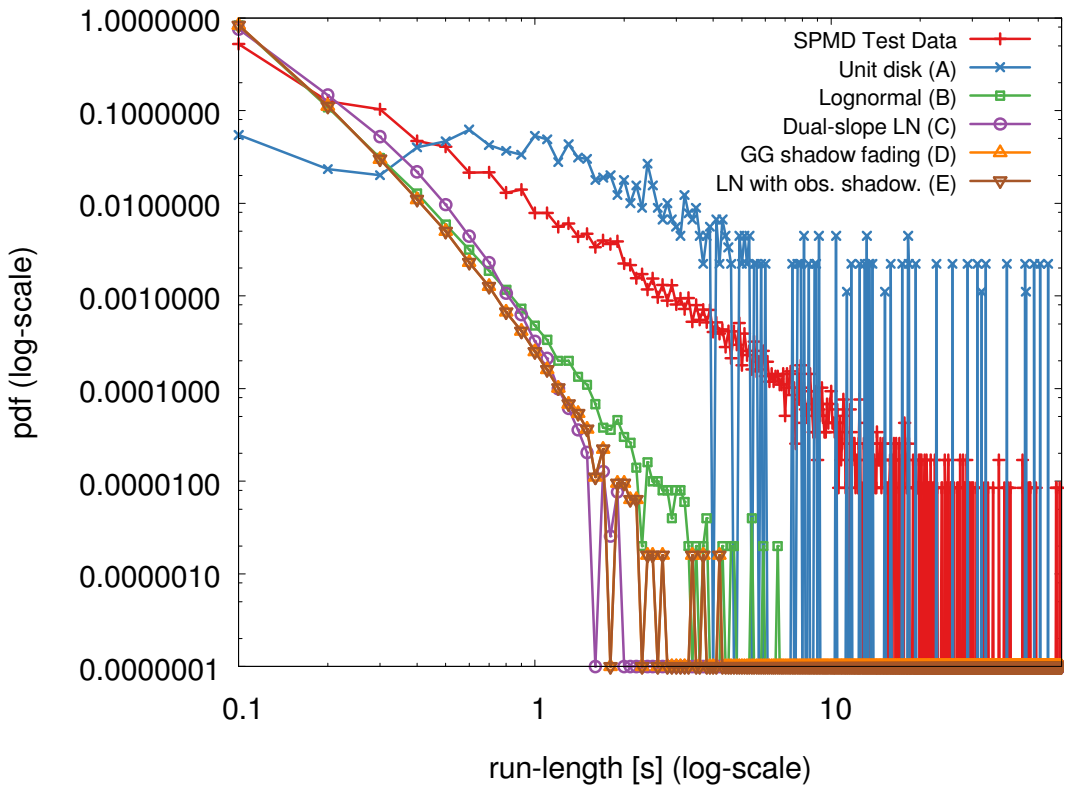

Figure 5.5 Log-log scale of the pdf of consecutive reception run-length (CRRL) as a function of time out to 60s.

likelihood of consecutively received packet runs greater than 0.2s, as compared to the SPMD test data.

5.4.5 Obstacle Shadowing Effects

Model *E* combines a stochastically evaluated path loss based on a lognormal model with deterministic shadowing using a geodata-based obstacle shadowing model. For the SPMD data set, approximately 60% of the inter-vehicle paths are obstructed by one or more items that can be identified by OSM geodata, suggesting potential shadowing effects of NLOS conditions (e.g., obstacles). Figure 5.6 shows the average number of obstacle borders (i.e., walls) penetrated (left axis) and the average total distances traveled through the interior of the obstacles (right axis) as a function of distances between two vehicles. As expected, the number of obstacle intersections is very low (i.e., 0) at very short inter-vehicle distances, as there are few obstacles, if any, between vehicles when they are close to each other with direct LOS

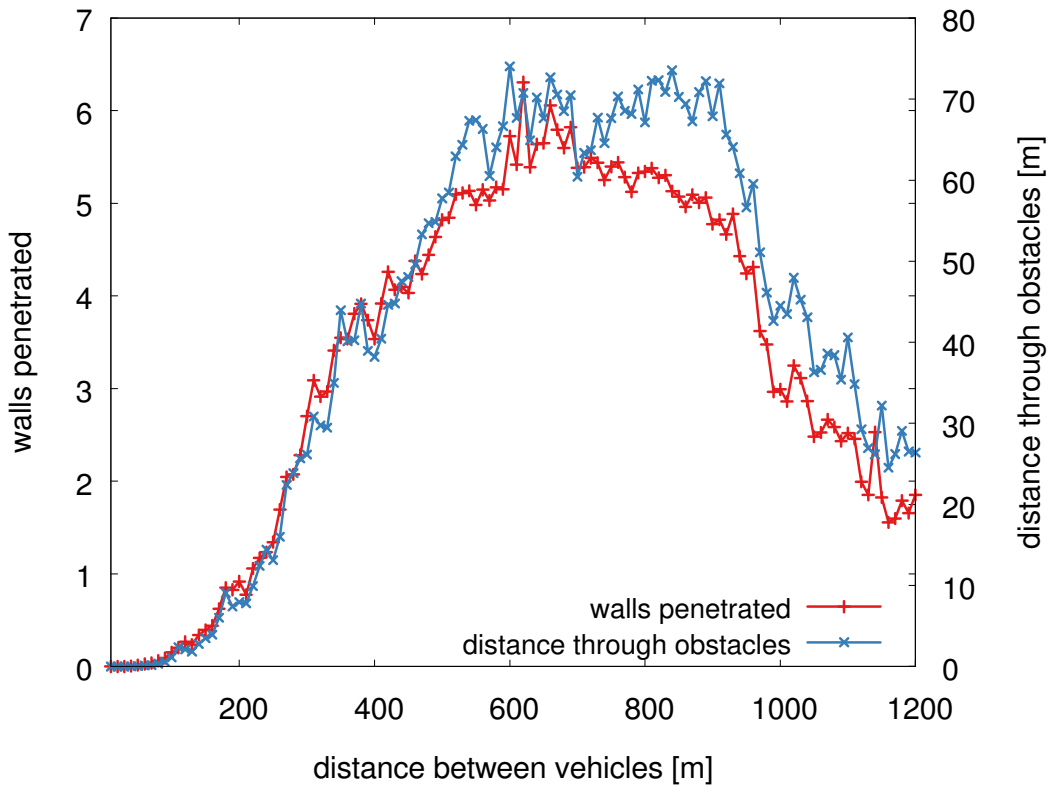

Figure 5.6 The average number of obstacle walls penetrated (left axis) and the average total distances traveled within them (right axis) as a function of total distance between vehicles, based on the SPMD test data set and geodata available from OSM. As expected, there are few obstacles between vehicles when they are close together, while the average obstacle interior distances traveled is approximately 10% of the total distance between vehicles, up to about 800m.

conditions. As the distance between vehicles increases, the trends of the number of obstacles and interior distances traveled within them increases with very similar trend (e.g., 100-600m) and then plateaus at approximately 5-6 obstacle intersection and 60-70m of interior distances (e.g., 600-950m) before beginning to decrease. The average obstacle interior distances traveled is approximately 10% of the total distance between vehicles, up to about 800m.

5.4.6 Numerical Results

Numerical results for the RSME and statistical bias of three metrics (PRR, IPG, and CRRL) for five VCMs as compared to the SPMD test data set are shown in Table 5.3. RSME values closer to zero indicate models that more closely match the actual behaviors exhibited throughout Ann Arbor. As expected, the unit disk model performs poorly in predicting PRR.

Table 5.3 Numerical results for the RSME of three metrics (PRR, IPG, and CRRL) for five VCMs as compared to the Ann Arbor SPMD test data set. As expected, the unit disk model performs poorly in predicting PRR. While all other models better predict PRR, they fail to accurately predict consecutive packet losses (i.e., IPG) and reception (i.e., CRRL). Use of geodata to deterministically estimate path loss through obstacles (i.e., Model *E*) improves CRRL, as compared to a purely stochastic model (i.e., Model *B*) that does not make use of such geodata.

Model		**Metric [RSME (bias)]**		
		PRR	**IPG**	**CRRL**
A	Unit disk	1.31 (0.31)	--	--
B	Lognormal	0.41 (0.28)	0.52 (-0.05)	0.32 (0.01)
C	Dual-slope lognormal	0.19 (0.42)	0.44 (-0.05)	0.25 (0.01)
D	Generalized gamma shadowed fading	0.28 (0.36)	0.47 (-0.04)	0.28 (0.02)
E	Lognormal fading with obstacle shadowing	0.22 (0.43)	0.40 (-0.04)	0.20 (0.02)

While all other models better predict PRR, they fail to accurately predict consecutive packet losses (i.e., IPG) and reception (i.e., CRRL). Use of geodata to deterministically estimate path loss through obstacles (i.e., Model *E*) improves CRRL, as compared to a purely stochastic model (i.e., Model *B*) that does not make use of such geodata. By evaluating the data set using several KFCV training and validation sets, the resulting non-zero statistical biases exhibited by all models indicate the large variations in V2V encounter behaviors throughout the Ann Arbor area.

5.5 Conclusions

Five VCMs were evaluated and compared to the large-scale FOT results from the SPMD test data set. A summary of results is shown in Table 5.4. The unit disk model *A* performs poorly and is highly unrealistic. While the other VCMs can predict well the average of the frequent PER observed in the FOT data, they over-estimate IPG lengths greater than 0.2s and under-estimate the likelihood of runs of three or more consecutively and successfully received

Table 5.4 Summary of five stochastic and/or deterministic VCMs evaluated against the Ann Arbor SPMD data set.

Model		Summary
A	Unit disk	Unrealistic and poorly estimates PRR.
B	Lognormal	Indicates strong fading, poorly matches PRR, and does not account for packet gap and reception behaviors that are exhibited by the test data.
C	Dual-slope lognormal	Indicates strong fading, better matches PRR, but does not account for packet gap and reception behaviors that are exhibited by the test data.
D	Generalized gamma shadowed fading	Indicates sub-Rayleigh fading with shadowing effects, better matches PRR, but does not account for packet gap and reception behaviors that are exhibited by the test data
E	Lognormal fading with obstacle shadowing	Better matches PRR, but does not account for behaviors exhibited by the test data. Use of geodata for obstacles improves some relationship tendencies in packet gaps and reception runs, but does not account for all fading effects.

packets. Such models that rely upon i.i.d. assumptions thus behave as WSSUS models that do not match the temporally-correlated effects of the Ann Arbor environment. Further work is needed to identify additional VCMs, especially ones that do not rely on i.i.d assumptions, that better reflect real world observations.

Models that deterministically evaluate path loss using geodata are highly reliant upon the existence of such geodata. Despite 60% of the V2V paths being obstructed by items available using OSM geodata, gaps in the geodata exist and many buildings in the Ann Arbor area are not represented in the OSM geodata. Additionally, while slightly improving the temporal relationship tendencies in an otherwise lognormal channel, the GBD obstacle shadowing model that uses available OSM geodata does not account for all shadowing effects.

The Ann Arbor environment shows significant fading (i.e., sub-Rayleigh) and/or shadowing effects that challenge the accuracy of traditional VCMs. Evaluating VCMs in terms of lifelike, large-scale experiments helps researchers better understand actual behaviors and allows for the development of new and/or improved models that more accurately reflect reality.

CHAPTER

6

BUR-GEN: Packet Generator for Bursty Vehicular Channel Models

DSRC-enabled VANET safety applications require high packet reception rates for reliability. Yet, the reception probabilities of basic safety messages are subject to losses due to path loss from separation distances between transmitting vehicles and receiving vehicles, multi-path fading, and obstacles that obstruct signals. Additionally, observations from DSRC field operational tests show that the vehicular channel is bursty, with occasional long periods of packet losses that thwart the ability of safety applications to assist drivers in improving their situational awareness.

While many research studies evaluate vehicular channel models in terms of PRR performance, the packet burstiness distributions that result from these models differs from real-world measurement campaigns. Modeling accuracy of consecutively received or dropped packets has safety implications in DSRC networks.

In this chapter, we describe a bursty packet generation algorithm called BUR-GEN that we evaluate through simulation and, along with several common VCMs, compare to the PRR, IPG, and CRRL of the DSRC measurement campaign, commonly referred to as the SPMD.

The model that incorporates the BUR-GEN packet generation process model outperforms all other i.i.d.-only packet generation models when the RSME of PRR, IPG, and CRRL are compared to the SPMD measurement campaign data set. The RSME of IPG and CRRL are improved by factors of six and four, respectively, by the inclusion of the BUR-GEN algorithm with a dual-slope distance-breakpoint path loss model.

Bursty packet losses are present in SPMD test data with burst distributions that result from packet generation processes that are not i.i.d.-based. Since VCM selection in simulation-based studies influences performance accuracy conclusions, it is important to select packet generation models that accuracy reflect the packet loss behaviors of real-world deployments in terms of average packet loss and burstiness distributions.

6.1 Introduction

The exchange of safety messages in a DSRC-enabled VANET requires consistently high packet reception rates for safety application reliability [104], yet such messages are subject to reception errors of various types. A packet can be lost due to separation distances between vehicles, multi-path fading effects, and obstacles (e.g., such as other vehicles, buildings, foliage, etc.) [14]. Unlike traditional static node wireless networks, bursty packet losses are common in VANET scenarios [104] [87] [14]. Furthermore, the burst patterns of consecutive packet losses and packet receptions, which can be described in terms of inter-packet gap (IPG) and consecutive reception run length (CRRL), respectively, greatly affects safety and situational awareness. A long-burst of lost packets (e.g., due to obstructions) reduces the likelihood of sufficient messages being successfully received to maintain a sense of safety, thus threatening the ability of VANET safety applications to adequately assist drivers in improving their situational awareness.

6.2 Motivation

VANET safety packet reception and loss probabilities are a function of the packet loss models that depend upon the path loss predications of the underlying wireless channel propagation models [105]. Model selection in simulation-based studies influences performance accuracy conclusions about VANET application reliability [106]. Many common models assume the generation of each packet as a probability event entirely independent of all

other packet generation events. Such models typically use probability distributions based on independent and identically distributed (i.i.d.) assumptions.

The ordering of packet receptions and losses, and hence the burst patterns of such packet streams, relies upon the underlying model's packet generation probabilities. Commonly referenced wireless packet loss models rarely assess their direct impact on safety measures [105]. Modeling accuracy of packet receptions has safety implications in DSRC networks, as safety may be dependent upon the number of consecutively received packets. For example, in an imminent crash situation, it may be imperative for a vehicle to successfully receive from another vehicle one or more packets in a very short period of time. Furthermore, while different VCMs may produce very similar long-term PRR performance, the burstiness of the packets they produce may differ from one another, and from real-world measurement campaigns.

Reliance on simplistic channel models leads to conclusions that fail to match real-world observations in packet reception probabilities [106] and burst patterns [105]. Despite recently proposed V2V shadow fading models derived from measurement campaign data (e.g., [107]), such models retain i.i.d. assumptions and have been developed using very limited equipment (e.g., two Volvo V70 station wagons) [106]. Simulation results of these models fail to evaluate the packet burst generation patterns of the models [106].

6.3 Problem Statement

While VCMs developed from measurement campaign data intend to improve model realism, simulation results [106] of recently proposed VCM models [107] fail to evaluate the packet burst generation patterns. In [105], we evaluated several common VCMs that rely upon i.i.d. assumptions and showed that these generally predict well packet loss patterns, yet fail to account for packet burst patterns, when evaluated against a real-world measurement campaign conducted throughout the Ann Arbor, MI USA area, of nearly 3000 vehicles over 18 months, commonly referred to as the Safety Pilot Model Deployment (SPMD).

Evaluation of VCM accuracy motivates the following research question:

RQ1: *Can improved vehicular channel models more accuracy match the results of large-scale DSRC measurement campaigns in terms of packet reception probabilities and bursty packet reception and loss behaviors?*

Model accuracy influences conclusions that can be drawn about them. In view of this, in this chapter, we propose a vehicular channel model derived from the SPMD measurement data that we evaluate using simulations and compare to the actual measurement campaign data. We compare our model to five other common models against the SPMD test data set in terms of PRR, IPG, and CRRL. Our results show our model maintains packet reception probabilities in line with the best of the models evaluated, while improving the modeling accuracy of packet gap and consecutive run burst patterns by factors of six and four, respectively.

6.4 Packet Loss / Reception Behaviors in the SPMD

6.4.1 Background

In [14], we analyzed the packet loss behaviors of the SPMD data set and found that:

i) packet reception probabilities were lower than expectations,

ii) IPG distributions were not uniformly distributed as a function of distances between transmitter and receiver, and

iii) packet losses occurred in bursty gaps that followed a power-law distribution.

In this section, we extend the data analysis of our previous work by including additional results that elaborate upon the packet loss and reception behaviors in the SPMD test data set, to provide background to further motivate the development of our campaign data-based packet generation model.

6.4.2 Field Operations

The SPMD was conducted from October, 2012 to April, 2013, involving over 2,700 vehicles, equipped with V2V wireless technologies, traversing Ann Arbor, MI. Selected data including BSM receptions from two months of operational data was provided to researchers by the USDOT [94].

Figure 6.1 depicts a general model (adapted from [108]) for two vehicles, A and B, moving with velocities v_A and v_B, respectively. Relative velocities between approaching vehicles affects safety and is an important component in TTC (i.e., see (7-2)). If the angle between

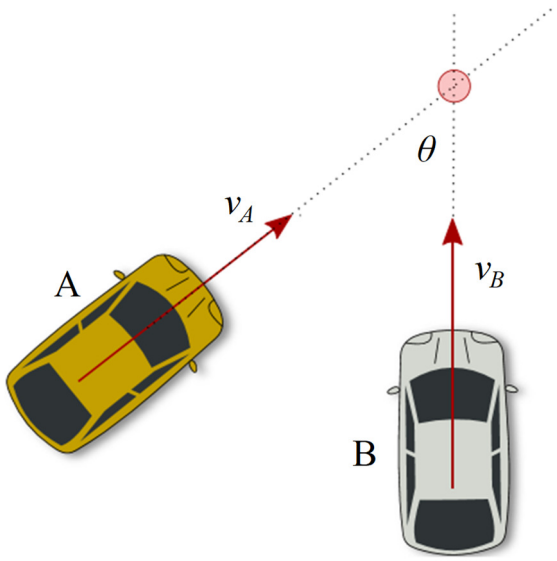

Figure 6.1 Relative velocity between two vehicles is a function of the individual vector velocities of the vehicles and the angle between them.

their vectors is θ, then the relative velocity of vehicle A with respect to vehicle B, v_{AB}, is given by $v_{AB} = v_A - v_B$, and the magnitude of the relative velocity is found by using the parallelogram law of vectors and the law of cosines, as:

$$|v_{AB}| = \sqrt{(v_A)^2 + (v_B)^2 - 2v_A v_B cos\theta}. \quad (6\text{-}1)$$

Figure 6.2 shows the pdf of the distribution of relative velocities of the nearly 2000 encounters that occurred during the SPMD. During V2V encounters, vehicles travel less than

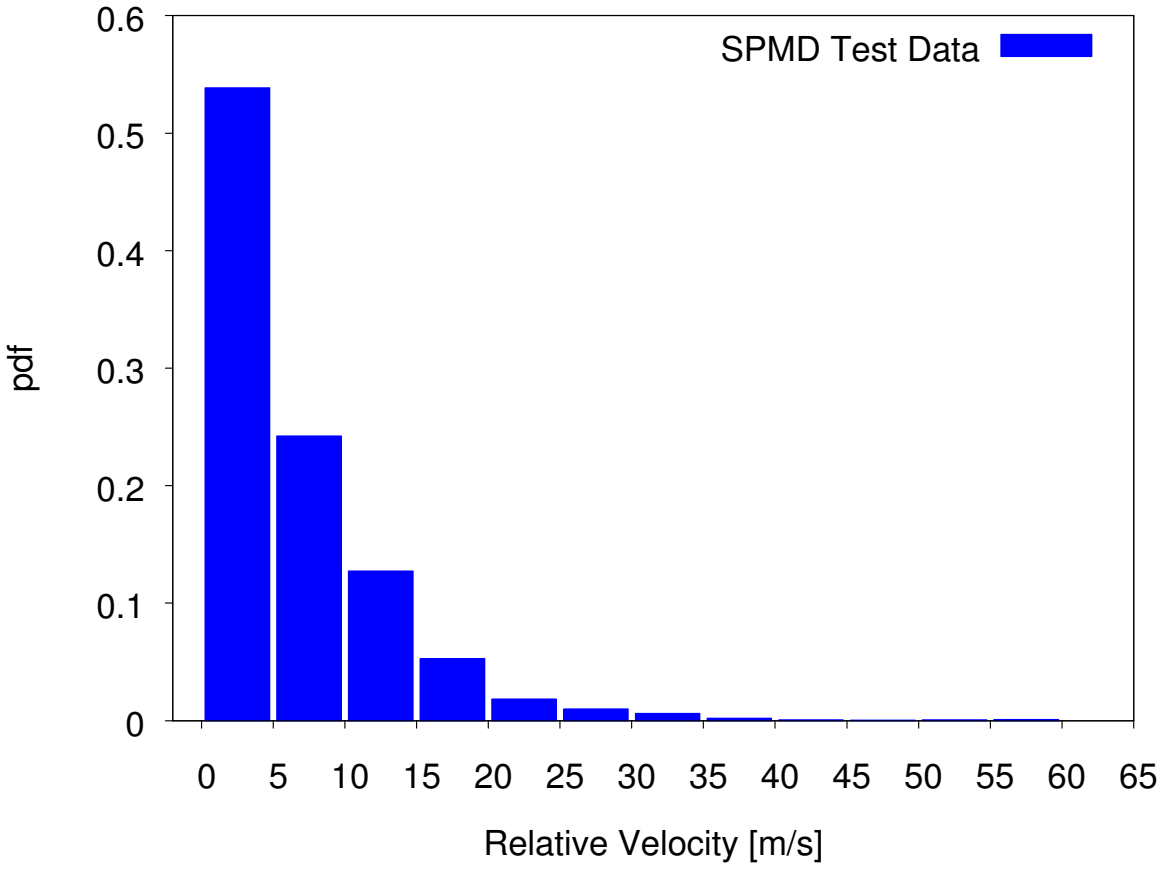

Figure 6.2 The pdf of relative velocity of vehicles during V2V communications encounters throughout the Ann Arbor-based Safety Pilot Model Deployment. Over half of the time vehicles move relative to one another less than 5 m/s, indicating that vehicles during encounters are stopped or following one another at similar speeds. The encounter data shows that there are few times when relative velocity is greater than 20 m/s, and there were no incidences of relative velocity of more than 60 m/s.

5 m/s (i.e., 18 kph or 11 mph), relative to one another over 53% of the time, indicating frequent periods during encounters of slow-following or stopped vehicles.

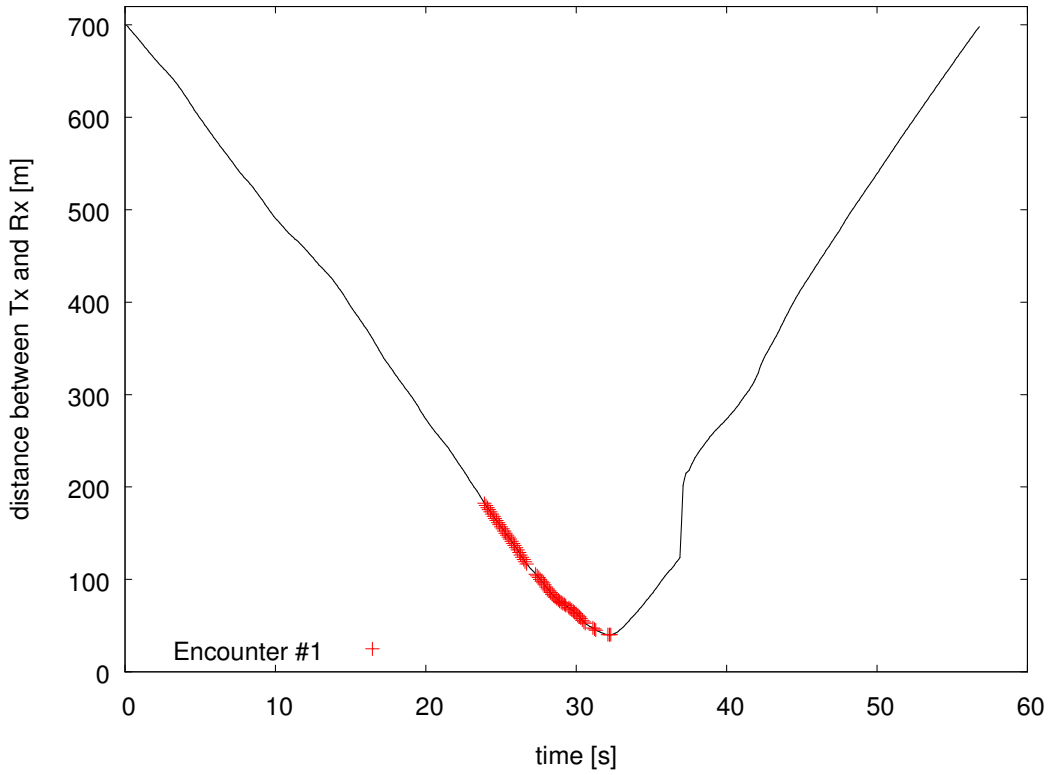

Figure 6.3 The communications pattern of an illustrative V2V encounter within the SPMD test data set of the inter-vehicle distance versus time. Packet receptions within 200m are bursty, and interspersed with inter-packet gaps. Communications is highly asymmetric with respect to distance, as there are no receptions after $t = 32s$, when the vehicles begin to separate away from one another. Prior to the receipt of the first packet, and after the reception of the last packet, there are long gaps of no receptions, even though the vehicles are quite close to one another.

Figure 6.3 plots the communications pattern of an illustrative V2V encounter. Successfully received BSMs are marked on the line that shows the relationship between inter-vehicle distance and time within the encounter. The two vehicles are initially separated by approximately 700m. As they approach each other midway through the encounter, periods of successful communications are observed. As the vehicles then continue moving and separation increases, communications success ceases. In this encounter, successful packet receipt as a function of inter-vehicle distance is highly asymmetric. There are periods of bursty losses, especially at distances beyond 200m, at which there are no successfully received packets.

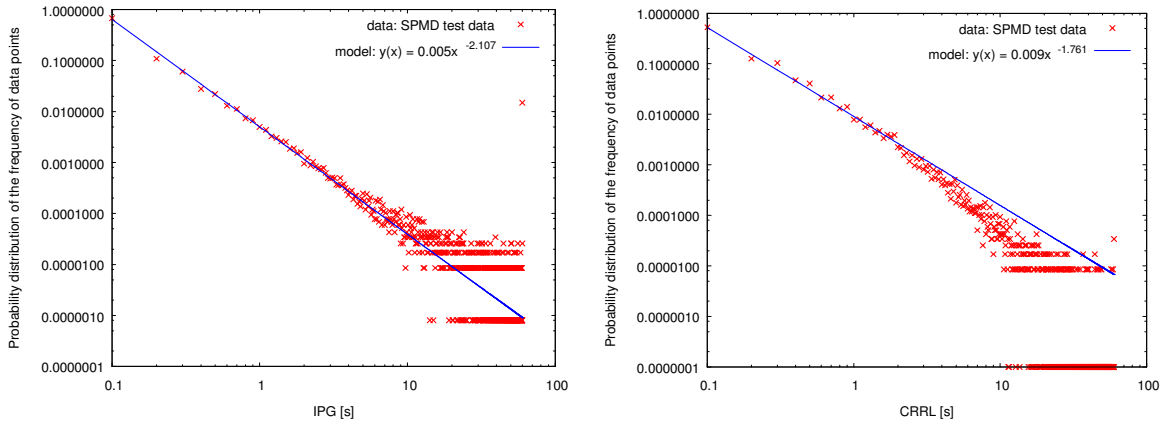

Figure 6.4 The log-log scale pdf of IPG and CRRL, respectively, within the SPMD test data set. Both IPG and CRRL follow power-law distributions.

6.4.3 Burstiness of Packet Gaps and Runs

The burst patterns within the SPMD test data set of IPG and CRRL out to 60s, respectively, are shown in Figure 6.4. Total frequency of gaps and runs were nearly equal, with a total of 116,977 gap events and 117,659 run events occurring. Burstiness trends following long-tailed power law distributions were identified using the approach in [98] and tested for goodness-of-fit using the Kolmogorow-Smirnov (KS) statistic (i.e., KS test) [98]. Both gaps and runs of length 0.1s (i.e., 1 packet) are predominant, while long bursts occur occasionally. For example, although rare, a gap length of 60s indicates a long period of communications failure that could threaten safety application reliability.

Figure 6.5 shows the cdf of the gap and run lengths, respectively, out to 600 packets. Short bursts are most common. Long runs and gaps are exceptionally rare, although gaps of 60s or longer occur approximately 1% of the time, on average.

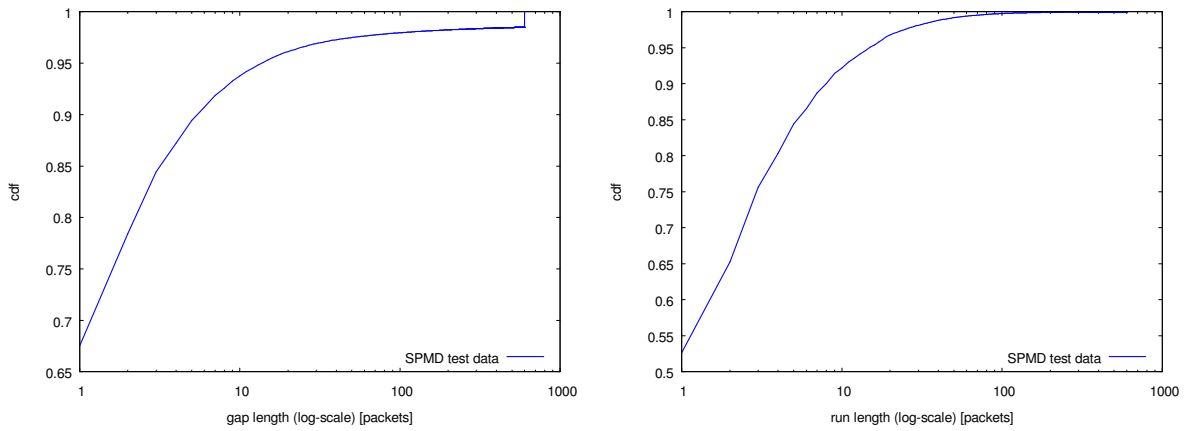

Figure 6.5 The cdf of IPG and CRRL, respectively, within the SPMD test data set. In both plots, the *x*-axis is log-scale. A majority of packet gaps are very short, with 95% of all gaps less than 11 packets (i.e., 1.1s). Although the analysis was limited to a maximum gap length of 600 packets (i.e., 60s), approximately 1.5% of all gaps are ≥ 600 packets. Consecutive runs of packet receptions are also typically short, with 95% of all runs being less than 11 packets in length (e.g., 1.1s). Long bursts of consecutively received packets are very rare, with no runs of more than 200 consecutive packets.

Using the pdf of IPG and CRRL, expected values can be determined. Given a pdf, $p_X(x)$, the expected value can be calculated as:

$$E[X] = \sum_i i p_X(i). \tag{6-2}$$

To assess expected burst lengths as a function of distance, the gap and run bursts previously plotted in Figure 6.4 were divided into distance-range bins of 0-100m, 100-300m, 300-600m, 600-900m, and 900-1200m. Expectation was calculated as in (6-2) for $X \in \{run\ length, gap\ length\}$ for the subset portions of V2V encounters in during which packet receptions occurred (i.e., leading and trailing gaps of V2V encounters were ignored). The resulting

Table 6.1 Expected run lengths and gap lengths for five distance bins. Expected run length increases when distance between transmitting and receiving vehicles decrease. Contrastingly, expected gap length increases as distances between vehicles increases.

Distance range [m]	***E*[*run length*] (packets)**	***E*[*gap length*] (packets)**
0-100	5.956	6.983
100-300	4.410	7.769
300-600	3.325	13.158
600-900	3.141	19.301
900-1200	3.296	23.345

Table 6.2 Expected PRR for five distance bins. PRR decreases as distance between transmitting and receiving vehicles increases.

Distance range [m]	***E*[*PRR*]**
0-100	46.03%
100-300	36.21%
300-600	20.17%
600-900	13.99%
900-1200	12.37%

expected values are shown in Table 6.1. As distance between transmitting and receiving vehicles increase, their expected run lengths decrease, while the expected gap lengths increase.

6.4.4 Expected PRR

Expected PRR, $E[PRR]$, is the ratio of the expected run length to the total expected run length plus the total expected gap length, calculated as:

$$E[PRR] = \frac{E[run\ length]}{E[run\ length] + E[gap\ length]}. \tag{6-3}$$

Expected PRR for the same five distance bins are before are shown in Table 6.2. Expected PRR, as a function of expected run length and gap length, decreases as distance increases.

6.4.5 Conditional Packet Reception

While we have thus far shown that packet gaps and runs exhibit bursty behaviors throughout the Ann Arbor measurement campaign, the contributing reasons for these bursts and the packet reception correlations between them remains unclear. To further explore this, we consider modeling wireless link burstiness using conditional probability delivery functions (CPDFs), which give the probability a packet will be received successfully after *n* consecutive successes or failures [109]. Thus, the probability of "the next packet" is conditional upon the number of prior consecutively received or lost packets.

More formally, the conditional packet delivery function, $C(n)$, is the probability the next packet will succeed given n consecutive packet successes (for $n > 0$) or failures (for $n < 0$). For example, $C(5) = 83\%$ means that the probability that a packet will arrive after five successful deliveries is 83%, while $C(-7) = 18\%$ means that the probability after seven consecutive losses of successfully receiving a packet is 18%. Note that a CPDF is only defined for $n \neq 0$ consecutive packets (lost or received) and is not defined for $n = 0$.

A link with independent losses will have a flat CPDF because the probability of reception is independent of any history.

The probability of receiving the n consecutive successes implies that $n - 1$ packets have thus far been successfully received, which can be expressed using conditional probability as:

$$\Pr(n \text{ successes}) = \Pr(X_n = 1 | X_{n-1} = 1) = \frac{\Pr(X_{n-1} = 1) \; and \; \Pr(X_n = 1)}{\Pr(X_{n-1} = 1)}. \quad (6\text{-}4)$$

Using (6-4), the CPDF was generated for the SPMD test data set, where the number of gap or length data points was greater than 10, thus limiting the analysis to gaps less than 1.2s and runs less than 7.5s. The CPDF is plotted in Figure 7.6. For gaps or lengths 3 or more, the average probability of receiving a packet is less than 10% and decreases as gap length increase. As run length increases, the conditional probability of receiving one more packet increases. Because the CPDF is not flat, reception probability is not independent of history, indicating

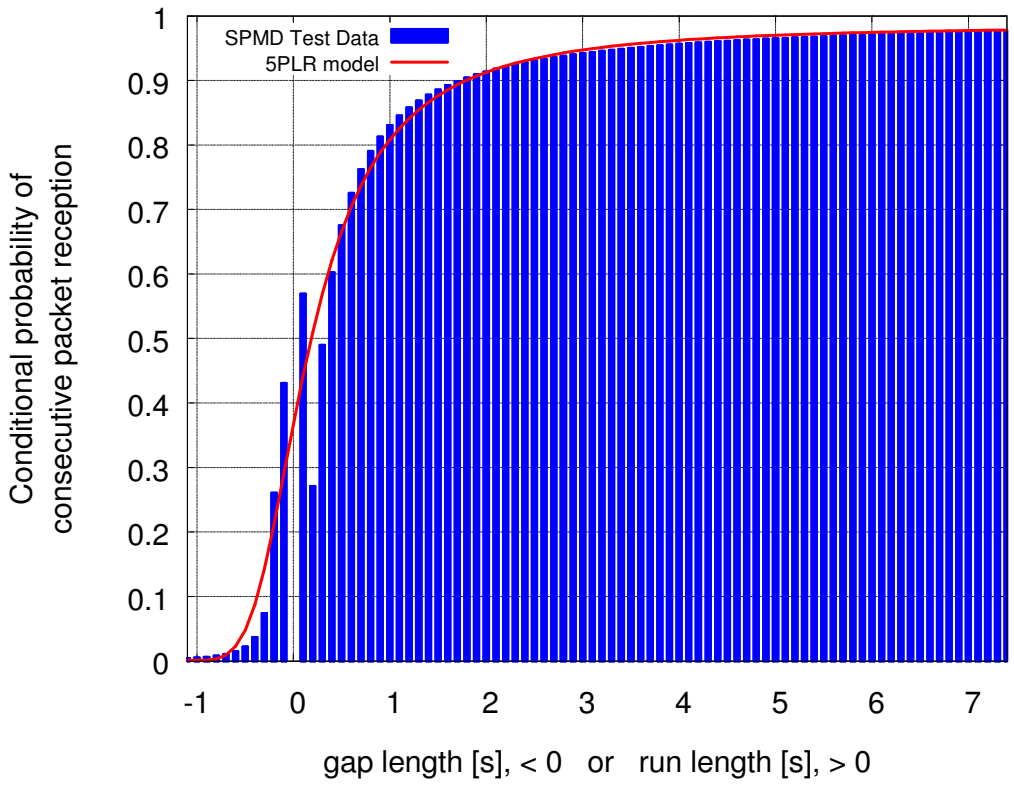

Figure 6.6 The CPDF of gap and run lengths for the SPMD test data set and a 5PLR estimation model. The probability of a gap ending or a run length continuing are not independent of the previous gap / run length history, indicating that bursty reception and loss behaviors within the environment are not the result of an i.i.d. packet generation phenomenon.

that packet burstiness in the SPMD data set is not the result of an i.i.d. packet generation phenomenon.

6.4.6 Temporal and Spatial Sensitivity

To further explore the burstiness patterns within the SPMD data set, temporal and spatial sensitivity analysis of the CPDFs were conducted.

The asymmetric S-curve of the CPDF in Figure 6.6 can be estimated using a 5-Parameter Logistic Regression (5PLR) curve, Y [110]:

$$Y = F(x; A; B; C; D; G) = D + \frac{(A - D)}{\left[1 + \left(\frac{x}{C}\right)^{B}\right]^{G}}, \tag{6-5}$$

where:

A is the estimated response at zero concentration,

B is the slope factor,

C is the mid-range concentration,

D is the estimated response at infinite concentration,

and G is the asymmetry factor.

A 5PLR estimation model of the SPMD-based CPDF is plotted in Figure 7.6.

For spatial sensitivity analysis, gaps and runs were divided into four distance-based bins (i.e., 0-300m,300-600m, 600-900m, and 900-1200m). The CPDF for each subset was computed and estimates of best fit were determined using linear regression of the RMSE between the model (6-5) and the data. Results are plotted in Figure 6.7. For very short runs and gaps, the conditional probability of receiving 1-3 packets varies with distance, but otherwise the conditional probability of a (gap or run) burst continuing appears independent of distance.

A similar approach was conducted for temporal sensitivity analysis of the CPDF. The full set of nearly 2000 V2V encounters found within the SPMD test data set represents encounters that occur at different times of the day and were thus divided randomly into five subsets. The CPDF for each subset was computed and estimates of best fit were determined as before. Results are plotted in Figure 6.8. Similar to the effect observed spatially, for very short runs and gaps, the conditional probability of receiving 1-3 packets varies with distance, but otherwise the conditional probability of a (gap or run) burst continuing appears independent of distance.

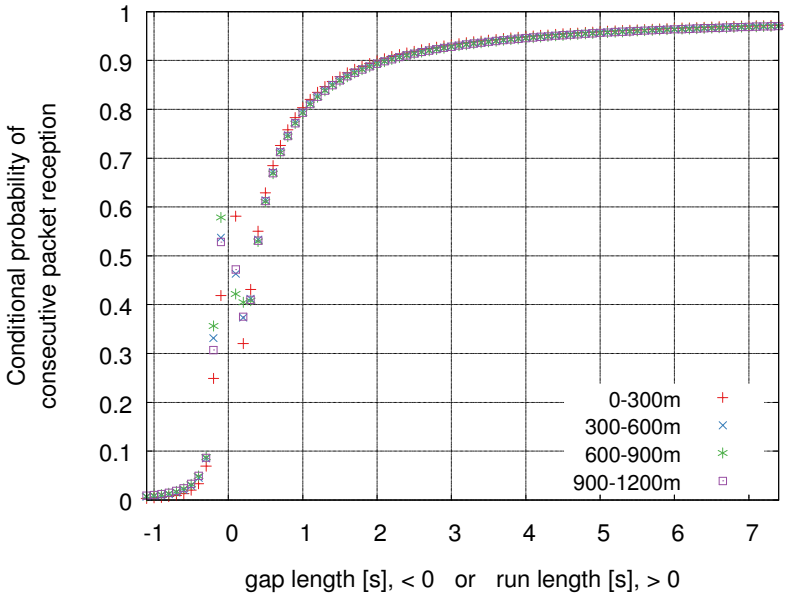

Figure 6.7 5PLR models of the CPDF of gaps < 1.2s and runs < 7.5s, for four distance bins. Conditional probabilities for short gaps and runs (e.g., lengths of 1-2) differ as a function of distance, but are nearly identical for other gap and run lengths, independent of distance bin.

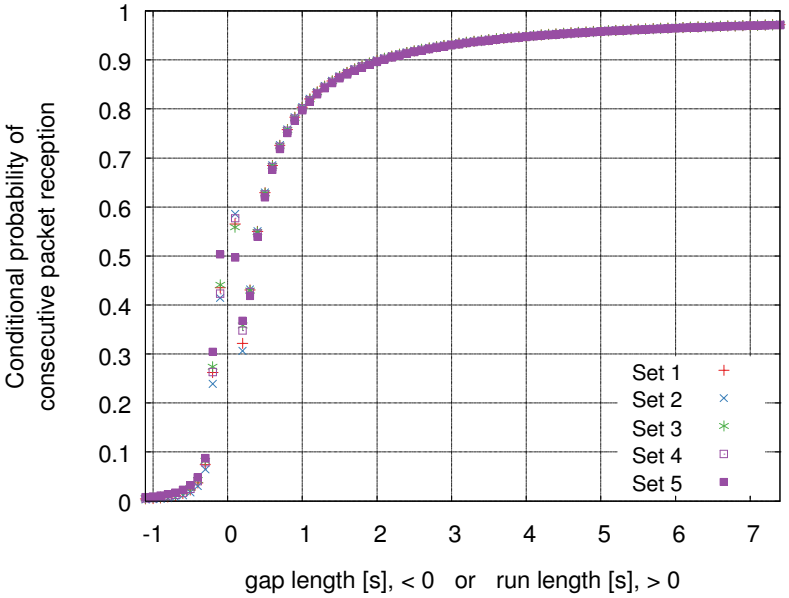

Figure 6.8 5PLR models of the CPDF of gaps < 1.2s and runs < 7.5s, for five different temporal subsets of the SPMD test data set. Conditional probabilities for short gaps and runs (e.g., lengths of 1-2) differ among the temporal data sets, but are nearly identical for other gap and run lengths, independent of the temporal subsets.

6.5 Packet Loss Models

We discuss here several packet loss models that we test for their abilities to replicate PRR, IPG, and CRRL and that we have compared to the especially bursty packet loss behaviors as observed in the SPMD test data set.

6.5.1 Bernoulli / Memoryless Packet Loss Model

A conceptually simple packet loss model is the Bernoulli Packet Loss Model, characterized by a reception parameter p and corresponding packet loss parameter $q = 1 - p$. The model is easily implemented by picking a random number $0 \leq n \leq 1$ for each packet, and deciding whether it is received (i.e., $n \leq p$) or lost (i.e., $n > p$). For a sequence of N packets, the number of received packets tends to Np for large values of N. Such a sequence is a Bernoulli process of N i.i.d. random variables $\{X_1, X_2, \ldots, X_N\}$, where each value of $X_i | 1 \leq i \leq N$ is either a 0 (i.e., packet is lost) or 1 (i.e., packet is received), where $\Pr(X_i = 1) = p$. Since, in a Bernoulli process, the outcome of future trials is independent of the outcome of past trials, a Bernoulli process exhibits the memoryless property of a Markov Chain. Thus, the Bernoulli Packet Loss Model is a Memoryless Packet Loss Model. While such a model is simple to understand and implement, its reliance on event independence does not adequately characterize bursts of lost and received packets that are observed in the SPMD test data [105] to have correlation tendencies with run and gap bursts that are conditionally related (Section 6.4.5).

6.5.2 Gilbert-Elliott Packet Loss Model

The simplest Markov chain model that accounts for bursty packet losses is the 2-state Markov chain Gilbert-Elliott Packet Loss Model shown in Figure 6.9.

The model is composed of two states, where state ‘0’ represents a lost packet, and state ‘1’ represents a received packet. The transition probability of receiving a packet is conditioned upon the success or failure of the previous packet. If the previous packet was lost, then the probability of receiving a packet occurs with probability p, while if the previous packet was successfully received, then probability of receiving another packet occurs with probability $1 - q$. Transition probabilities for lost packets are similar. If the previous packet was received, then the probability of losing a packet occurs with probability q, while if the previous packet was also lost, then probability of losing another packet occurs with probability $1 - p$. These probabilities can be represented in a transition probability matrix,

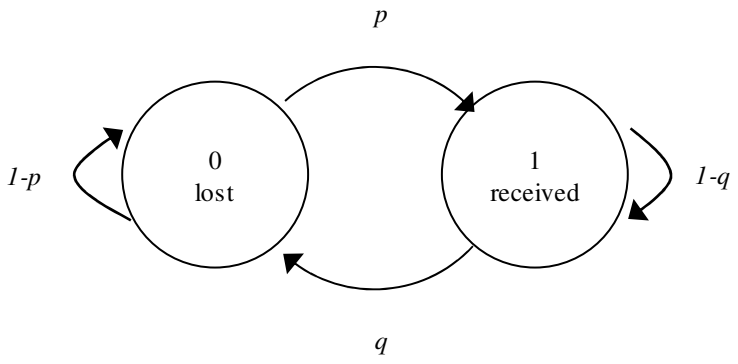

Figure 6.9 The 2-state Markov chain Gilbert-Elliott Packet Loss Model.

$$\begin{bmatrix} p = p_{01} & 1-q = p_{11} \\ 1-p = p_{00} & q = p_{10} \end{bmatrix}, \tag{6-6}$$

where we denote $p_{xy} = \Pr(X_i = y | X_{i-1} = x)$. Note that the Gilbert-Elliott model generally assumes conditional behaviors: subsequent packet loss or reception is conditional upon the previously received / lost packet. In the Gilbert-Elliott 2 state Markov chain model, typically $p + q < 1$. In the special case where $p + q = 1$, the model reverts to a stationary Bernoulli model. When considering no more than $n = 2$ consecutive packets, a CPDF degenerates into the Gilbert-Elliott two-state Markov model, whereas evaluations for $n > 2$ allows for evaluations of longer runs of consecutive receipts/losses that can be expressed by CPDFs.

By analyzing the SPMD data set in terms of the 2-state Gilbert Elliott model, we find that $p = 0.231$ and $q = 0.01$. Since $p + q \approx 0.24 < 1$, we observe that the packet loss behaviors in Ann Arbor do not follow an i.i.d. Bernoulli process and instead exhibit non-stationary tendencies.

An evaluation of the Gilbert-Elliott model using the techniques of [105] showed slight improvements in IPG and CRRL burst generation patterns over i.i.d.-based models when compared to the results of the SPMD data set. This result showed that extending conditional packet loss and receptions to a 2 state Markov chain model improved IPG and CRRL model accuracy over purely i.i.d.-based models, However, the results were sufficiently lacking in precision, with burstiness predictions often over- and under-estimated. This led us to consider

$$S_1 = \{0, 1, 0, 1, 0, 1, 0, 0, 1, 1\}$$

$$S_2 = \{0, 1, 1, 1, 1, 0, 0, 1, 0, 0\}$$

Figure 6.10 Two binary streams, S1 and S2, that illustrate packet generation results with equivalent PRR but different packet gap and consecutive runs.

additional approaches to burst distribution models that better reflect the actual patterns observed in the SPMD test data set.

6.6 Approach

Packet receptions in the SPMD data set exhibit IPG and CRRL burstiness trends that both follow different long-tailed power law distributions [14] (Section 6.4.3). Our analysis provides evidence that the packet generation processes do not follow i.i.d. processes (Section 6.4.5) (Section 6.5.2), assumptions upon which many common path loss models are based [105].

Model accuracy depends upon the evaluation of packet production processes in terms of average PRR and also packet loss and reception burstiness (e.g., IPG and CRRL). For example, let sequences of packet losses and receptions be modeled as binary strings, where a '0' represents a lost packet and a '1' represents a successfully received packet. For illustrative purposes, let us consider two example binary strings in Figure 6.10, S_1 and S_2 of total length $N = 10$ packets, $R = 5$ successfully received packets, and $L = N - G = 5$ lost packets.

Both S_1 and S_2 show 5 successfully received packets out of 10 total packets, and thus have identical PRR = $\frac{R}{N} = \frac{5}{10} = 50\%$. In S_1, the longest packet gap occurs with one occurrence of two consecutive 0's, and similarly, the longest consecutive run length occurs with one occurrence of two consecutive 1's. In S_2, the longest gap occurs again where there are two consecutive 0's, with two occurrences of this pattern, while there is one occurrence of the longest consecutive run length of four consecutive 1's.

Strings S_1 and S_2 are each a different combination of five 0's and five 1's. While they have identical PRR, the ordering of the 1's and 0's leads to different packet gap and reception burst lengths.

We address safety packet generations by proposing a new packet generation model, BUR-GEN, that uses a *burst generator*. Results are compared to the SPMD test data set and evaluated in terms of three metrics (PRR, IPG, and CRRL) that compare BUR-GEN to several common VCMs.

6.7 Packet Generation Model

6.7.1 Process Flow

The architecture and data flow diagram for a packet generation and evaluation model is shown in Figure 6.11. The *Packet Generator* employs a path loss model (commonly i.i.d.-based) that produces a randomized *Flow Stream* of packet receptions and losses that appear in the stream as alternating gaps and runs. The *Flow Stream Analyzer* evaluates the *Flow Stream* and compares it to a measurement campaign data, such at the SPMD test data set, and in terms of metrics such as PRR, IPG, and CRRL. Our contribution of the Burst Generator Model (BUR-GEN) augments a path loss model by producing packet runs and gaps from *burst generation distributions* (BDFs) that are derive from the distributions of IPG a nd CRRL from the SPMD test data set; the Packet Generator thus combines a path loss model and the Burst

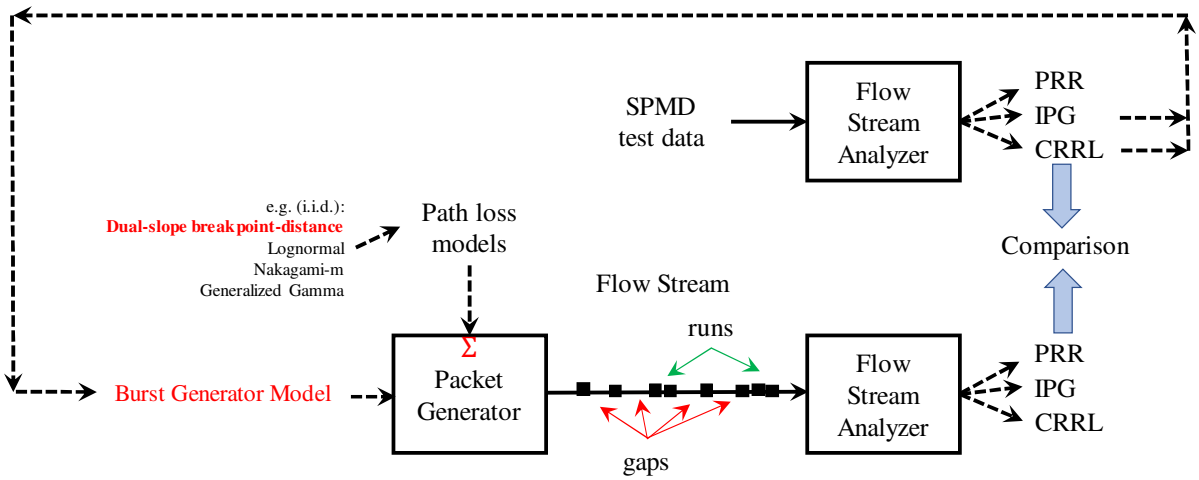

Figure 6.11 Architecture and data flow diagram for a packet generation and evaluation model. A Flow Stream Analyzer is used to evaluate the PRR, IPG, and CRRL of the SPMD test data. The resulting distributions are used as inputs into a Burst Generator model that the Packet Generator combines with a path loss model to produce a modeled Flow Stream of alternating gaps and runs of packets. The model results are also analyzed by a Flow Stream Analyzer and the results of the test data and model are compared.

Generator Model to produce a Flow Stream that differs from a purely i.i.d.-based packet generator.

Common path loss models that rely on i.i.d. assumptions generate each packet reception or loss as an event that is independent of all other events (i.e., an uncorrelated channel). When the average PRR is prr, then the probability in an uncorrelated channel of a gap of n consecutively missed packets, $p_{gap}(n)$, of length $t[s] = n/10$,:

$$p_{gap}(n) = (1 - prr)^n. \tag{6-7}$$

and the probability of a run of n consecutively received packets, $p_{run}(n)$ is:

$$p_{run}(n) = prr^n. \tag{6-8}$$

6.7.2 Burst Generator (BUR-GEN) Model

A packet generator that relies on an i.i.d.-based distribution for packet reception/loss probabilities produces a flow stream of packets that consist of alternating gaps and runs that are drawn from the probability distributions of (6-7) and (6-8), respectively.

Since evidence shows that burstiness distributions do not follow i.i.d. generation patterns in the Ann Arbor data set [14] (Sections 6.4.5, 6.4.6,and 6.5), we propose BUR-GEN, a Burst

Let X be a random variable with cdf F_X.

1. Generate a random number, u, from the uniform distribution in the interval $[0, 1]$.
2. Find the maximum value x such that $F_X(x) \leq u$.
3. Take x to be a random number drawn from F_X, i.e., $x = F_X^{-1}(u)$

Figure 6.12 The inverse transformation method.

Generation Model that generates streams of consecutive runs and gaps that are each drawn, respectively, from a *burst distribution function* (BDF). For example, a sequence of packet gaps length can be drawn from the cdf of the SPMD measurement campaign data. Randomized samples are produced using the inverse transformation method. This method takes uniform samples of a number u between 0 and 1, and then returns the largest number X from the domain of the distribution $P(X)$ such that $P(-\infty < X < x) \leq u$. Figure 6.12 elaborates the method for generating packet gaps and consecutive runs, where F_X is replaced by the cdf of the SPMD measurement campaign for gaps and runs, respectively (e.g., as plotted in Figure 6.5). Five different distance bins are used (i.e., 0-100m, 100-300m, 300-600m, 600-900m, 900-1200m) with a cdf derived for each separate distance bin.

6.7.3 Packet Reception Rate

As evidenced by Table 6.1, expected run length and expected gap length are distance-dependent within the measurement campaign data, supported by the expected PRR values shown in Table 6.2 are related to expected IPG (i.e., $E[gap]$) and expected CRRL (i.e., $E[run]$) and result from the application of (6-2). However, the expected PRR value as shown in Table 6.2 is an average that is derived from a distance range over the appropriate distance bin. For example, for all distances in the range bin of 100-300m, the expected PRR from Table 6.2 is 36.21%.

For furthering our discussion of PRR, we differentiate between two terms: *expected PRR* which is a value derived from expected gap length and run length as in (6-2), while *average PRR* is a value typically calculated using a path loss model. While slightly different in meaning, we will relate these terms shortly.

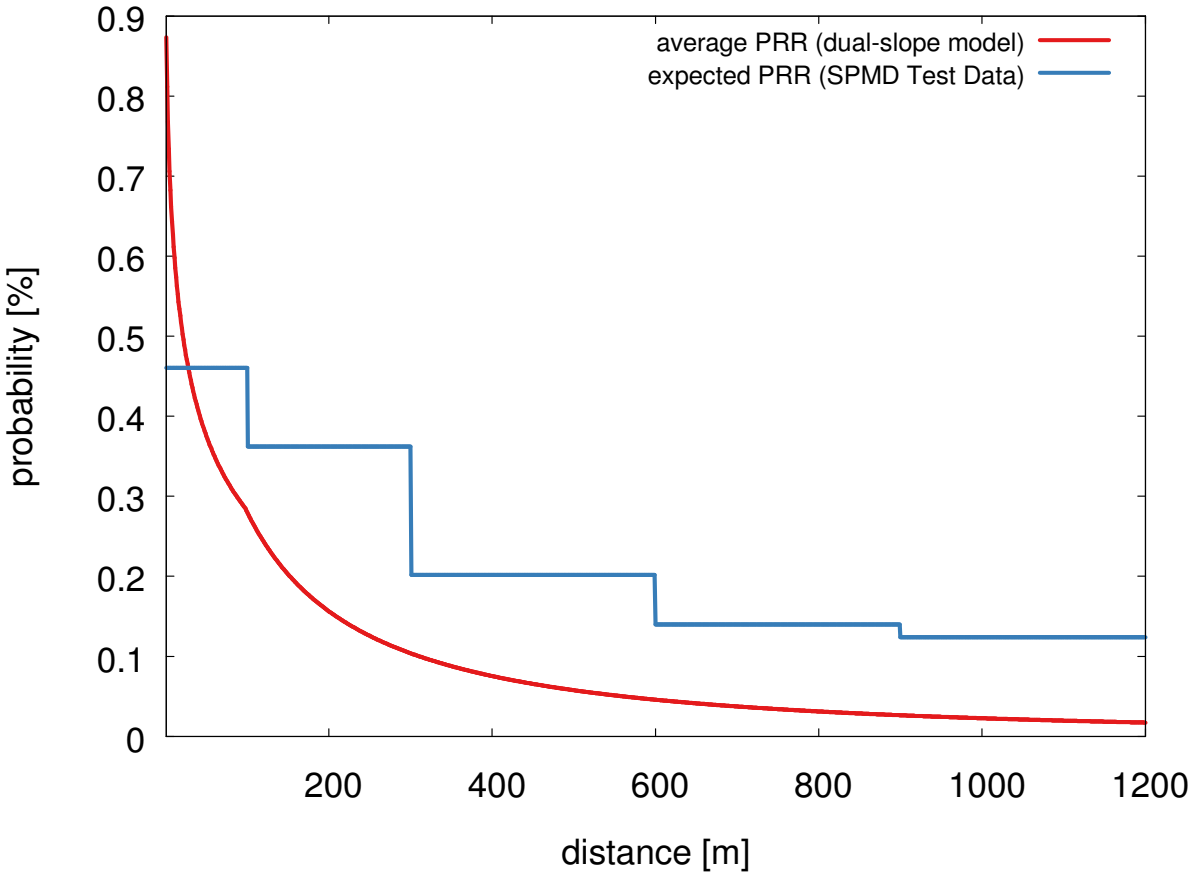

Figure 6.13 Comparison of average PRR and expected PRR. Average PRR (i.e., using the dual-slope distance-breakpoint path loss model derived from the SPMD test data) decreases smoothly as distance increases, while expected PRR drops in a stepwise manner consistent with the distance bins used for their evaluation. Expected PRR is calculated using the subset of data points that occur only during active communications, while the average PRR includes all data points throughout an entire encounter. As expected PRR excludes long periods of leading and trailing packet gaps, the value of expected PRR often exceeds that of the path-loss-modeled average PRR.

Average PRR depends on distance when it is derived from distance-dependent path loss models. For example, assuming a dual-slope distance-breakpoint path loss model (2-13) with parameters $d_b = 97.5m, \gamma_1 = 4.3, \sigma_1 = 63.7, \gamma_2 = 7.1,$ and $\sigma_2 = 34.9,$ then $PRR(d = 100) = 20.21\%$ and $PRR(d = 300) = 3.56\%$. It is immediately observed that average PRR using a distance-based path loss model varies with distance (i.e., PRR = 20.21% at distance = 100m, and PRR = 3.56% at distance = 300m). However, the expected PRR = 36.21% is not distance-dependent, and is applied over the entire distance range of 100-300m. Furthermore,

the expected PRR value (36.21%) is higher than the average PRR values that the path loss model produces (3.56 – 20.21%).

Figure 6.13 compares average PRR and expected PRR. Several observations are notable. First, average PRR (i.e., that uses the dual-slope path loss model derived from the SPMD data) decreases smoothly as distance increases, whereas expected PRR drops in a stepwise manner consistent with the distance range bins (i.e., as used in Table 6.2). Second, expected PRR is higher than average PRR for most distances. This is due to the different data points used in calculating average PRR and expected PRR. Average PRR is calculated for all possible data points in which two vehicles participate in a V2V encounter, whereas expected PRR is calculated from the subset periods from the first through the last successfully received packets. For example, referring back to Figure 6.3, the average PRR will include all periods during the encounter, regardless of separation distance or time, whereas the calculation of expected PRR is limited to the periods of active communications (i.e., $22 \leq t \leq 32$). Specifically, in this scenario, the long gaps of packet losses that exist for periods $t < 22$ and $t > 32$ are excluded from the calculation of expected PRR. Since these packet losses are excluded from the calculation, expected PRR will be higher than average PRR for this encounter. Intuitively, average PRR gives the average long-term packet reception probability of V2V encounters over all time, whereas expected PRR is calculated from a subset of those data points and describes packet reception probabilities during the times of active communications.

It is observed that expected PRR:

i) fails to account for long periods of packet loss (i.e., gaps) that occur before and/or after periods of successful communications, and

ii) does not estimate PRR in a distance-dependent manner.

Our analysis of the SPMD test data shows that long periods of packet losses occur throughout the data set. Thus, we introduce a mechanism to adjust the expected PRR by occasionally injecting long gaps into the packet generation process to as to give the resulting desired average PRR.

Let us consider a means by which we can equate *average PRR*, $\overline{PRR}$, to some function of the *expected PRR*, $f(E[PRR])$:

$$\overline{PRR} \propto f(E[PRR]). \tag{6-9}$$

Since expected PRR does not account for periods of packet losses before and after successful communications, let us augment this (i.e., through function f) with a weighted average function that will occasionally introduce additional packet gaps into the flow stream. Let α be the weighted probability that packet bursts are generated using a BDF that produces an expected PRR, $E[PRR] = \frac{E[run]}{E[run]+E[gap]}$, and let $(1-\alpha)$ be the probability that a gap of length G is generated that replaces either the run or the gap that would have otherwise been generated (i..e, hence the term $G + G = 2G$ in (6-10)). Note that the expected PRR of the G-length gap is 0%. Thus, the average PRR of the weighted average function is:

$$f(E[PRR]) = \frac{E[run]}{\alpha(E[run] + E[gap]) + (1-\alpha)2G}. \tag{6-10}$$

We can now set $f(E[PRR]) = \overline{PRR}$ and solve (6-10) for α:

$$\alpha(G, E[run], E[gap], \overline{PRR}) = \frac{2G - \frac{E[run]}{\overline{PRR}}}{2G - (E[run] + E[gap])}. \tag{6-11}$$

As an example calculation, let us assume that with probability $(1-\alpha)$ we will generate a gap of length $G = 600$ packets. At an assumed distance of $d = 200m$, $E[run] = 4.410$ and $E[gap] = 7.769$ packets (i.e., from Table 6.1). Using the dual-slope distance-breakpoint model with parameters as given above, we find $\overline{PRR(d = 200m)} = 7.4\%$. Substituting into (6-11), we find $\alpha = 96\%$. Thus, at a distance of 200m, $\alpha = 96\%$ of the time on average we can randomly draw gap and run bursts from the BDF, and $(1-\alpha) = 4\%$ of the time we will replace the gap or run with a gap of 600 packets. This results in a weighted average PRR of 7.4%.

The sensitivity of the $(1-\alpha)$ term of (6-11) compared to the expected gap length, $E[gap]$, is plotted in Figure 6.14. As distance increases, the expected gap also increases (i.e., Table 6.1). However, because the expected PRR does not account for leading and trailing packet loss gaps, the expected PRR is often higher than the path loss model (i.e., as shown and discussed in Figure 6.13). The term $(1-\alpha)$ of (6-11) accounts for the frequency with which a long burst of lost packets (i.e. $G = 600$ of (6-10)) is injected into the packet stream. Such injections are infrequent at short distances, with rising frequency as distance increases.

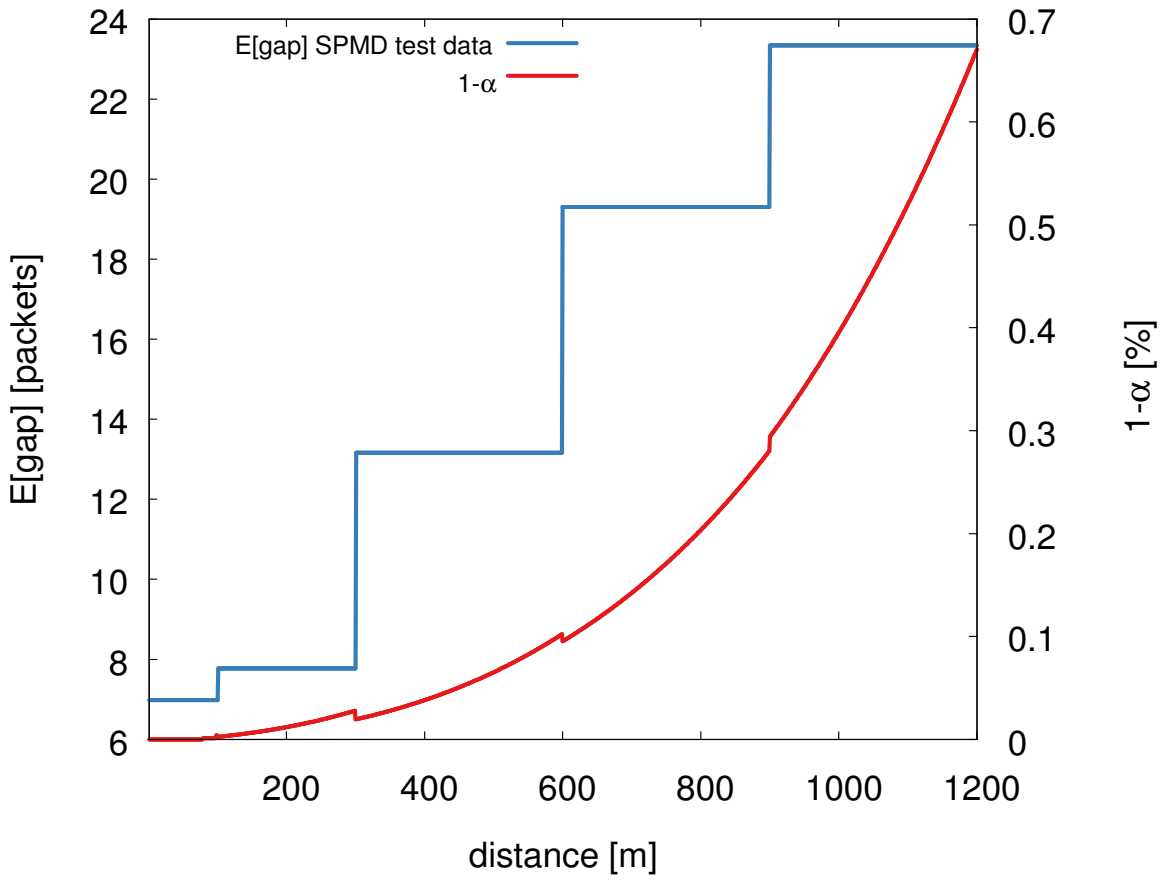

Figure 6.14 Sensitivity of $(1-\alpha)$ as compared to expected gap length. Expected gap length increases as distance increases. However, since leading and trailing long packet gaps are excluded from the calculation of expected gap, the resulting expected PRR is higher than desired average PRR. By injecting long packet gaps into a packet stream with frequency $(1-\alpha)$, expected PRR can be related to average PRR. The need for such injections is infrequent as short distances and increases as distance increases.

6.7.4 Packet Generator

If the general packet generator model of Figure 6.11 uses only a i.i.d.-based path loss model, then packets are independently generated one packet at a time. Consecutive runs occur randomly with run length probabilities defined by (6-8). The resulting flow stream consists of alternating runs and gaps.

The packet generator model can now be described that produces a flow stream of packets that maintains the average PRR of a path loss model and the desired burst distributions of a BDF. Instead of generating packets one at a time, the algorithm draws run lengths (and gap lengths) from the respective BDFs, and then alternatively emits the consecutive runs or packet

```
1  function packet_generator(L, PL(d), F_gap, F_run):
2      // return s, a stream of length L of 0's and 1's
3
4      s ← zeros(L) // the packet stream, initially all 0's
5      count ← 1
6      next = "gap" // start with a gap, then alternate gap-run-gap-run…
7      G = 600
8      α = f(G, PL(d), F_gap, F_run) // See Eqn. (7-11)
9
10     while count < L
11         u_1 = rand[0, 1]
12         if u_1 <= α  // w.p. α
13             u_2 = rand[0, 1]
14             if next == "gap"
15                 L_gap = F_gap^-1(u_2)  // pick next gap from cdf
16                 count = count + L_gap
17                 next = "run"
18             else
19                 L_run = F_run^-1(u_2)  // pick next run from cdf
20                 emit L_run 1's into s
21                 count = count + L_run
22                 next = "gap"
23             endif
24         else  // w.p. 1-α
25             count = count + G  // long-gap
26             next = "run"
27         endif
28     return s
```

Figure 6.15 The BUR-GEN (burst generator) packet stream generator algorithm. The algorithm returns a packet stream S of length L that consists of alternating gaps and runs that are drawn from gap and run burst distribution functions (i.e., line 15 and 19, respectively). With probability $(1-\alpha)$, a long burst of length G of lost packets is injected into the stream.

gaps into the flow stream. The process is augmented with a typically small probability $(1-\alpha)$ to replace an otherwise expected run or gap with a long-gap of 600 packets. Pseudocode for the packet generator algorithm that combines a path loss model with the BUR-GEN burst generator model is provided in Figure 6.15.

6.8 Experimental Setup

The BUR-GEN packet generation model is evaluated through simulation, with results for PRR, IPG, and CRRL compared to the SPMD data set. The results of this new model (i.e.,

Simulation Parameters		
Encounters		
Vehicles per encounter	2	
Encounters per experiment	10,000	
Number of experiments	100	
Total trips simulated	1,000,000	
Mobility		
Trip length [s]	uniform [5, 300]	
Initial relative velocity	[1-60 m/s] randomly drawn using cdf of SPMD data analysis	
Car-following	Krauss model	
Path loss		
Model	Dual-slope distance-breakpoint (Eqn. 2.13)	
d_b [m]	97.5	
γ_1	4.3	
σ_1	63.7	
γ_2	7.1	
σ_2	34.9	
Burst Distribution		
	Model *C*	Model *F* (BUR-GEN)
gaps (IPG)	1 packet at a time based on PRR from i.i.d. path loss model	from cdf of SPMD measurement campaign
runs (CRRL)		

Figure 6.16 Simulation parameters. Vehicle mobility is modeled as randomly generated V2V encounters. Path loss is modeled using the dual-slope distance-breakpoint model and using the "best fit" parameters identified in Chapter 5. The i.i.d. packet burst generation Model *C* is evaluated against a model that includes the BUR-GEN algorithm (i.e., Model *F*).

Model *F*) are compared with the results of five common VCMs as previously evaluated in Chapter 5 (i.e., Models *A*-*E*).

Each trip involves a pair of vehicles representing a V2V encounter in which one vehicle is a transmitter (Tx), and the other is a receiver (Rx). One experiment involves the creation of 10,000 random encounters. Each experiment is repeated 100 times (i.e., a total of 100 x 10,000 = 1,000,000 simulated encounters), with results averaged and examined for confidence intervals.

Simulation parameters are divided into mobility model, path loss model, and burst distribution model, and are listed in Figure 6.16.

The mobility of each V2V encounter is generated as a random trip between two vehicles, assumed moving throughout urban and highway environments. The length in time of each encounter is randomly drawn from a standard uniform distribution of [5, 300]s (i.e., 50-3000

possible packets). The inverse transformation method (i.e., Figure 6.12) is used to randomly drawn initial relative velocities between vehicles from the distributions derived from the SPMD measurement campaign data as given in Figure 6.2, and vehicles update their relative speeds over time using a standard car-following model (e.g., the Krauss model [69]) that handles vehicle velocity changes as vehicles approach and separate from one another. Vehicles update their positions, based on these simulation parameters, and the relative distances between each pair of vehicles is calculated every 100ms. The resulting separation distances are used as inputs to the path loss and packet generation models.

The dual-slope distance-breakpoint path loss model is used to estimate desired PRR for a given distance, d. The model parameters used are those found in Chapter 5 that give the "best fit" for PRR when common path loss models were evaluated with respect to the SPMD test data set (i.e., (2-13) with $d_b = 97.5m, \gamma_1 = 4.3, \sigma_1 = 63.7, \gamma_2 = 7.1,$ and $\sigma_2 = 34.9$). The transmitting vehicle Tx emits a BSM every 100ms.

Run and gap burst lengths are randomly drawn from the burst distribution functions. Two models are evaluated through simulations:

i) Model *C* – the dual-slope distance-breakpoint path loss model as previously evaluated in Chapter 5, and

ii) Model *F* – the dual-slope distance breakpoint model path loss augmented with the BUR-GEN packet stream generator algorithm from Figure 6.15.

For Model *C*, packets are generated one at a time from the PRR distribution produced by the dual-slope distance-breakpoint path loss model. For Model *F*, burst lengths of runs and gaps are drawn from the burst distribution functions that are derived from the SPMD measurement campaign data (i.e., as given in Figure 7.5) using the inverse transformation method (i.e., Figure 7.12).

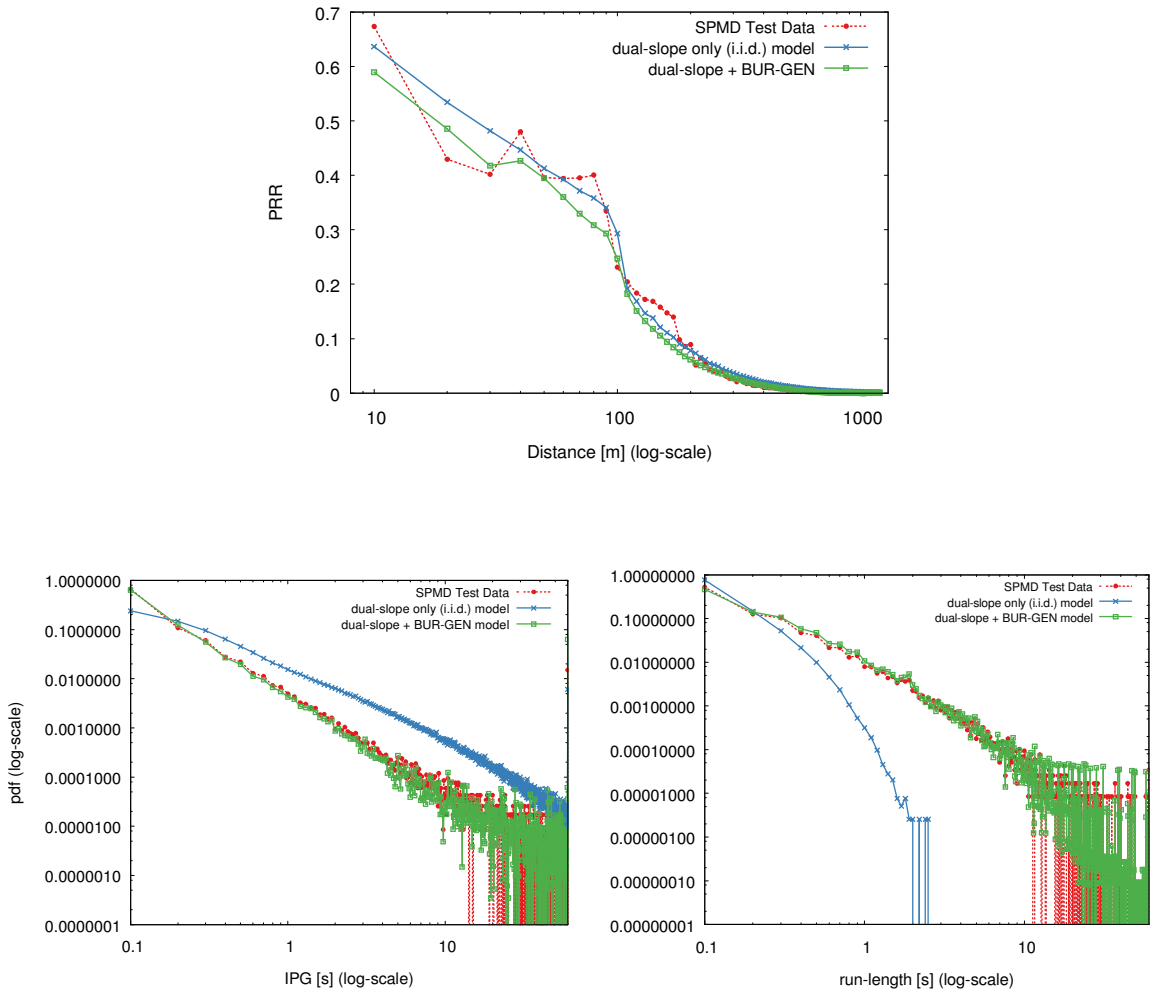

Figure 6.17 PRR comparison of the dual-slope distance-breakpoint model (only) and the combined dual-slope distance-breakpoint model with the BUR-GEN burst generation model.

6.9 Results and Discussion

6.9.1 Results

Results for PRR, IPG, and CRRL are plotted in Figure 6.17. Table 6.3 shows numerical results that compare the RSME o.25f the PRR, IPG, and CRRL metrics of Model *F* (i.e., the dual-slope distance-breakpoint model with the BUR-GEN burst distribution function), to Models *A*-*E* (i.e., five common VCMs as evaluated in Chapter 5).

Table 6.3 Numerical results of the RSME for three metrics – PRR, IPG, and CRRL – of the combined dual-slope distance-breakpoint model with the BUR-GEN burst distribution function (i.e, Model *F*, compared to five common (i.i.d. only) VCMs (i.e., Models *A*-*E*).

Model		Metric value (rank)		
		PRR	**IPG**	**CRRL**
A	Unit disk	1.31 (6)	--	--
B	Lognormal	0.41 (5)	0.52 (5)	0.32 (5)
C	Dual-slope distance-breakpoint (i.i.d. only)	0.19 (1)	0.44 (3)	0.25 (3)
D	Generalized gamma shadowed fading	0.28 (4)	0.47 (4)	0.28 (4)
E	Lognormal fading with obstacle shadowing	0.22 (3)	0.40 (2)	0.20 (2)
F	Dual-slope distance-breakpoint + BUR-GEN	0.21 (2)	0.07 (1)	0.07 (1)

6.9.2 Discussion

The inclusion of the BUR-GEN model with the dual-slope distance-breakpoint path loss model produces burst distributions of IPG and CRRL that very closely match the SPMD measurement campaign data. The PRR trend produced when BUR-GEN is included (i.e., Model *F*) appears to preserve the PRR behaviors of the dual-slope distance-breakpoint (i.i.d.) model (i.e., Model *C*), although the resulting PRR is slightly lower than the i.i.d. model alone. Still, the resulting RSME of the combined model (*F*) (i.e., 0.21) ranks it better than all other i.i.d.-only models, making it, in terms of PRR, second only to the i.i.d.-only model (*C)* (i.e., 0.19).

When the combined model (*F*) is compared to each of the five common VCMs, the improvements are notable. For example, in comparing Model *F* to Model *C*, the minor degradation in PRR (an increase in Model *F* vs. Model *C* of +12.4%) is offset by the improvements is IPG and CRRL that are six times and four times better, respectively. When compared to all other i.i.d.-based VCMs, the BUR-GEN inclusive model improves the RSME of PRR, IPG, and CRRL in all cases.

6.10 Conclusions

The packet generation process that uses the dual-slope distance-breakpoint path loss model was augmented with BUR-GEN, a burst distribution function that randomly generates gap and

run bursts using probability distribution functions derived from the SPMD measurement campaign. In simulation of one million trips, the combined model outperforms all other i.i.d.-only packet generation models when the RSME of PRR, IPG, and CRRL are compared to the SPMD measurement campaign data set. The RSME of IPG and CRRL are improved by factors or six and four, respectively, by the inclusion of the BUR-GEN algorithm, with a minor decrease to the RSME of PRR, although this result still ranks the PRR predictions of the combined model second only to the dual-slope distance-breakpoint (i.i.d.-only) path loss model.

Our analysis shows that bursty packet losses are present in SPMD test data and that burst distributions such as IPG and CRRL result from packet generation processes that are not i.i.d.-based. Since VCM selection in simulation-based studies influences performance accuracy conclusions, it is important to select packet generation models that accuracy reflect the packet loss behaviors of real-world deployments in terms of average packet loss and burstiness distributions.

CHAPTER

7

SAFERELAY: IMPROVING SAFETY IN TIME-CONSTRAINED VANETS WITH GEO-ADDRESSING RELAYS

In a VANET, vehicles attempt to improve safety by transmitting messages that others receive to increase their awareness of one another. Yet, the data delivery requirements of various safety applications are often inconsistent, thus potentially jeopardizing safety performance. While many information dissemination techniques have been proposed to improve data delivery in a VANET, such as flooding and geocasting, evaluations do not focus on measuring safety efficiency in terms of safety application requirements and often fail to include mobility considerations, such as time to contact (TTC). To improve safety in a VANET, we propose SafeRelay, a flooding-based message dissemination technique that relays safety messages within a geographically addressed forwarding zone (FZ). We evaluate different FZ sizes in terms of several metrics, including safety awareness probability, which combines both communications and mobility performance. Simulation results of an urban downtown scenario show that SafeRelay can significantly improve safety awareness using moderately-sized nearby FZs.

7.1 Introduction

Modern technical advances provide connected vehicles the potential to improve driving safety. To make driving safer in a VANET, each vehicle regularly generates pertinent "here I am" information about itself (e.g., location, speed and heading) that is encapsulated within a BSM [11] and rapidly broadcast as a safety beacon (i.e., beaconcasting) to make other nearby vehicles aware of its presence so they can alert drivers of unsafe situations such as pre-crash scenarios. Safety success requires high probability of packet delivery while considerable mobility and environmental issues (e.g., obstacles such as other vehicles, buildings, foliage, etc.) jeopardize safety by impeding radio-wave transmissions. Although DSRC standards [12] attempt to address requirements for the rapid dissemination of safety messages in highly mobile conditions, packet delivery remains especially challenged when nodes at high densities need to deliver messages in time-limited intervals under harsh environmental conditions, resulting in channel congestion that defeats delivery attempts.

Paradoxically, data delivery requirements of safety applications can potentially jeopardize safety itself. For example, to improve situational awareness in others, emergency vehicles may boost transmission power and/or use intermediate nodes to forward their own alert messages. However, higher transmission power may prevent message delivery if channel collisions occur due to concurrent transmissions, while the multiplicity of forwarded messages adds to the communications overhead within the channel, especially in the broadcast environment of a VANET. Techniques such as increased power and message frequency work counter to mitigation techniques that adaptively reduce messaging, transmission power, and/or congestion window size [111] to reduce channel pressures. Thus, an approach that attempts to improve the delivery potential of one transmission may, in fact, reduce the delivery potential of others, thus jeopardizing safety effectiveness.

To improve safety in a VANET, we propose *SafeRelay*, a flooding-based message distribution technique that uses idle channel time to relay safety messages within a geolocationally specified *forwarding zone* (FZ). We compare *SafeRelay* to no flooding and One Zero Flooding (OZF) [112] by simulating different safety use case scenarios that vary FZ parameters, such as coverage area, and we present results and comparative analysis using a new safety metric that combines mobility and communications effectiveness, *safety awareness probability.*

The rest of this chapter is organized as follows: Section 6.2 elaborates the motivation for safety information dissemination. Section 6.3 describes the safety evaluation model, and Section 6.4 describes the approach to safety evaluation. Section 6.5 presents evaluation results and Section 6.6 concludes the chapter.

7.2 Motivation

7.2.1 Safety Applications

Quantifying safety effectiveness in a VANET remains difficult. Many VANET safety applications have been proposed [77] [11] that differ in safety intentions based upon expected messaging effectiveness. Proposed applications [11] help vehicles move through intersections (Intersection Movement Assist), alert drivers to specialized vehicles (Emergency Vehicle Alert / Stopped School Bus), and/or increase drivers' awareness of road conditions (Situational Awareness). However, current limited deployments and testing evaluations (e.g., [113]) have not conclusively provided necessary performance and operational standards that quantify safety.

7.2.2 Safety Information Model

Broadening the works of others, we further evaluate performance of the safety-based VANET by

i) extending the range of safety coverage beyond single hop transmission limits,

ii) making packet reception requirements distance dependent (e.g., closer vehicles should successfully receive more messages), and

iii) incorporating mobility awareness using the relative velocities, directions, and distances between vehicles.

To illustrate these characteristics, refer to the safety system snapshot in Figure 7.1, where vehicle *A* (i.e., moving left to right) broadcasts its safety message that others within its communications range limit (i.e., moving right to left, vehicle *B*, but not *C* and *D*) can receive.

To improve safety awareness, vehicle *A* wishes to make vehicle *D* more aware of its presence by transmitting its safety message toward a geocast region (GR), centered at *v* with radius R_{GR}. Because some of the GR (e.g., in this case, the entire GR) lies beyond the communications range limit of vehicle *A*, the FZ specifies the area within which the safety messages of *A* should be relayed (i.e., through vehicles *B* and *C* towards the GR that contains

D). Geometrically, we assume that the FZ covers the single hop transmission range of the sender, its intended geocast region, and the area between them.

Safety effectiveness requires successful message delivery, but also depends on additional measures that capture aspects of mobility. For example, since vehicle *A* is closer to vehicle *B* than it is to vehicle *C*, we would expect that safety awareness carries a higher importance between vehicles *A* and *B* vs. vehicles *A* and *C*. Additionally, vehicles with higher relative velocity and headed towards one another would be more likely to collide than vehicles heading away from one another. Because vehicle *D* is further away from *A* than *B* or *C*, it is not clear if vehicle *D* receiving the safety messages of vehicle *A* would, in fact, improve safety. This demonstrates a potential relationship between communications effectiveness and relative distances and velocities between two nodes.

To address the relationship between proximity and safety awareness, assume that safety requires receipt of more messages per second for shorter distances than for longer distances. For illustrative purposes, let us assume that in order to be considered "safely aware" of the 10 messages per second generated by vehicle *A*, vehicle *B* requires receipt of 5 of them, vehicle *C* requires 3, and vehicle *D* requires 1 message. Without message relay vehicles *C* and *D* do not receive any of the BSMs from vehicle *A* due to the communications range limit and thus cannot be considered "safely aware" of *A*. Thus, to achieve safety awareness, a hypothetical

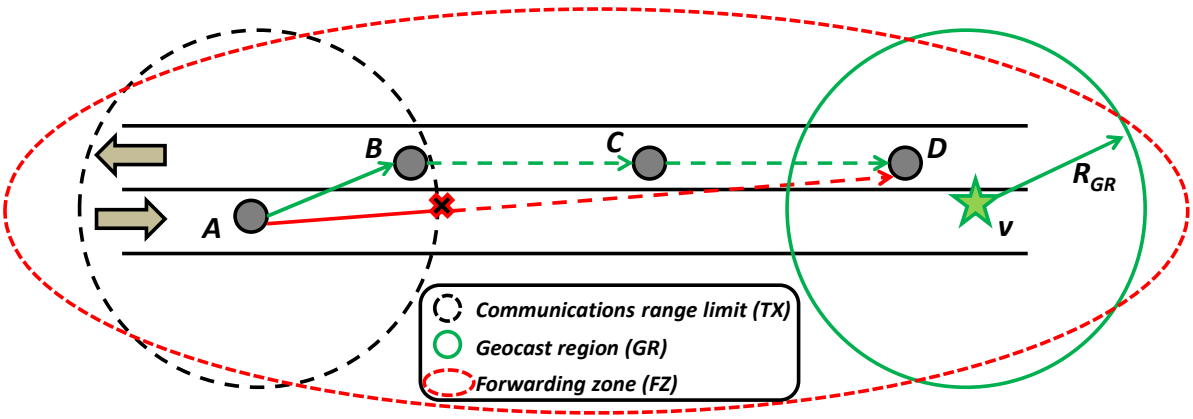

Figure 7.1 Conceptual view of the safety system in which vehicle *A* desires to target safety messages towards the geocast region (GR) centered at *v* with radius R_{GR}, requiring messages to be relayed through the entire *forwarding zone* (FZ) that covers the entire area.

relay mechanism must successfully deliver the minimum percentage of BSMs that *A* generates (i.e., 50% to *B*, 30% to *C*, and 10% to *D*).

7.2.3 Channel Pressure

According to the current standards [11] each vehicle generates a new BSM at regular intervals (10Hz) that is intended to be delivered within a short (e.g., 100 ms) *safety transmission interval* (STI) to improve safety. Figure 7.2 shows a timing diagram for typical channel access in a beaconcasting VANET. In this example, five vehicles are shown that may contend for access to the vehicular channel, generating their BSMs in the following order: $vehicle_3$, $vehicle_1$, $vehicle_5$, $vehicle_2$, and $vehicle_4$. $Vehicle_3$ defers access to the channel for one arbitration interframe space (AIFS), and sensing no carrier on the channel, begins transmitting its BSM. After sensing the completion of the transmission by $vehicle_3$ of its BSM, $vehicle_1$, $vehicle_5$, and $vehicle_2$ all defer for an AIFS and then begin counting down their backoff time that each vehicle chooses randomly as per the IEEE 802.11 standards [5]. $Vehicle_2$ completes its countdown first and begins transmitting its BSM, during which time the BSM for $vehicle_4$ arrives. The backoff countdowns resume for $vehicle_1$, $vehicle_5$, and $vehicle_4$. In this example, the backoff countdowns for $vehicle_5$ and $vehicle_4$ complete at the same time, and both then simultaneously transmit their BSMs. The resulting concurrent channel access causes both transmissions to collide, resulting in neither BSM being successfully received by nearby receivers that are in range of both transmissions. Because of the broadcast nature of the

beaconcasting VANET, the transmitted BSMs are neither acknowledged nor unacknowledged and so they are not rebroadcast. Thus, concurrent access to the vehicular channel can result in potentially lost safety packets that vehicles may not receive (e.g., the BSMs of $vehicle_5$ and $vehicle_4$ are "lost packets"). When there are no vehicles that desire to transmit a BSM within a safety transmission interval, residual time period(s) may exist during which the channel may be idle. Underutilized channel idle time may potentially be used instead to relay BSMs by rebroadcasting them (e.g., the technique used in this chapter). After 100ms, the safety transmission interval begins anew, and if any vehicle has not successfully transmitted a BSM within 100ms of its arrival at the MAC, then the transmission is cancelled, assuming the safety data contained within it has expired and will be soon replaced with a newly generated BSM with updated information.

Channel pressure can be alleviated by utilizing idle time to spread out safety message transmissions more uniformly across the STI. However, such an approach may delay a safety message transmission until later in the STI, thus jeopardizing safety by deferring the

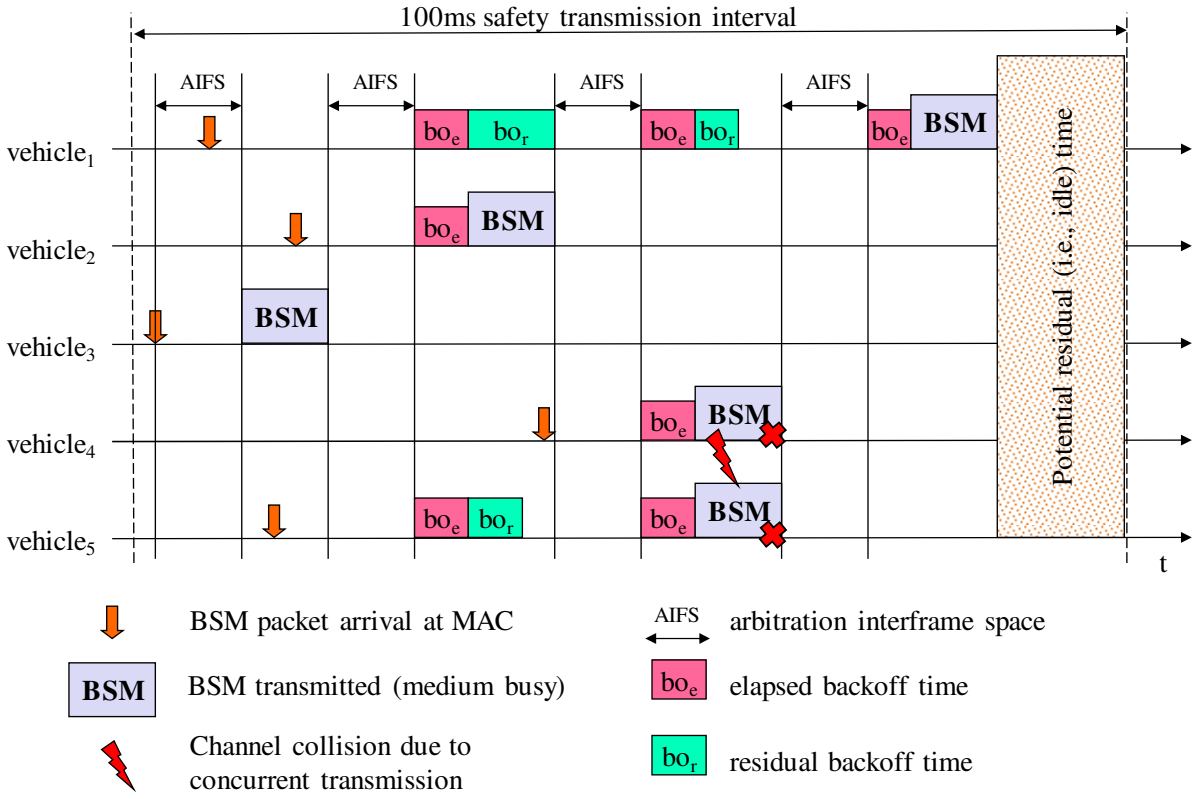

Figure 7.2 An example timing diagram for the beaconcasting VANET.

transmission of safety information that would otherwise have been sent earlier. Thus, a balanced and fair approach to safety message transmission is desired.

7.2.4 Information Dissemination

Since current standards [11] limit the effective coverage area of safety message content to the single hop transmission range, additional techniques, such as flooding and georouting protocols [62], are employed [60] [114] [63], [64], [65], [66] to further extend situational awareness to other vehicles. However, such approaches are often counter to the safety requirements of the beaconcasting VANET.

Figure 7.3 lists our generic pseudocode for broadcast flooding (i.e., based on [112]). In the case of no flooding, *criteria(m)* always returns `false`, meaning that received messages are never rebroadcasted. In the case of OZF [112], *criteria(m)* returns `true` when two criteria are met:

Pseudocode 1 *Broadcast flooding: receive message m*

```
1.  Function f ← m
2.      if criteria(m)
3.          m' ← amend(m)
4.          t ← getSendTime()
5.          sendBroadcast(m', t, timeout=100ms)
6.      end if
```

Figure 7.3 Pseudocode (based on [12] for broadcast flooding. Line 1 receives a message, *m*; line 2 decides if *m* should be forwarded; line 3 generates a new message, *m'*, by potentially amending the original message, *m*; line 4 determines the time at which the message should be resent; and line 5 schedules the rebroadcast of the amended message *m'* at some future time, *t*.

i) broadcast storm is prevented by continuing the flood only if the message is received for the first time, and

ii) a form of directional flooding occurs by which the message is only rebroadcast if the relaying node lies between the source and destination.

Furthermore, OZF amends the original message, *m*, by updating the sending position to the relaying node's local position and then schedules the rebroadcast for time *t = now()*. Many flooding techniques further amend the general approach given in Fig. 3 by using additional distance-based, direction-based and/or probabilistic driven criteria (i.e., line 2 in Figure 7.3) to make the decision to rebroadcast. However, such approaches fail to adequately control channel pressure and meet safety delivery constraints of the safety-based VANET.

7.3 Safety Evaluation

7.3.1 Communications Effectiveness

Especially in emergency situations, it is critical to inform surrounding vehicles quickly [115]. For example, avoiding a rear-end collision may require that a vehicle within 50 meters from the sender successfully receives with high probability 4 out of 5 packets in 1 second [116], whereas an emergency vehicle warning system may require hypothetically that a vehicle within 500 meters from the sender successfully receives at least 1 packet in 1 second.

We evaluate communications efficiency using *Awareness Probability* [116] [52] [85], the probability of successfully receiving at least *n* packets in the tolerance time window, T_{Tol}:

$$P_A(x, n, T_{Tol}) = \sum_{k=n}^{\left\lfloor \frac{T_{Tol}}{\tau} \right\rfloor} \binom{\left\lfloor \frac{T_{Tol}}{\tau} \right\rfloor}{k} P_s(x)^k (1 - P_s(x))^{\left\lfloor \frac{T_{Tol}}{\tau} \right\rfloor - k} \quad (7\text{-}1)$$

.

where, τ is the BSM generation interval (i.e., the STI length = 100ms), and $P_s(x)$ is the node reception probability at distance x between vehicles.

7.3.2 Mobility Effects

The most often used standard indicator [108] used to assess the potential for collision between two vehicles is the metric *time to contact* (TTC) [117] [108], which corresponds to the amount of time before two vehicles will come within contact range of one another (i.e., collision in the worst case). TTC often represents a threshold measure that distinguishes safe situations from unsafe ones. Although opinions differ, TTC values typically less than 4-6s imply higher risk, with the safety limit being as low as 1.5s in urban areas [118] [119].

The ratio of the relative distance between two nodes and their relative speeds determine TTC [120] [121] [118]. TTC applies when vehicles approach one another and is undefined otherwise. For two vehicles, *i* and *j*, with positions p_i, p_j, and velocities v_i, v_j, respectively, and length of vehicle *i* being l_i, the TTC for vehicle *i* with respect to vehicle *j*, TTC_i, is given by [118]:

$$TTC_i = \frac{d_{rel}(p_i, p_j)}{v_{rel}(v_i, v_j)} = \frac{p_j - p_i - l_i}{v_i - v_j}, \quad \forall\, v_i > v_j. \quad (7\text{-}2)$$

From TTC, a probability of contact can be derived. Typically, threshold values are defined, such as TTC_{min} and TTC_{max}, where values of TTC less than TTC_{min} imply 100% contact probability, values of TTC greater than TTC_{max} mean 0% probability of contact, and values of TTC between TTC_{min} and TTC_{max} are linearly interpolated.

$$P_c(TTC) = \begin{cases} 1, \; TTC \leq TTC_{min} \\ \frac{TTC - TTC_{max}}{TTC_{min} - TTC_{max}}, TTC_{min} < TTC < TTC_{max}. \\ 0, \; TTC \geq TTC_{max} \end{cases} \quad (7\text{-}3)$$

Where $P_c(TTC)$ is the probability of contact, then the probability of safety, $P_c(TTC)$, is defined as:

$$P_s(TTC) = 1 - P_{c,}(TTC), \forall\, TTC > 0. \quad (7\text{-}4)$$

7.3.3 Safety Awareness Probability

Intuitively, safety awareness increases when the probability of contact between vehicles decreases and when communications effectiveness increases. There are thus two components of evaluating safety that we will consider in turn:

i) mobility effects, and

ii) ii) communications effectiveness.

Since safety messages expire quickly, safety awareness must reflect recent reliability indicators instead of long-term averages. Thus, Successful Packet Delivery Probability (PDP) [115] is extended by defining BSM Reception Ratio (BRR), $BRR(i, j, T)$, that measures the BSM reception rate of a receiving node, i, for a sender node, j, within some recent time Window, T, (e.g., the most recent 3 seconds).

$$BRR(i,j,T) = \frac{R(i,j,T)}{T(i,j,T)}, \tag{7-5}$$

where $R(i, j, T)$ is the number of BSMs transmitted by node j and received successfully by node i (regardless of the number of hops) within time window T, and $T(i, j, T)$ is the total number of BSMs transmitted by node j within time window T that node i could possibly receive.

Awareness probability (7-1) depends on the number of expected messages received, n, within some time tolerance, T_{tol}. Additionally, n can be a function of distance, d, between vehicles. For example, avoiding a rear-end collision may require receipt of more messages at shorter distances. Since safety messages are emitted at regular intervals, the required number of messages to be received (i.e., within one second), $n(d)$, can be represented by a step-down function that depends on the distance between nodes, d:

$$n(d) = \begin{cases} n_{max}, & d \le d_{min} \\ \left\lfloor \dfrac{n_{min}(d - d_{min}) + n_{max}(d_{max} - d)}{d_{max} - d_{min}} \right\rfloor, & d_{min} < d < d_{max}. \\ n_{min}, & d \ge d_{max} \end{cases} \tag{7-6}$$

Communications effectiveness and mobility effects can now be combined into an appropriate VANET safety index. Between a pair of vehicles, the pairwise *safety awareness probability* (P_{SA}) is:

$$P_{SA} = P_S \cdot P_A, \tag{7-7}$$

where P_s is as given by ((7-4), and P_A is derived from ((7-1) by substituting $n = n(d)$ of ((7-6), and $P_s(x) = BRR(i,j,T)$ of ((7-5), yielding:

$$P_{SA}(i,j,T,n(d),T_{Tol}) = (1-P_c)\sum_{k=n(d)}^{\left\lfloor \frac{T_{Tol}}{\tau} \right\rfloor} \binom{\left\lfloor \frac{T_{Tol}}{\tau} \right\rfloor}{k} BRR(i,j,T)^k \left(1-BRR(i,j,T)\right)^{\left\lfloor \frac{T_{Tol}}{\tau} \right\rfloor - k}. \quad (7\text{-}8)$$

7.4 Evaluation and Results

7.4.1 Simulation Setup

Simulation studies evaluate the impact to safety of rebroadcast strategies for different message dissemination requirements. To reflect largely random but accurate vehicular mobility traces, SUMO is used to capture the mobility patterns of 250 vehicles moving along random routes throughout a two square mile urban downtown scenario for 2000 seconds (i.e., > 30 min.) of simulation time. To evaluate network performance of the VANET, the *ns-3* network simulator framework enables each vehicle to emit 250-byte BSMs at a rate of 10Hz as supported by the simulator's IEEE 802.11 and WAVE implementations.

To evaluate the effects of message forwarding strategies, OZF [112] is implemented and compared to no flooding. Additionally, we implement *SafeRelay*, a strategy that handles the decision to rebroadcast BSMs under timing constraints. Specifically, OZF uses directed rebroadcast to relay a message as soon as it is received (i.e., potentially interfering with the primary BSM transmissions of other vehicles), whereas *SafeRelay* defers the rebroadcast until a vehicle senses the channel idle for at least 10ms (i.e., an arbitrary period that was found to not adversely impact safety success), but gives up if the rebroadcast cannot be completed within 100ms. Table 7.1 compares the message dissemination techniques that are evaluated in terms of the generic broadcast flooding algorithm of Figure 7.3.

7.4.2 Parameters

To evaluate the effects of forwarding strategies on the number of packets forwarded and safety awareness probabilities, simulations are conducted for four different application requirements that vary the center points and sizes of the GRs, with parameters as described in Table 7.2. In all configurations, all vehicles transmit BSMs at 10Hz. A subset (e.g., 0%, 5%, or 100%) of the BSMs are tagged for potential relay throughout a FZ towards a GR. Other vehicles within the FZ that receive tagged BSMs rebroadcast them. The four configurations are:

Table 7.1 Three message dissemination strategies that are evaluated.

	Message Dissemination Strategy		
	No Flooding	**One Zero Flooding (OZF)**	**SafeRelay**
criteria	FALSE	TRUE if first time message received and towards the destination	
amend	N/A	update source transmitter's position to relay node's position	set transmitter's source address to originating node's source address
getSendTime	N/A	now()	delay until after channel sensed idle for 10ms but before expiration of 100ms safety transmission interval
% of vehicles that transmit BSMs	100%	100%	100%
% of BSMs that are tagged for relay	0%	100%	5%
% of vehicles that rebroadcast tagged BSMs	N/A	100%	100%
geocast region	N/A	directed towards a destination point, or possibly a circle	directed towards a circle centered potentially ahead of the vehicle

A. Base case in which all vehicles emit BSMs, but 0% of the BSMs are tagged for relay, resulting in no forwarding of any of the BSMs beyond their one-hop communications range.
B. Use OZF to forward the first receipt of 100% of all messages towards a geocast region (GR) located at the vehicle's expected position in 5 seconds, and with a R_{GR} of 1000m.
C. Use SafeRelay for "moving emergency vehicle" such that 5% of tagged vehicles' BSMs are forwarded towards a GR located at the tagged vehicle's expected position in 10 seconds and with a R_{GR} of 2000m.
D. Use SafeRelay for "stopped school bus" such that 5% of tagged vehicles' BSMs are forwarded towards a GR located at the tagged vehicle's current position and with a R_{GR} of 2000m.

Figure 7.4 illustrates the GRs for the four configurations, with the vehicle that originates a BSM located at the point labeled *v*, and the corresponding GRs shown as circles.

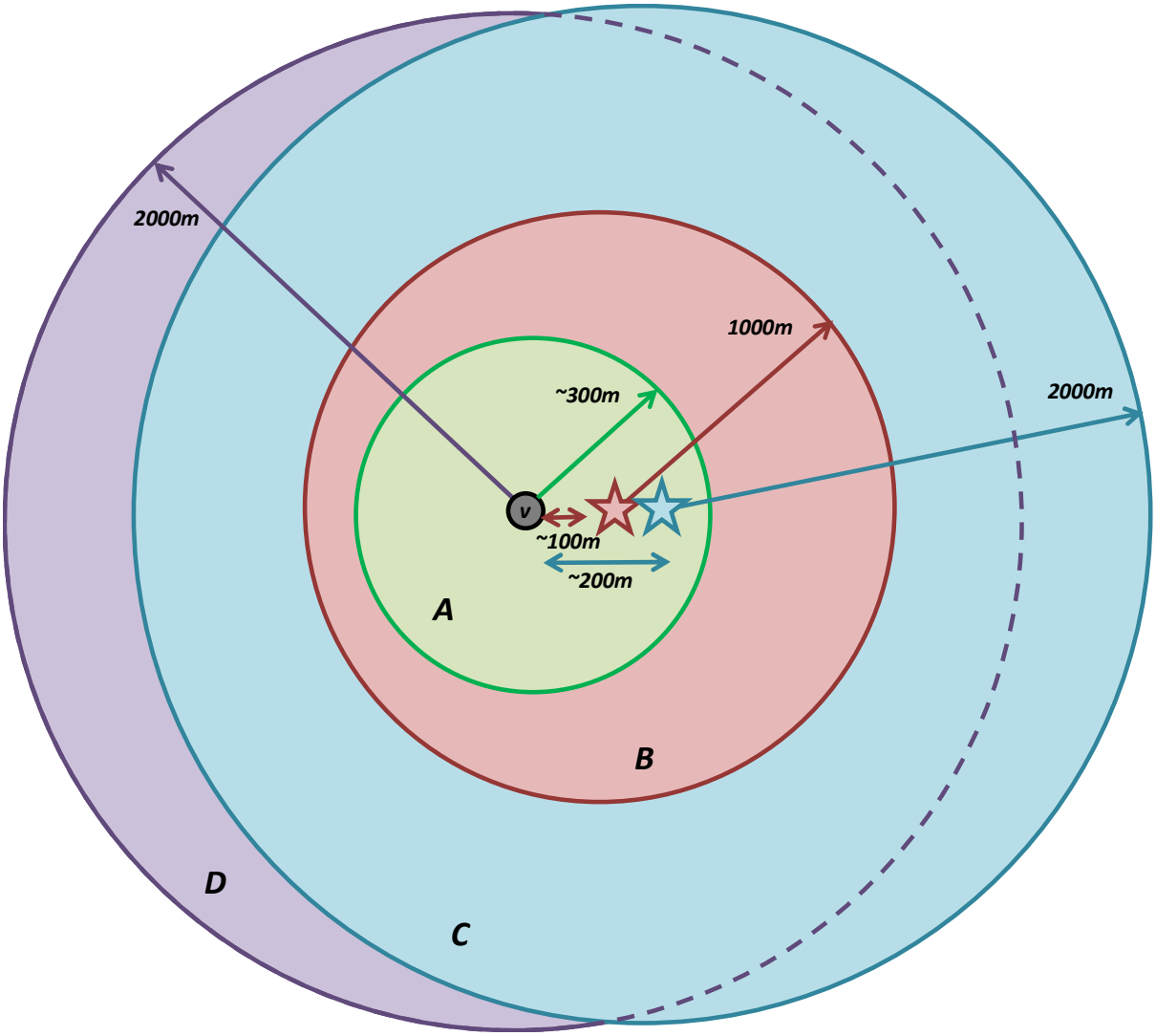

Figure 7.4 Pictorial illustration of geocast regions for four configurations (i.e., *A*, *B*, *C*, and *D*) that represent different application requirements. The vehicle transmitting a BSM is located at the point labeled *v* and is assumed to be moving left to right at approximately 20 m/s.

Configuration *A* (no flooding) serves as the base case in that no forwarding is conducted by any of the participating vehicles and so the GR is limited to the transmission range of the emitted BSM. Contrastingly, configuration *B* stresses the total communications attempts by enacting OZF so that all vehicles attempt to relay 100% of their safety messages to all other vehicles within a GR centered at the location where the transmitted vehicle would be located in 5s (e.g., at 20 m/s = 100m ahead of the vehicle), assuming it continues to travel at its current velocity and heading, with a GR area covered by a radius of 1000m from that center point.

Configurations *C* and *D* (*SafeRelay*) restrict message forwarding to a tagged subset (i.e., 5%) of the vehicles' BSMs, analogous to a smaller number of safety messages from higher priority vehicles, such as ambulances or school buses, that specify their BSMs to be forwarded while the remaining vehicles do not. While both *C* and *D* thus reduce the expected number of messages that are expected to be forwarded, they also double the radius of the GR (i.e., quadrupling the GR coverage area) as compared to the GR in *A*. The center of the GR for *C* is projected ahead of the high priority vehicle to the location where it will be located after 10s, assuming it continues at its current velocity and heading (e.g., to create a GR in advance of a moving ambulance), whereas in *D* the GR center point is not projected forward and remains centered with vehicle (e.g., a broken-down car needing emergency assistance). At the times when vehicles are not moving (i.e., velocity = 0), then the GRs for *C* and *D* will be identical.

For performance evaluation, we assess BSM reception probability over the most recent 3 seconds (i.e., $BRR(i,j,3)$), and we use values for the number of required messages received

Table 7.2 Four configuration that vary forwarding zone parameters based on different application requirements.

	Configuration			
	A	***B***	***C***	***D***
Simulation time (s)	2000			
Configuration space (km^2)	16			
Number of vehicles	250			
Car-following model	Krauss			
Maximum speed (m/s)	20			
Arrival rate (veh. / s)	1			
Traffic routing	Every vehicle repeats its route after reaching destination (until simulation ends).			
Radio propagation model	Two-ray ground			
Channel access	continuous			
BSM generation rate (Hz)	10			
BSM size (bytes)	250			
% of BSMs tagged for rebroadcast	0%	100%	5%	5%
Geocast region (GR) center point, longitudinally forward (in seconds) given current velocity and heading	N/A	5	10	0
R_{GR} (m)	N/A	1000	2000	2000

(i.e., $n(d)$ as in ((7-6)) that vary as a function of the distance between vehicles. The minimum number of messages required and corresponding effective distance are found arbitrarily by examining the resulting data from our experiments. Successful single-hop packet reception is never more than 10% beyond approximately 500m within the data. Thus, it would not be expected that vehicles could receive more than an average of 1 out of 10 messages per second beyond this range. Therefore, we have defined (i.e., albeit somewhat arbitrarily) the minimum number of messages required for safety effectiveness to be 1 message out of 10 at distances greater than or equal to 500m.

7.4.3 Results and Discussion

7.4.3.1 Vehicular Density and BSM Forwarding Policies

Although all configurations are repeated within the same urban, downtown scenario, examining the distribution of vehicle placement within the scenario helps convey where larger concentrations of vehicles occur (i.e., intersections, or popularly traveled routes). Furthermore, since for all scenarios the same vehicles travel exactly the same routes, the only effects that differ between configurations are the inter-vehicle communications, and the effects to the safety awareness.

Figure 7.5 (a) shows the average vehicular density for a subset of the 4000m x 4000m configuration space of the environment, as plotted in 40m x 40m squares. Some darker regions (i.e., "hot spots") show where higher concentrations of vehicles occur. For example, since vehicles start with a zero velocity and begin entering the scenario on roadway edges that are at the fringe of the scenario, higher densities of vehicles are seen in those locations that introduce vehicles into the scenario. An especially darker, solid area on the left-side indicates a highly travelled area.

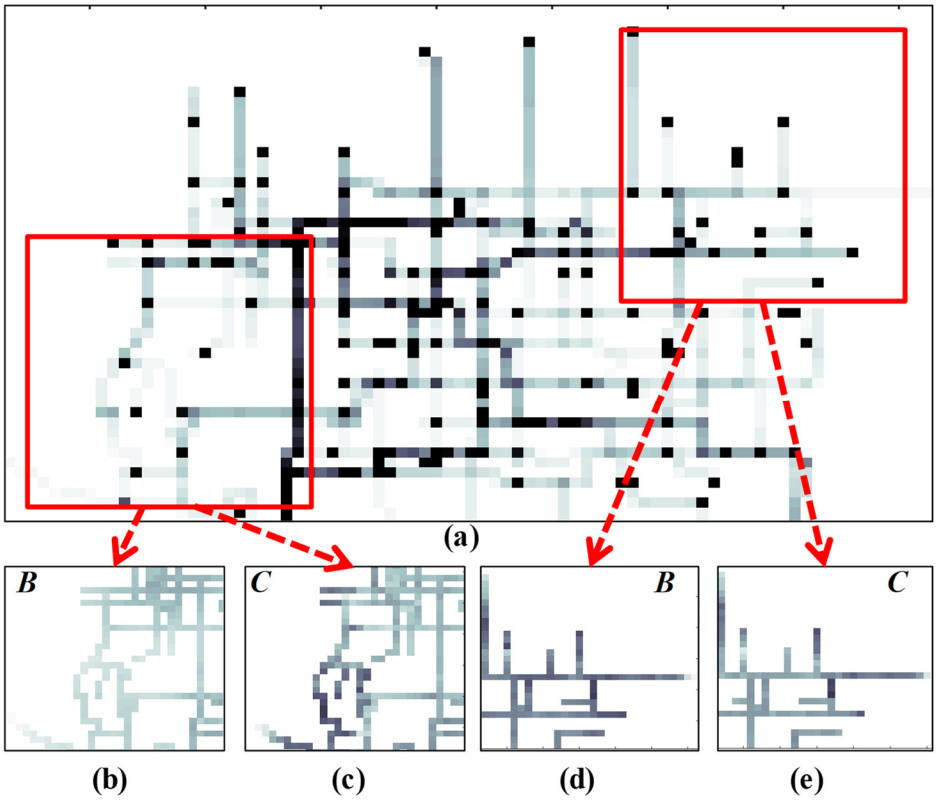

Figure 7.5 Vehicular density (a) for a subset of the configuration space, where darker-colored regions indicate areas through which more vehicles have traveled, and average BRR (b-e) for two different subsets of the scenario space and two different configurations (*B* and *C*), where darker-colored regions indicate higher BRR. Average BRR between scenarios is localized and may improve (e.g., (c) vs. (b)), or degrade (e.g., (e) vs. (d)).

Whereas the vehicular density is the same among all configurations, BRR differs due to the BSM message forwarding policies (e.g., configuration *B* vs. C). Figure 7.5 (b-e) shows the average BRR for two different configurations (i.e., *B* and *C*), where darker-colored regions indicate higher BRR, for the two sections highlighted in Figure 7.5 (a). For the left highlighted region, BRR increases in *C* as compared to *B* (i.e., Figure 7.5 (c) vs. Figure 7.5 (b)). Contrastingly, for the top, right section BRR decreases in *C* as compared to *B* (i.e., Figure 7.5 (e) vs. Figure 7.5 (d)). This implies that BSM forwarding policies can affect BRR positively or negatively in different localized regions.

7.4.3.2 Performance Evaluation

The decision for each vehicle to tag a BSM for relay varies with its forwarding policy. For example, in *A*, each vehicle only generates a primary BSM but does not tag it, and so no vehicles relay any BSMs, whereas in *B*, all vehicles tag all their BSMs and so they all forward all received messages. Contrastingly, in *C* and *D*, only 5% of the BSMs are tagged for relay, whereas the remaining BSMs (i.e., 95% of them) are not relayed.

The total number of *distinct* tagged BSMs received, as a function of distance between the vehicle that originally transmits a tagged BSM and potential receiving vehicles, is shown in Figure 7.6. Any tagged BSM that is received by a vehicle is only counted the first time it is received, regardless of whether the tagged BSM was transmitted by a nearby originating vehicle that is within the single hop communications range, or forwarded through one or more relay nodes. Several effects are noticeable within Figure 7.6:

i) The highest number of received tagged messages occurs at short ranges. Vehicles are most likely to collocate near each other (e.g., at very short separational distances when they are queued up and stopped at intersections).

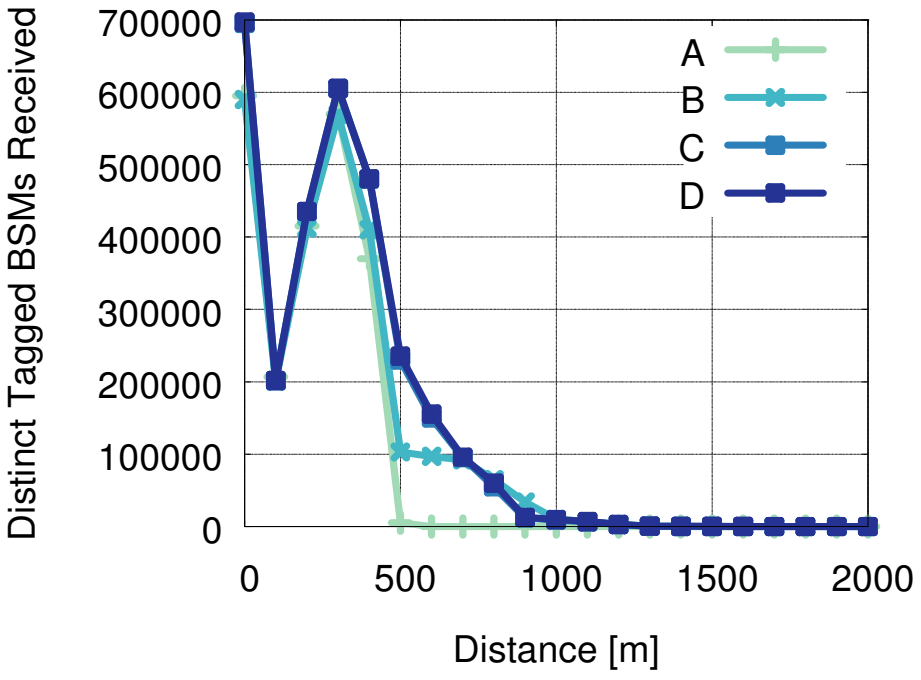

Figure 7.6 A comparison for four different scenarios of the total number of distinct tagged BSMs that are received, as a function of distance between the vehicle that originates the tagged BSM and receiving vehicles.

ii) There is a drop in tagged messages that are received in the range of 50-150m: For all configurations, few potential receivers are close to transmitting vehicles in the 50-150m range, providing insight into the non-uniform distribution of vehicles throughout the downtown roadway network (e.g., see Figure 7.5) in which traffic lights control vehicular flow through intersections. Specifically, in addition to be near one another near intersections, vehicles are also likely to be near each other when separated by 200-400m (e.g., when the transmitting vehicle is partway between multiple nearby intersections that each have numerous receiving vehicles lined up at the cross roads).

iii) Beyond 300m, there is a decreasing trend in tagged BSMs that are received: There are decreasingly fewer potential receiving vehicles beyond 300m, as a result of the distribution of vehicles throughout the configuration space and signal attenuation cause by separational distance. Specifically, there are few vehicles that are separated by 400-500m (e.g., nearing the single hop communications range of a single BSM) that successfully receive an originally transmitted BSM and then relay it. Thus, fewer tagged BSMs are received by vehicles beyond 700m.

iv) There is an increase in tagged messages received beyond 500m for configurations other than *A*: For *A* (i.e., no relaying), no vehicles beyond approximately 600m receive BSMs, whereas relatively small numbers of tagged BSMs are received for the other configurations out to distances of 1600m. Configuration *B* only relays tagged messages (i.e., 100%) out to a distance of 1000m, whereas *C* and *D* relay tagged messages (i.e., 5%) out to 2000m. This difference in forwarding policy and GR size causes more tagged messages to be successfully relayed by *C* and *D*, as compared to *B*, which is more evident in the range of 500-700m.

BSM Reception Rate (BRR) as a function of distance from the vehicle that originates the BSM to receiving vehicles, regardless off the number of hops that tagged BSMs travel, is shown in Figure 7.7. Generally, BRR increases slightly at 100m, and thereafter drops as distance increases. BRR is slightly lower when receiving vehicles are very close to transmitting vehicles (e.g., near 0m), as the high densities of collocated vehicles (e.g., see Figure 7.6) increases the likelihood of transmission collisions. For *A*, in which no BSMs are relayed, the BRR range extends to only approximately 600m. By relaying tagged BSMs, the

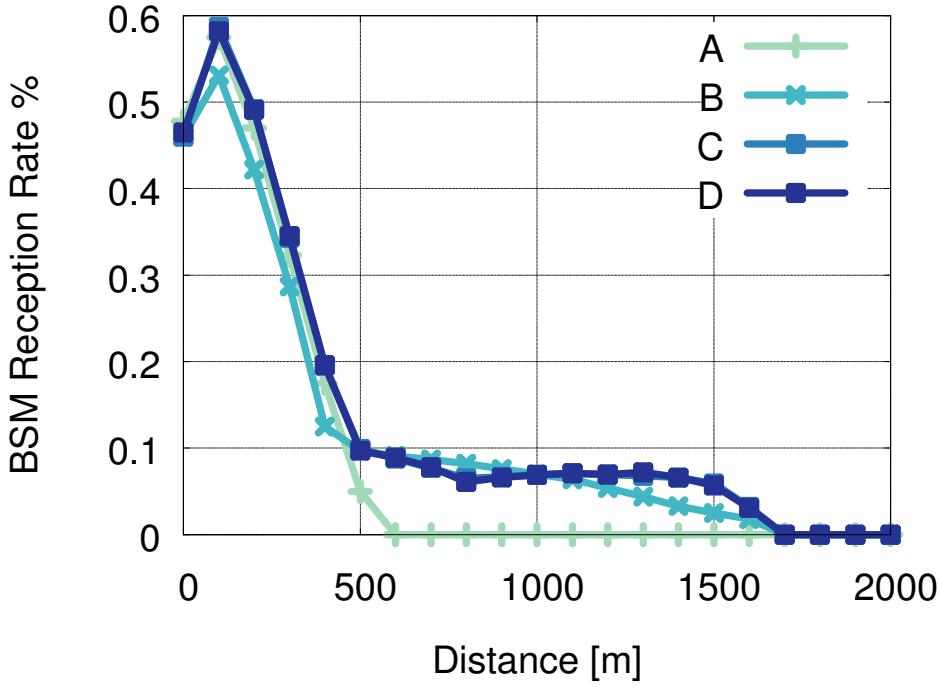

Figure 7.7 A comparison for four different scenarios of the averages of BRR as a function of distance between the vehicle that originally transmits a BSM and vehicles that receive it.

other configurations extend delivery range to approximately 1600m but at lower probability, although the effects in the extended range are difficult to discern among configurations. For example, in the range of 500-1000m, configurations *B*, *C*, and *D* attempt to relay tagged BSMs (i.e., if they can do so successfully before the BSM expires). However, as previously noted (e.g., see Figure 7.6), there are few vehicles in the range of 400-500m that successfully receive and then forward tagged BSMs, thus decreasing BRR as a function of distance between the originating vehicle and potential receiving vehicles.

Awareness probability is compared in Figure 7.8. While the awareness probability range for *A* (no relaying) extends to only approximately 600m, the range extends with comparatively high probability for other configurations. In particular, configuration *B*, *C*, and *D* show awareness probability of at least 40% out to approximately 900m, and at least 20% out to approximately 1600m. Configurations using SafeRelay (*C* and *D*) outperform OZF in the range of 1000-1500m.

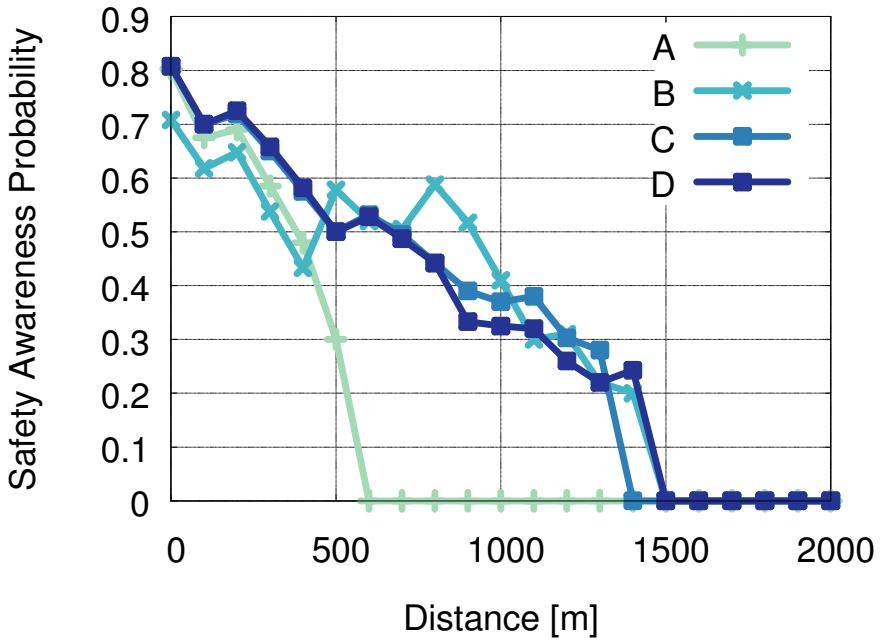

Figure 7.9 A comparison for four different scenarios of the averages of safety awareness probabilities as a function of distance between transmitting and receiving vehicles. Application requirements that increase forwarding zone coverage area help receiving vehicles that are likely to come in contact with one another improve their safety awareness of the sending vehicle.

Differing from awareness probability by additionally considering the mobility factors between two nodes moving towards one another, safety awareness probability is compared in Figure 7.9. While safety awareness probability begins a steep decrease for *A* around approximately 400m and extends only to 600m, the range extends significantly and with relatively high probabilities for other configurations, implying that BSM relay improves considerably a receiving vehicles safety awareness of a sender. In particular, safety awareness probability of at least 50% extends to approximately 600m for configurations *C* and *D*, to approximately 900m for *B*, and is approximately 25% out to 1300m for all BSM relay configurations.

7.5 Conclusions

Safety messaging policies that relay BSMs throughout a FZ can extend safety awareness range without impacting the BSM Reception Rate, thus improving safety awareness without

jeopardizing communications efficiency. For example, in comparing the case in which no BSMs are forwarded to configurations that relay BSMs throughout FZs with GR radius up to 2000m, safety awareness probability of at least 25% is extended from approximately 500m to 1300m, an increase of approximately 160%.

BSM forwarding policy parameters can have a large impact on safety effectiveness, which must account for efficient communications and inter-vehicle mobility concerns. Specifically, it is shown that effects to safety are impacted by the number of vehicles that desire BSMs to be forwarded, the radius and center of the GR that they specify, and the safety message receipt requirements. Greater numbers of vehicles relaying messages improves safety. Safety messages can be disseminated to the range limit of the FZ, although larger zone sizes can lead to greater message interferences that decrease delivery probabilities.

While many previous works evaluate various routing protocols and flooding techniques in a VANET, they do not directly compare results quantitatively in terms of safety-specific metrics that combine both communications (e.g., packet delivery) and mobility (e.g., TTC). Selecting appropriate FZ size, number of participating vehicles, messaging requirements, and flooding algorithm can effectively extend safety range. Improved safety message dissemination makes connected vehicles more aware of one another, thus improving vehicle situational awareness, one of the key goals of the safety-based VANET.

CHAPTER

8

Assessing the Safety Reliability of Modeling the Bursty Vehicular Channel

Many VANET safety applications have been proposed that differ in reliability requirements based upon expected messaging effectiveness that require low latency and high packet delivery probabilities. Yet, communications-level safety performance requirements are not standardized, making it difficult to quantify safety effectiveness in a VANET. Large-scale DSRC deployments suggest harsh operational conditions in which low packet reception rates, bursty channel conditions, and strong shadow fading are observed. Safety evaluations derived from such measurement campaigns are rare, leaving simulation researchers to rely on common VCMs that do not accuracy reflect the conditions of the bursty vehicular channel.

In this chapter we explore through simulation a vehicular channel model that incorporates BUR-GEN, a packet burst generation algorithm that accurately predicts packet reception and loss burstiness. Our results show that safety reliability estimates for V2V safety applications are increased by a factor of 31for maximum safety tolerances, as compared to an i.i.d.-based model that produces that same PRR but does not account for bursty channel behaviors. Simulation studies that do not address packet loss patterns as observed in real-world, large-scale DSRC measurement campaigns, such as the SPMD, fail to accurately predict safety

application reliability, which require low latency and highly successful packet delivery probabilities to occur within harsh environmental conditions.

8.1 Introduction

Modern technical advances provide connected vehicles the potential to improve driving safety. By regularly generating pertinent "here I am" information about itself (e.g., location, speed and heading), vehicles transmit information that is encapsulated within a BSM [11] and rapidly broadcast as a safety beacon to make other nearby vehicles aware of its presence so they can alert drivers of unsafe situations such as pre-crash scenarios. DSRC standards [12] attempt to address requirements for the rapid dissemination of safety messages in highly mobile conditions. Safety success requires high probability of packet delivery while considerable mobility and environmental issues (e.g., obstacles such as other vehicles, buildings, foliage, etc.) jeopardize safety by impeding radio-wave transmissions.

Many VANET safety applications have been proposed [77] [11] that differ in safety intentions based upon expected messaging effectiveness. Proposed applications [11] help vehicles move through intersections (Intersection Movement Assist), alert drivers to specialized vehicles (Emergency Vehicle Alert / Stopped School Bus), increase drivers' awareness of road conditions (Situational Awareness), and warn of imminent pre-crash scenarios (Pre-Crash Warning).

Quantifying safety effectiveness in a VANET remains difficult. Current limited deployments and testing evaluations (e.g., [113]) have not conclusively provided necessary performance and operational standards that quantify safety. Metrics that assess safety effectiveness [52] [81] [85] are not standardized and lack definitions on how they should be applied to real-world test conditions [122].

Large-scale DSRC deployments are rare. To date, the largest real-world measurement campaign involved nearly 3000 vehicles transmitting J2735 BSMs using DSRC, and was conducted over 18 months throughout the Ann Arbor, MI USA area. A two-month subset of data [94] from this study, commonly referred to as the Safety Pilot Model Deployment (SPMD), provided limited data of packet transmission and reception events [14]. Safety performance results were not provided as part of the data release, and to the best of our

knowledge, a detailed assessment of safety effectiveness from the SPMD test data set has not been previously released.

DSRC-based field operations indicate harsh, problematic conditions that may jeopardize safety measures themselves. Analysis of the SPMD measurement campaign data set shows that packet reception rates are low [14]. Shadow fading is strong and the vehicular channel is bursty [14], with occasional long periods of packet losses (Chapter 6). Common models do not accurately characterize the non-ideal vehicular channel [105] (Chapter 6), calling into question the conclusions about safety that may be drawn from results that are based upon such models.

The rarity of large-scale technology deployments, imperfections of simulation-based modeling, and lack of agreed measures to quantify safety effectiveness presents researchers with continued challenges in assessing safety in the safety-based, DSRC-enabled VANET.

8.2 Problem Statement

While high packet reception probabilities are required to ensure high safety application reliability [1] [104], successful packet delivery is not always consistently observed in large-scale DSRC deployments [14] [105] (Chapter 6). Low PRR and bursty communications are common in DSRC environments [14] [87].

Especially troublesome to the low-latency, high-delivery requirements of V2V safety applications, such as imminent crash conditions [104], is the presence of bursty gaps between packet receipts. For example, Figure 8.1 shows the packet receptions derived from the SPMD test data set for a subset of a V2V encounter when the receiving vehicles is less than 100m from the transmitting vehicle. Receptions (i.e., denoted with a red "+") are bursty and inconsistent, with packet loss gaps occurring within the packet stream. Occasional small gaps, and short bursts of consecutively received packets are observed. Additionally, long gaps of packet losses are present, such as before $t = 146s$, between $t = 153s$ and $t = 163s$, and after $t = 174s$. Communication is inconsistent and asymmetric with respect to inter-vehicle separational distance.

Common VCMs do not accurately depict the packet loss behaviors observed in large-scale, real-world DSRC measurement campaigns, especially in their representations of the channel burstiness and packet losses [105] (Chapter 6). Safety evaluations using metrics such as

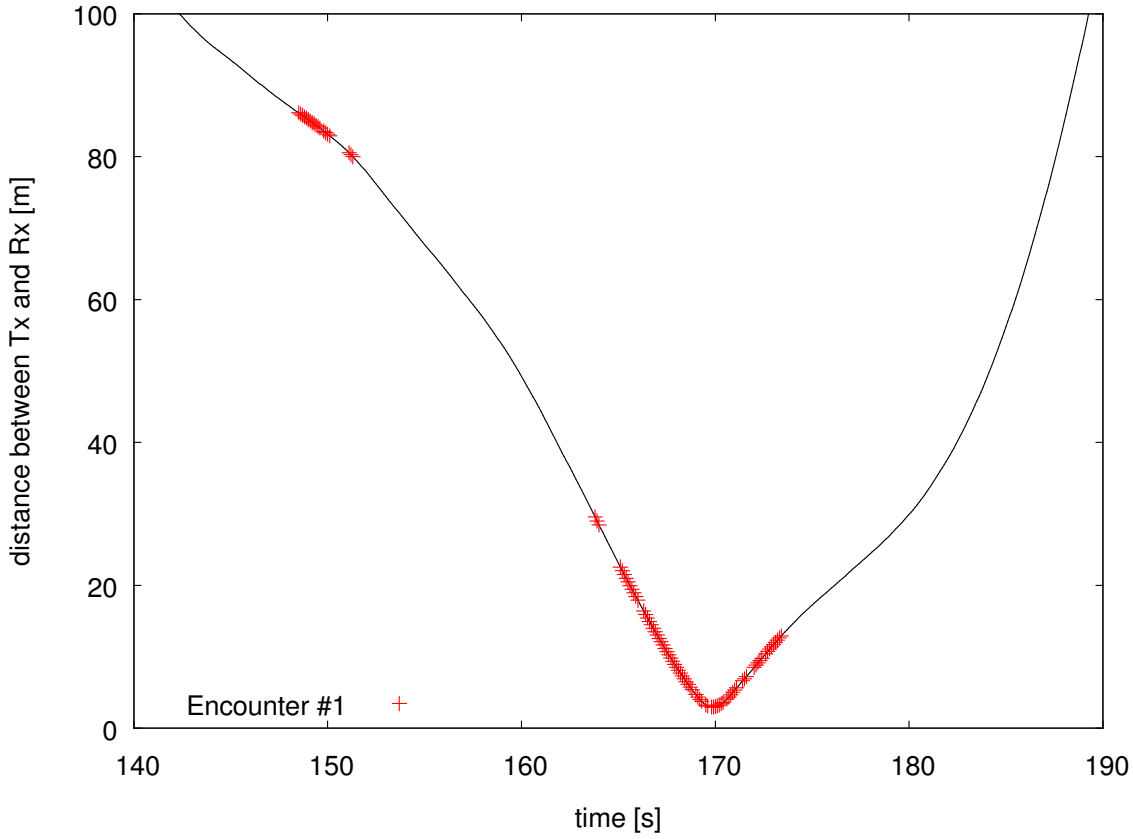

Figure 8.1 Packet reception for a subset of a V2V encounter derived from the SPMD test data set for trip 365 of vehicle 10160 and trip 661 of vehicle 10135 that occurred on 4/13/2013 between 20:11:01 and 20:14:23 UTC, for inter-vehicle separational distances less than 100m. Successful packet receptions are marked with a red "+", and their absence indicates periods of packet loss. Packet receptions and losses are bursty, and highly asymmetrical.

awareness probability (2-28) require minimum packet success rates (i.e., at least $n = 1$ packets in $t \leq T$ seconds, where T is often a small, low-latency requirement) that long packet loss bursts may fail to satisfy. Simulation studies that are based upon such common models may therefore inaccurately represent safety performances if applied to real-world campaigns. For example, in our earlier work [16], we evaluated probability awareness using simulations based on the Nakagami-m fading model (2-1). Our subsequent data analysis of the applicability of common VCMs to the SPMD test data set indicated consistently strong shadow fading [105] throughout the environment that the generalized gamma model (2-23) indicates can be expressed as sub-Nakagami fading.

Evaluation of safety application reliability resulting from vehicle channel models that are suitable for large-scale DSRC deployments (e.g., the SPMD test data set) motivates the following research question:

RQ1: *How do simulation studies that use vehicular channel models affect the safety application reliability estimates as compared to real-world measures gathered from a large-scale DSRC field operational test?*

8.3 Approach

To assess the affect that VCMs have on safety application reliability, we conduct simulation studies of 1,000,000 V2V encounters, that we repeat using two packet generation models:

i) an i.i.d. path loss model (i.e., dual-slope distance-breakpoint model (2-13)) and,

ii) a model that combines an i.i.d. path loss model (i.e., again the dual-slope distance-breakpoint model) with a burst pattern generation algorithm (i..e., BUR-GEN (Chapter 6)).

For each experiment, we calculate the awareness probability for maximum and minimum safety tolerances as derived from expected VSC safety application requirements, and we compare results generated by the simulation models to ground-truth values gleaned from the SPMD test data set.

Table 8.1 lists the application range and message tolerances for maximum and minimum safety requirements for four VSC safety applications (adapted from [104]). These representative safety applications operate over a range of relatively close distances (e.g., 100-300m) with various safety message tolerances. For example, for maximum effective safety,

Table 8.1 Application range and message tolerance for four VSC safety applications.

VSC Application	Application Range [m]	Message Tolerance	
		Maximum Safety	Minimum Safety
Service Vehicle Alert	300	At least 1 in 0.5s	At least 1 in 3.0s
Emergency Electronic Brake Lights	250	At least 1 in 0.3s	At least 1 in 2.0s
Cooperative Forward Collision Warning	150	At least 1 in 0.3s	At least 1 in 1.0s
Lane Change Assist	100	At least 1 in 0.3s	At least 1 in 2.0s

Table 8.2 Minimum and maximum safety performance requirements used for evaluation, as a function of distance.

Range [m]	Maximum Safety Tolerance	Minimum Safety Tolerance
0-150	At least 1 msg in 0.3s	At least 1 msg in 1.0s
150-250	At least 1 msg in 0.3s	At least 1 msg in 2.0s
250-300	At least 1 msg in 0.5s	At least 1 msg in 3.0s

Lane Change Assist requires successful reception of at least 1 message in 300ms, while Service Vehicle Alert requires as a minimum at least 1 message in 3000ms.

8.4 Experimental Setup

The experimental setup repeats exactly the conditions presented in section 6.8 of Chapter 6.

8.5 Results and Discussion

For minimum and maximum levels of safety performance, safety application range and message receipt tolerances were inferred from Table 8.1 and are given in Table 8.2. The packet streams of the simulation model outputs and the SPMD test data set were examined for awareness probability in terms of these safety application performance requirements. Results to 400m comparing the maximum safety tolerance are shown in Figure 8.2 and those for minimum safety tolerances are shown in Figure 8.3.

In maximum safety tolerances shown by Figure 8.2, awareness probability within the SPMD test data set starts relatively high at short distances, and steadily decreases as distance

increases. The presence of long bursts of gaps of dropped packets within the SPMD test data set presents challenges in achieving high awareness probabilities. At short distances of approximately 10m, the awareness probability is nearly 80%, dropping to 30% at 100m. The awareness probability continues to decrease to approximately 10% at 200m. The results produced by the dual-slope distance-breakpoint model significantly overstate the awareness probability for distances less than approximately 100m, and understate it for distances greater than 100m, as compared to the SPMD test data. For this dual-slope distance-breakpoint (only) model, awareness probability is 100% at 10m, indicating that the i.i.d.-based model overestimates the likelihood that at least one packet will be received at short distances, as compared to the real-world SPMD data set, in which packet loss bursts are prevalent. Awareness probability drops sharply and is 0% beyond 140m, indicating that this model predicts that it is extremely rare that at least 1 message will be received within 500ms. Contrastingly, the model that combines the dual-slope distance-breakpoint path loss model with a packet burst algorithm matches well the expected awareness probability observed with the SPMD test data set.

When safety application tolerances are relaxed to the minimum requirements, awareness probabilities of the SPMD test data set increase only slightly. At short distance of approximately 10m, awareness probability is nearly 85%, dropping to 35% at 100m. The awareness probability continues to decrease to approximately 10% at 250m. The results produced by the dual-slope distance-breakpoint model significantly overstate the awareness probability, as compared to the SPMD test data. For the i.i.d. dual-slope distance-breakpoint model, awareness probability is 100% for distances out to 90m, indicating that the i.i.d.-based model overestimates the likelihood that at least one packet will be received at short distances, as compared to the real-world SPMD data set, in which packet loss bursts are prevalent. Additionally, spikes occur in the trendline at 150m and 250, coincident with the changes in requirements in receiving at least n packet. For example, as per Table 8.2, at 150m, the safety reliability requirements change from a minimum of 1 packet in 1.0s to 1 packet in 2.0s. Contrastingly, the model that combines the dual-slope distance-breakpoint path loss model with a packet burst algorithm matches well the expected awareness probability observed with the SPMD test data set.

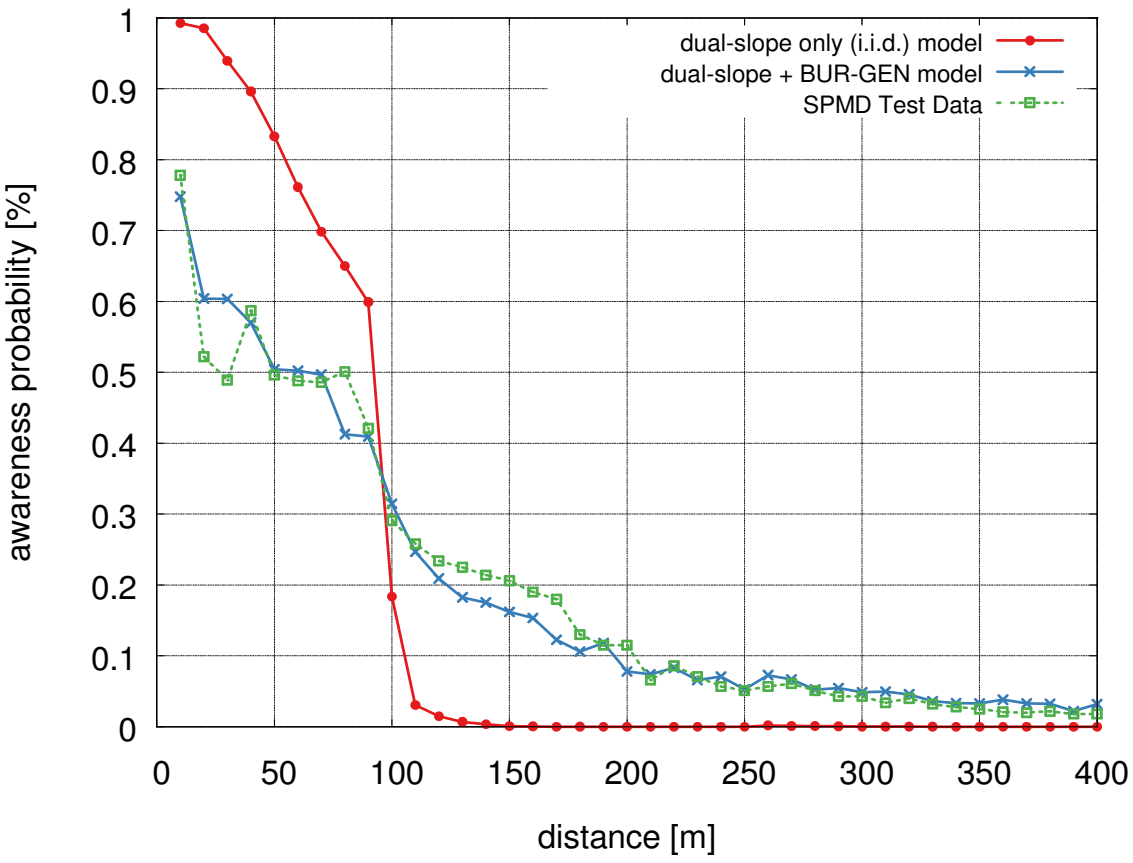

Figure 8.2 Awareness probability as a function of distance between transmitter vehicle and receiving vehicle for maximum safety tolerance requirements

Numerical results comparing the RMSE of awareness probability of each model as compared to the SPMD test data set are given in Figure 8.4. The model that combines the dual-slope distance-breakpoint path loss model with the BUR-GEN packet burst algorithm improves awareness probability estimation, as compared the same path loss model that does not include BUR-GEN, by factors of 31 (maximum safety tolerances) and 128 (minimum safety tolerances), respectively.

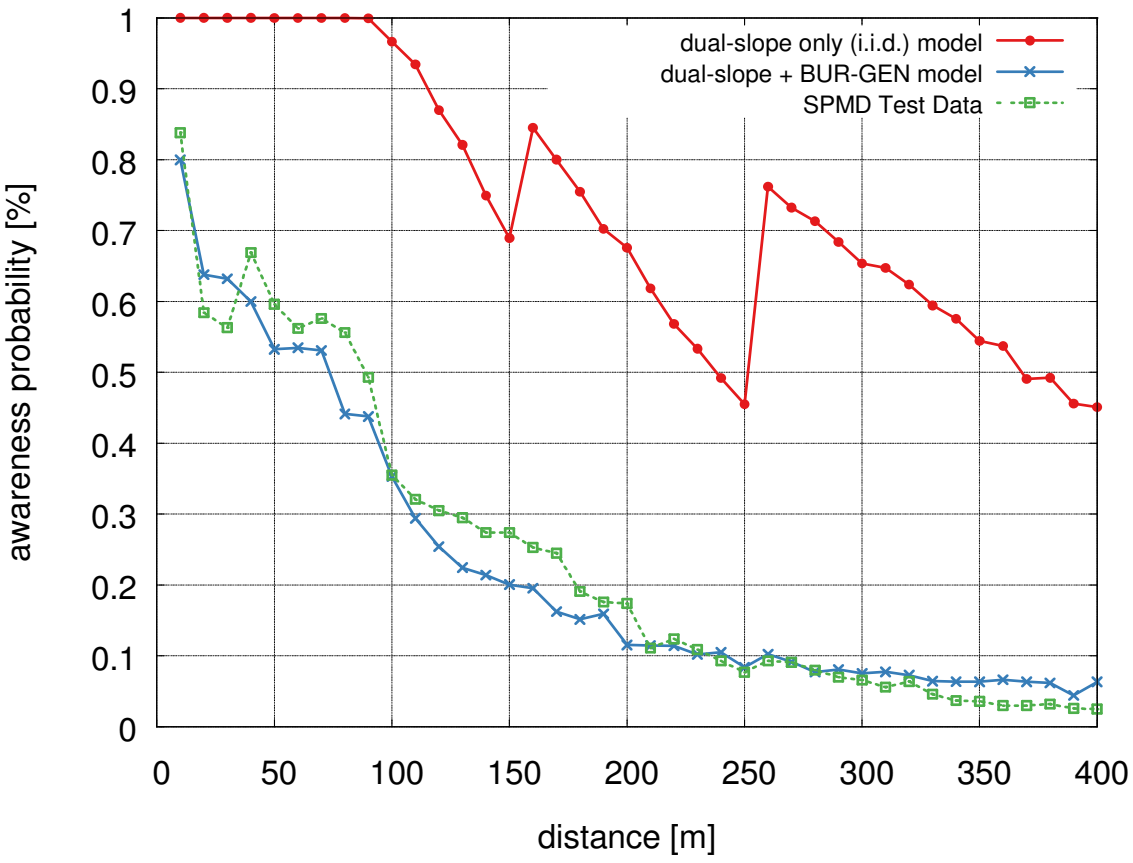

Figure 8.3 Awareness probability as a function of distance between transmitter vehicle and receiving vehicle for minimum safety tolerance requirements.

	RMSE vs. SPMD test data set	
Model	**Min. safety tolerance**	**Max. safety tolerance**
dual-slope only (i.i.d.)	10.22	1.24
dual-slope + BUR-GEN	0.08	0.04

Figure 8.4 Numerical results of the RMSE of awareness probability between the model and the SPMD Test Data, for maximum and minimum safety tolerances

8.6 Conclusions

In simulation, a vehicular channel model that incorporates BUR-GEN and accurately predicts packet reception and loss burstiness improves the safety reliability estimates for V2V safety applications by a factor of 31 for maximum safety tolerances, as compared to i.i.d.-based model that produces that same PRR but does not account for bursty channel behaviors. Simulation studies that do not address packet loss patterns as observed in real-world, large-scale DSRC measurement campaigns, such as the SPMD, fail to accurately predict safety application reliability, which require low latency and highly successful packet delivery probabilities to occur within harsh environmental conditions.

CHAPTER

9

Conclusions and Future Work

9.1 Conclusions

This dissertation presents evidence that advances the modeling accuracy of VCMs by better-matching authentic observations, and additionally enhances VANET safety measures themselves, thus supporting our thesis statement outlined in Chapter 1. In Chapter 3, we consider deterministic path loss models, such as the Obstacle Model implemented in the *ns-3* simulator [13], and show that such models tend to improve accuracy of vehicular channel modeling but are highly dependent upon the availability of geodata that describes buildings and obstacles that may interfere with radio wave propagations and do not account for mobile obstructions [105]. In the absence of complete geodata, such deterministic shadowing models fail to account for all fading and shadowing outcomes that are found in truthful measurement data sets. We present in Chapter 4 data analysis of safety packet loss behaviors for a large, field operational test utilizing nearly 3000 vehicles near Ann Arbor, Michigan, and show that packet losses in the vehicular channel differ significantly from static-node networks, such as Roofnet, and that DSRC packet losses are not necessary independent events, but show temporal and/or spatial correlation tendencies in many encounters [14]. In Chapter 5 we provide analysis of five common radio-wave propagation models suitable for vehicular channel modeling, and show that these mostly i.i.d. models often accurately account for average packet loss behaviors, but fail to address the IPG and consecutive run/loss behaviors that are observed

in real deployments [105]. To address problems with vehicular channel models that fail to address the bursty packet patterns that measurement campaigns, we present in Chapter 6 a new bursty packet generator algorithm, BUR-GEN, that improves the accuracy of packet loss and reception probabilities by factors of six and four, respectively, as opposed to common, i.i.d.-base packet generation models, when compared to the SPMD results.

In Chapter 7, we explore safety message dissemination and show that situational awareness can be improved greatly in the time-constrained safety VANET using SafeRelay, a simple flooding-based technique that honors the safety channel constraints of the safety VANET, and which we evaluate with a newly-defined metric, safety awareness probability that combines communications and vehicular mobility into a single metric [16]. Finally, in Chapter 8, we present evidence of the improvements to safety measures, such as awareness probability, that an improved VCM that includes a bursty packet generation algorithm (i.e., BUR-GEN) has when evaluating VCMs. As compared to common, i.i.d.-based packet generation models that often mis-predict safety, we show that BUR-GEN improves awareness probability factors of 31 and 128, respectively, for maximum and minimum safety tolerances, when results generated using BUR-GEN are compared against those from commonly available VCMs, and compared to the actual awareness probabilities of the SPMD measurement campaign.

Simulation studies that do not address packet loss patterns as observed in real-world, large-scale DSRC measurement campaigns, such as the SPMD, fail to accurately predict safety application reliability, which require low latency and highly successful packet delivery probabilities to occur within harsh environmental conditions. Model selection in simulation-based studies influences performance accuracy conclusions about VANET application reliability. To improve the accuracy of simulation-based results and safety performance assessments, as compared to real-world, large-scale DSRC measurement campaigns, the bursty conditions of the vehicular channel cannot be ignored when properly modeling the channel behaviors.

9.2 Future Work

The motivation for our future work lies in potential means to further elaborate our thesis, especially in the development of VCMs and safety measures that further improve accuracy w.r.t. DSRC FOTs. Therefore, future efforts may include the following:

- Test the BUR-GEN model approach in network simulation, by implementing the model (and perhaps other path loss models, such as the dual-slope distance-breakpoint, and generalized gamma path loss models) in a network simulator, such as *ns-3*.
- Evaluate the effect of bursty packet generation functions (e.g., such as BUR-GEN) on safety evaluations that use other safety performance measures, such as the impact of incorporating TTC within a safety performance assessment (i.e., application through simulation of BUR-GEN through the measure of safety awareness probability).
- Consideration of additional DSRC-based measurement campaigns, aside from the Ann Arbor SPMD study, as data becomes available, to see if bursty channel behaviors exist in similar or different conditions within other FOT data sets.
- Further augment deterministic obstacle shadow modeling with abilities to incorporate richer data set of obstacle data. For example: extend data modeling beyond OSM data, include 3D characteristics, and apply obstacle modeling to (moving) vehicles (i.e., beyond the limited data for static buildings that is commonly available).
- Evaluate further the concepts of burst distribution functions to identify sets of functions that model well the observed behaviors of packet burstiness. For example, examine the use of long-tailed power-law distributions, and CPDFs in their "next packet burst" prediction capabilities.
- Refine VCMs on a more microscopic-level by sensitivity analysis of isolated V2V encounters (e.g., downtown intersection, highway, residential area, tunnel, parking garage, etc.) to better describe bursty packet loss behaviors on an individual geographically-based scenario, as opposed to analysis derived from wide-scale, city-based data.

REFERENCES

[1] M. Shulman and R. Deering, "Vehicle safety communications in the united states," in *Conference on Experimental Safety Vehicles,* 2007.

[2] *National Highway Traffic Safety Administration, Fatality Analysis Reporting System (FARS) Encyclopedia, Online: [http://www-fars.nhtsa.dot.gov/Main/index.aspx], Accessed: [July 12, 2014].*

[3] M. L. Sichitiu and M. Kihl, "Inter-vehicle communication systems: a survey," *Communications Surveys & Tutorials, IEEE,* vol. 10, *(2),* pp. 88-105, 2008.

[4] *U.S. Department of Transportation, Connected Vehicle Research, Online: [http://www.its.dot.gov/connected_vehicle/connected_vehicle.htm], Accessed: [July 12, 2014].*

[5] IEEE, "IEEE Standard for Information technology--Telecommunications and information exchange between systems Local and metropolitan area networks--Specific requirements Part 11: Wireless LAN Medium Access Control (MAC) and Physical Layer (PHY) Specifications," *IEEE Std 802. 11-2012 (Revision of IEEE Std 802. 11-2007),* pp. 1-2793, 2012. . DOI: 10.1109/IEEESTD.2012.6178212.

[6] IEEE, "IEEE Draft Guide for Wireless Access in Vehicular Environments (WAVE) - Architecture," *IEEE P1609. 0/D6. 0, June 2013,* pp. 1-96, 2013.

[7] IEEE, "IEEE Standard for Wireless Access in Vehicular Environments Security Services for Applications and Management Messages," *IEEE Std 1609. 2-2013 (Revision of IEEE Std 1609. 2-2006),* pp. 1-289, 2013. DOI: 10.1109/IEEESTD.2013.6509896.

[8] IEEE, "IEEE Standard for Wireless Access in Vehicular Environments (WAVE)--Networking Services Corrigendum 1: Miscellaneous Corrections," *IEEE Std 1609. 3-2010/Cor 1-2012 (Corrigendum to IEEE Std 1609. 3-2010),* pp. 1-19, 2012. DOI: 10.1109/IEEESTD.2012.6239546.

[9] IEEE, "IEEE Standard for Wireless Access in Vehicular Environments (WAVE)--Multi-channel Operation," *IEEE Std 1609. 4-2010 (Revision of IEEE Std 1609. 4-2006),* pp. 1-89, 2011. DOI: 10.1109/IEEESTD.2011.5712769.

[10] IEEE, "IEEE Guide for Wireless Access in Vehicular Environments (WAVE) - Architecture," *IEEE Std 1609. 0-2013,* pp. 1-78, 2014. DOI: 10.1109/IEEESTD.2014.6755433.

[11] SAE, "J2735 Dedicated Short Range Communications (DSRC) Message Set Dictionary," 2009.

[12] J. B. Kenney, "Dedicated short-range communications (DSRC) standards in the United States," *Proc IEEE,* vol. 99, *(7),* pp. 1162-1182, 2011.

[13] S. E. Carpenter and M. L. Sichitiu, "An obstacle model implementation for evaluating radio shadowing with ns-3," in *Proceedings of the 2015 Workshop on Ns-3,* 2015.

[14] S. E. Carpenter and M. L. Sichitiu, "Analysis of packet loss in a large-scale DSRC field operational test," in *5th IFIP International Conference on Performance Evaluation and Modeling in Wired and Wireless Networks (PEMWN 2016),* Paris, France, 2016.

[15] S. E. Carpenter and M. L. Sichitiu, "Evaluating the accuracy of vehicular channel models in a large-scale DSRC test," in *14th International Conference on Mobile Ad-Hoc and Sensor Systems (to Appear),* 2017.

[16] S. E. Carpenter and K. Harfoush, "SafeRelay: Improving safety in the time-constrained VANET with geoaddresing relay," in *Vehicular Electronics and Safety (ICVES), 2017 IEEE International Conference on,* 2017.
[17] http://www-fars.nhtsa.dot.gov/Trends/TrendsGeneral.aspx.
[18] *Google Self-Driving Cars Incidents: [https://google-self-driving-car-incidents.silk.co/], Accessed: [January 7, 2017*].
[19] Anonymous "National Transportation Safety Board (NTSB), Preliminary Report, Highway HWY16FH018.
Online: [https://www.ntsb.gov/investigations/AccidentReports/Pages/HWY16FH018-preliminary.aspx], Accessed: [January 7, 2017]," .
[20] Cable News Network (CNN), "http://www.cnn.com/interactive/2014/02/tech/cnn10-future-of-driving/ [Accessed 02/09/2015]," .
[21] http://www.its.dot.gov/connected_vehicle/connected_vehicle.htm.
[22] D. Jiang, Q. Chen and L. Delgrossi, "Optimal data rate selection for vehicle safety communications," in *Proceedings of the Fifth ACM International Workshop on VehiculAr Inter-NETworking,* 2008.
[23] M. van Eenennaam, A. Remke and G. Heijenk, "An analytical model for beaconing in VANETs," in *Vehicular Networking Conference (VNC), 2012 IEEE,* 2012, . DOI: 10.1109/VNC.2012.6407451.
[24] A. Kumar, D. Manjunath and J. Kuri, *Wireless Networking.* 2008.
[25] S. Eichler, "Performance evaluation of the IEEE 802.11 p WAVE communication standard," in *Vehicular Technology Conference, 2007. VTC-2007 Fall. 2007 IEEE 66th,* 2007.
[26] J. Lantz, "FEDERAL COMMUNICATIONS COMMISSION 47 CFR Part 90".
[27] USDOT, Research and Innovative Technology Administration and W. Fehr, "System requirement description: 5.9GHz DSRC vehicle awareness device specification, v3.6,".
[28] J. Harding *et a*l. Vehicle-to-vehicle communications: Readiness of V2V technology for application. National Highway Traffic Safety Administration. Washington, D. C. 2014.
[29] W. Viriyasitavat *et al*, "Vehicular Communications: Survey and Challenges of Channel and Propagation Models," *Vehicular Technology Magazine, IEEE,* vol. 10, *(2),* pp. 55-66, 2015. DOI: 10.1109/MVT.2015.2410341.
[30] E. Giordano *et al*, "Corner: a radio propagation model for VANETs in urban scenarios," *Proc IEEE,* vol. 99, *(7),* pp. 1280-1294, 2011.
[31] C. Sommer *et al*, "A computationally inexpensive empirical model of IEEE 802.11 p radio shadowing in urban environments," in *Wireless on-Demand Network Systems and Services (WONS), 2011 Eighth International Conference on,* 2011.
[32] S. Kokalj-Filipovic *et al*, "V2V propagation modeling with imperfect RSSI samples," *ArXiv Preprint arXiv:1409.1846,* 2014.
[33] A. F. Molisch *et al*, "A survey on vehicle-to-vehicle propagation channels," *Wireless Communications, IEEE,* vol. 16, *(6),* pp. 12-22, 2009.
[34] N. Akhtar, O. Ozkasap and S. C. Ergen, "VANET topology characteristics under realistic mobility and channel models," in *Wireless Communications and Networking Conference (WCNC), 2013 IEEE,* 2013.
[35] R. Meireles, M. Ferreira and J. Barros, "Vehicular connectivity models: From single-hop links to large-scale behavior," in *Vehicular Technology Conference Fall (VTC 2009-Fall), 2009 IEEE 70th,* 2009.

[36] E. Van Eenennaam, "A survey of propagation models used in vehicular ad hoc network (vanet) research," *Paper Written for Course Mobile Radio Communication, University of Twente,* pp. 1-7, 2008.
[37] G. Yan and S. Olariu, "A probabilistic analysis of link duration in vehicular ad hoc networks," *Intelligent Transportation Systems, IEEE Transactions on,* vol. 12, *(4),* pp. 1227-1236, 2011.
[38] O. Renaudin *et al*, "Non-stationary narrowband MIMO inter-vehicle channel characterization in the 5-GHz band," *Vehicular Technology, IEEE Transactions on,* vol. 59, *(4),* pp. 2007-2015, 2010.
[39] L. Cheng *et a*l, "Mobile vehicle-to-vehicle narrow-band channel measurement and characterization of the 5.9 GHz dedicated short range communication (DSRC) frequency band," *IEEE J. Select. Areas Commun.,* vol. 25, *(8),* 2007.
[40] S. Marinoni and H. H. Kari, "Ad hoc routing protocol performance in a realistic environment," in *Networking, International Conference on Systems and International Conference on Mobile Communications and Learning Technologies, 2006. ICN/ICONS/MCL 2006. International Conference on,* 2006.
[41] A. Mahaja*n et a*l, "Modeling vanet deployment in urban settings," in *Proceedings of the 10th ACM Symposium on Modeling, Analysis, and Simulation of Wireless and Mobile Systems,* 2007.
[42] F. J. Martinez *et al*, "Realistic radio propagation models (RPMs) for VANET simulations," in *Wireless Communications and Networking Conference, 2009. WCNC 2009. IEEE,* 2009.
[43] M. Boban *et al*, "Impact of vehicles as obstacles in vehicular ad hoc networks," *Selected Areas in Communications, IEEE Journal on,* vol. 29, *(1),* pp. 15-28, 2011.
[44] R. Scopigno and H. A. Cozzetti, "Signal shadowing in simulation of urban vehicular communications," in *Wireless and Mobile Communications (ICWMC), 2010 6th International Conference on,* 2010.
[45] F. J. Martinez *et al*, "Assessing the impact of a realistic radio propagation model on VANET scenarios using real maps," in *Network Computing and Applications (NCA), 2010 9th IEEE International Symposium on,* 2010.
[46] M. Fogue *et al*, "Analysis of the most representative factors affecting warning message dissemination in VANETs under real roadmaps," in *Modeling, Analysis & Simulation of Computer and Telecommunication Systems (MASCOTS), 2011 IEEE 19th International Symposium on,* 2011.
[47] J. S. Otto, F. E. Bustamante and R. A. Berry, "Down the block and around the corner the impact of radio propagation on inter-vehicle wireless communication," in *Distributed Computing Systems, 2009. ICDCS'09. 29th IEEE International Conference on,* 2009.
[48] S. A. Hosseini Tabatabaei *et al*, "Improving propagation modeling in urban environments for vehicular ad hoc networks," *Intelligent Transportation Systems, IEEE Transactions on,* vol. 12, *(3),* pp. 705-716, 2011.
[49] C. Sommer, D. Eckhoff and F. Dressler, "IVC in Cities: Signal Attenuation by Buildings and How Parked Cars Can Improve the Situation," 2013.
[50] R. Chen *et al*, "Performance analysis of connectivity for vehicular ad hoc networks with moving obstructions," in *Vehicular Technology Conference (VTC Fall), 2014 IEEE 80th,* 2014.

[51] M. Nakagami, "The m-distribution-A general formula of intensity distribution of rapid fading," *Statistical Method of Radio Propagation,* 1960.
[52] X. Yin *et al*, "Performance and reliability evaluation of BSM broadcasting in DSRC with multi-channel schemes," *IEEE Trans. Comput.,* vol. 63, *(12),* pp. 3101-3113, 2014.
[53] M. Killat and H. Hartenstein, "An empirical model for probability of packet reception in vehicular ad hoc networks," *EURASIP Journal on Wireless Communications and Networking,* vol. 2009, *(1),* pp. 721301, 2009.
[54] P. M. Shankar, *Fading and Shadowing in Wireless Systems.* 2011.
[55] V. A. Aalo, T. Piboongungon and C. Iskander, "Bit-error rate of binary digital modulation schemes in generalized gamma fading channels," *Communications Letters, IEEE,* vol. 9, *(2),* pp. 139-141, 2005.
[56] F. J. Martinez *et al*, "Computer simulations of VANETs using realistic city topologies," *Wireless Personal Communications,* pp. 1-25, 2013.
[57] F. J. Martinez *et al*, "A survey and comparative study of simulators for vehicular ad hoc networks (VANETs)," *Wireless Communications and Mobile Computing,* vol. 11, *(7),* pp. 813-828, 2011.
[58] J. Harri, F. Filali and C. Bonnet, "Mobility models for vehicular ad hoc networks: a survey and taxonomy," *Communications Surveys & Tutorials, IEEE,* vol. 11, *(4),* pp. 19-41, 2009.
[59] R. Nagel and S. Eichler, "Efficient and realistic mobility and channel modeling for VANET scenarios using OMNeT and INET-framework," in *Proceedings of the 1st International Conference on Simulation Tools and Techniques for Communications, Networks and Systems & Workshops,* 2008.
[60] T. L. Willke, P. Tientrakool and N. F. Maxemchuk, "A survey of inter-vehicle communication protocols and their applications," *Communications Surveys & Tutorials, IEEE,* vol. 11, *(2),* pp. 3-20, 2009.
[61] S. K. Bhoi and P. M. Khilar, "Vehicular communication: a survey," *Networks, IET,* vol. 3, *(3),* pp. 204-217, 2014.
[62] F. Cadger *et al*, "A survey of geographical routing in wireless ad-hoc networks," *Communications Surveys & Tutorials, IEEE,* vol. 15, *(2),* pp. 621-653, 2013.
[63] B. Blaszczyszyn *et al*, "Opportunistic broadcast in vanets (ob-van) using active signaling for relays selection," in *ITS Telecommunications, 2008. ITST 2008. 8th International Conference on,* 2008.
[64] Y. Zhuang, J. Pan and L. Cai, "A probabilistic model for message propagation in two-dimensional vehicular ad-hoc networks," in *Proceedings of the Seventh ACM International Workshop on VehiculAr InterNETworking,* 2010.
[65] D. Abada and A. Massaq, "Improving Relay Selection Scheme for Connecting VANET to Internet over IEEE 802.11 p," *International Journal of Computer Applications,* vol. 132, *(2),* pp. 1-8, 2015.
[66] S. Oh, M. Gruteser and D. Pompili, "Coordination-free Safety Messages Dissemination Protocol for Vehicular Networks," *IEEE Transactions on Vehicular Technology,* 2012.
[67] Simulation for Urban Mobility (SUMO), "http://sumo-sim.org/ [Accessed 02/09/2015]".
[68] M. Behrisch *et al*, "Sumo-simulation of urban mobility-an overview," in *SIMUL 2011, the Third International Conference on Advances in System Simulation,* 2011, .

[69] S. Krauss, P. Wagner and C. Gawron, "Metastable states in a microscopic model of traffic flow," *Physical Review E,* vol. 55, *(5),* pp. 5597, 1997.
[70] T. Honda *et al*, "Effect of buildings in VANETs communication: Performance of OLSR protocol for video streaming application," in *Broadband and Wireless Computing, Communication and Applications (BWCCA), 2013 Eighth International Conference on,* 2013.
[71] Y. H. Ho, A. H. Ho and K. A. Hua, "Routing protocols for inter-vehicular networks: A comparative study in high-mobility and large obstacles environments," *Comput. Commun.,* vol. 31, *(12),* pp. 2767-2780, 2008.
[72] W. Cha *et al*, "An adaptive link management for vehicular ad hoc networks," in *Wireless Communications and Signal Processing (WCSP), 2010 International Conference on,* 2010, .
[73] http://www.its.dot.gov/testbed.htm.
[74] http://www.omnetpp.org/.
[75] http://veins.car2x.org/.
[76] ns-3 network simulator, "http://www.nsnam.org/ [Accessed 02/09/2015]".
[77] CAMP Vehicle Safety Communications Consortium, "Vehicle safety communications project: task 3 final report: identify intelligent vehicle safety applications enabled by DSRC," *National Highway Traffic Safety Administration, US Department of Transportation, Washington DC,* 2005.
[78] http://www.its.dot.gov/connected_vehicle/connected_vehicle_policy.htm.
[79] G. Bianchi, L. Fratta and M. Oliveri, "Performance evaluation and enhancement of the CSMA/CA MAC protocol for 802.11 wireless LANs," in *Personal, Indoor and Mobile Radio Communications, 1996. PIMRC'96., Seventh IEEE International Symposium on,* 1996.
[80] J. Lin *et al*, "Wireless communication performance based on IEEE 802.11 p R2V field trials," *Communications Magazine, IEEE,* vol. 50, *(5),* pp. 184-191, 2012.
[81] F. Ba*i et a*l, "Towards characterizing and classifying communication-based automotive applications from a wireless networking perspective," in *Proceedings of IEEE Workshop on Automotive Networking and Applications (AutoNet),* 2006.
[82] X. Yin *et al*, "Performance and Reliability Evaluation of BSM Broadcasting in DSRC with Multi-channel Schemes," 2013.
[83] M. Khairnar, D. Vaishali and D. Kotecha, "Simulation-Based Performance Evaluation of Routing Protocols in Vehicular Ad-hoc Network," *ArXiv Preprint arXiv:1311.1378,* 2013.
[84] J. Haerri, F. Filali and C. Bonnet, "Performance comparison of AODV and OLSR in VANETs urban environments under realistic mobility patterns," *Department of Mobile Communication BP,* vol. 193, pp. 06904, 2006.
[85] N. An, T. Gaugel and H. Hartenstein, "VANET: Is 95% probability of packet reception safe?" in *ITS Telecommunications (ITST), 2011 11th International Conference on,* 2011. DOI: 10.1109/ITST.2011.6060037.
[86] D. Aguay*o et a*l, "Link-level measurements from an 802.11 b mesh network," in *ACM SIGCOMM Computer Communication Review,* 2004.
[87] F. Bai, D. D. Stancil and H. Krishnan, "Toward understanding characteristics of dedicated short range communications (DSRC) from a perspective of vehicular network

engineers," in *Proceedings of the Sixteenth Annual International Conference on Mobile Computing and Networking,* 2010.
[88] D. Bezzina and J. Sayer, "Safety pilot model deployment test conductor team report," National Highway Transportation Safety Administration, Washington, D. C., Tech. Rep. DOT HS 812 171, June 2015. 2015.
[89] Anonymous, "U-M Mobility Transformation Center Announces Founding Corporate Partners," *UMTRI Research Review,* vol. 45, *(3),* pp. 3-4, 2014.
[90] T. Geller, "Car talk," *Commun ACM,* vol. 58, *(3),* pp. 16-18, 2015.
[91] D. LeBlanc, S. E. Bogard and R. Goodsell, *Connected Commercial Vehicles—Retrofit Safety Device Kit Project: Model Deployment Operational Analysis Report,* 2014.
[92] Open Street Map (OSM), "http://www.openstreetmap.org/#map=5/51.500/-0.100 [Accessed 02/09/2015]".
[93] *Safety Pilot Model Deployment*. Available: http://www.umtri.umich.edu/our-results/projects/safety-pilot-model-deployment.
[94] USDOT. *Research Data Exchange*.
[95] J. Sayer, "Connected Vehicle Safety Pilot," April 24, 2012, 2012.
[96] Anonymous, "Data-Driven Approach: UMTRI Researchers Embrace Technology to Gather, Manage, and Analyze Data," *UMTRI Research Review,* vol. 46, *(1),* pp. 4-7, 2015.
[97] D. Henclewood, M. Abramovich and B. Yelchuru, "Safety pilot model deployment - one day sample data environment data handbook, V. 1.2," USDOT Research and Technology Innovation Administrations, July 1, 2014. 2014.
[98] A. Clauset, C. R. Shalizi and M. E. Newman, "Power-law distributions in empirical data," *SIAM Rev,* vol. 51, *(4),* pp. 661-703, 2009.
[99] R. L. Sydnor, *The Selection and use of Precise Frequency and Time Systems,* 1996.
[100] D. W. Allan, *Tutorial: Clock and Clock Systems Performance Measures,* 1995.
[101] R. Hernández-Pérez, "Allan deviation analysis of financial return series," *Physica A: Statistical Mechanics and its Applications,* vol. 391, *(9),* pp. 2883-2888, 2012.
[102] W. Riley, "NIST Special Publication 1065," *NIST (Unpublished),* 2008.
[103] T. S. Wiens *et a*l, "Three way k-fold cross-validation of resource selection functions," *Ecol. Model.,* vol. 212, *(3),* pp. 244-255, 2008.
[104] F. Bai and H. Krishnan, "Reliability analysis of DSRC wireless communication for vehicle safety applications," in *Intelligent Transportation Systems Conference, 2006. ITSC'06. IEEE,* 2006.
[105] S. E. Carpenter and M. L. Sichitiu, "Evaluating the accuracy of vehicular channel models in a large-scale DSRC test," in *14th International Conference on Mobile Ad-Hoc and Sensor Systems,* 2017.
[106] S. Bastani, D. T. Ozalla and M. Karaca, "On the performance of vehicular communications with a measurement-based radio propagation model," in *Computer Aided Modelling and Design of Communication Links and Networks (CAMAD), 2016 IEEE 21st International Workshop on,* 2016.
[107] T. Abbas *et al*, "A measurement based shadow fading model for vehicle-to-vehicle network simulations," *International Journal of Antennas and Propagation,* vol. 2015, 2015.
[108] S. Lefèvre, D. Vasquez and C. Laugier, "A survey on motion prediction and risk assessment for intelligent vehicles," *Robomech Journal,* vol. 1, *(1),* pp. 1-14, 2014.

[109] K. Srinivasan *et al*, "The β-factor: Measuring wireless link burstiness," in *Proceedings of the 6th ACM Conference on Embedded Network Sensor Systems,* 2008.
[110] P. G. Gottschalk and J. R. Dunn, "The five-parameter logistic: a characterization and comparison with the four-parameter logistic," *Anal. Biochem.,* vol. 343, *(1),* pp. 54-65, 2005.
[111] A. Koubaa, M. Alves and E. Tovar, "A comprehensive simulation study of slotted CSMA/CA for IEEE 802.15. 4 wireless sensor networks," in *5th IEEE International Workshop on Factory Communication Systems,* 2006.
[112] P. Costa *et al*, "Towards lightweight information dissemination in inter-vehicular networks," in *Proceedings of the 3rd International Workshop on Vehicular Ad Hoc Networks,* 2006.
[113] CAMP Vehicle Safety Communications Consortium 2, "Vehicle Safety Communications – Applications (VSC-A) Final Report: Appendix Volume 1 System Design and Objective Test," *National Highway Traffic Safety Administration, US Department of Transportation, Washington DC,* 2011.
[114] S. K. Bhoi and P. M. Khilar, "Vehicular communication: a survey," *Networks, IET,* vol. 3, *(3),* pp. 204-217, 2014.
[115] X. Ma, X. Yin and K. S. Trivedi, "On the reliability of safety applications in VANETs," *International Journal of Performability Engineering,* vol. 8, *(2),* pp. 115, 2012.
[116] X. Ma *et al*, "MAC and application-level broadcast reliability in vanets with channel fading," in *Computing, Networking and Communications (ICNC), 2013 International Conference on,* 2013.
[117] S. Toma, E. Swanson and W. G. Najm, *Light Vehicle Crash Avoidance Needs and Countermeasure Profiles for Safety Applications Based on Vehicle-to-Vehicle Communications,* 2013.
[118] K. Vogel, "A comparison of headway and time to collision as safety indicators," *Accident Analysis & Prevention,* vol. 35, *(3),* pp. 427-433, 2003. . DOI: http://dx.doi.org.prox.lib.ncsu.edu/10.1016/S0001-4575(02)00022-2.
[119] B. Sultan and M. McDonald, "Assessing the safety benefit of automatic collision avoidance systems (during emergency braking situations)," in *Proceedings of the 18th International Technical Conference on the Enhanced Safety of Vehicle. (DOT HS 809 543),* 2003, .
[120] J. C. Hayward, "Near-miss determination through use of a scale of danger," *Highway Research Record, (384),* 1972.
[121] S. Pundlik, E. Peli and G. Luo, "Time to collision and collision risk estimation from local scale and motion," in *Advances in Visual Computin*g, 2011.
[122] W. Li *et al*, "Analytical model and performance evaluation of long-term evolution for vehicle safety services," *IEEE Transactions on Vehicular Technology,* vol. 66, *(3),* pp. 1926-1939, 2017.

APPENDIX

Appendix A - Abbreviations

AC	–	Access Class
ADEV	–	Allan deviation
AIFS	–	Arbitration Interframe Spacing
API	–	application programming interface
BDF	–	burst distribution function
BRR	–	BSM reception ratio
BSM	–	Basic Safety Message
BSP	–	Binary space partition
BSS	–	Basic Service Set
CAMP	–	Crash Avoidance Metrics Partnership
CCH	–	control channel
CCRL	–	Consecutive reception run-length
CFCW	–	Cooperative Forward Collision Warning
CGAL	–	Computational Geometry Algorithms Library
CPDF	–	conditional probability distribution function
CSMA/CA	–	Carrier-Sense Multiple Access with Collision Avoidance
CW	–	congestion window
DAS	–	Data Acquisition System
dB	–	decibel
DE	–	data environment
DSRC	–	Dedicated Short-Range Communications
EDCA	–	Enhanced Distributed Channel Access
EEBL	–	Emergency Electronic Brake Lights
FCC	–	Federal Communications Commission
FEC	–	forward error correction
FOT	–	Field operational test
FSPL	–	Free space path loss
FZ	–	Forwarding Zone
GB	–	geometry-based
GBD	–	geometry-based deterministic
GG	–	generalized gamma (model)
GHz	–	Gigahertz
GPS	–	global positioning satellite
GR	–	geocast region
Hz	–	Hertz
i.i.d.	–	independent and identically distributed
IEEE	–	Institute of Electrical and Electronics Engineers
IP	–	Internet Protocol
IPG	–	inter-packet gap

ITS	–	Intelligent Transportation Systems
JPO	–	Joint Program Office
KS	–	Kolmogorow-Smirnov
KVCV	–	k-Fold Cross Validation
LOS	–	line of sight
MANET	–	Mobile ad hoc network(ing)
MLE	–	Maximum likelihood estimate
MTC	–	Mobility Transportation Center
NG	–	non-geometry-based
NHTSA	–	National Highway Transportation Administration
NLOS	–	non-line of sight
OBU	–	On-Board Unit
OCB	–	Outside the context of a BSS
OFDM	–	Orthogonal Frequency Division Multiplexing
OLOS	–	obstructed line of sight
OSM	–	Open Street Map
OZF	–	One Zero Flooding
PCS	–	Pre-Crash Warning
PDP	–	Packet Delivery Probability
PDR	–	Packet delivery ratio
PER	–	Packet Error Rate
PLBL	–	Packet Loss Burst Length
PRR	–	Packet reception ratio
QoS	–	Quality of Service
RMSE	–	root-mean-square-error
RPM	–	radio propagation model
RQ	–	research question
RSE	–	Roadside equipment
RSS	–	received signal strength
RSSI	–	received signal strength indicator
RSU	–	Roadside Unit
SCH	–	service channel
SINR	–	signal-to-interference-plus-noise ratio
SPMD	–	Safety Pilot Model Deployment
STI	–	safety transmission interval
SUMO	–	Simulator for Urban Mobility
TTC	–	time to contact
UMTRI	–	University of Michigan Transportation Research Institute
USDOT	–	United States Department of Transportation
V2I	–	Vehicle to infrastructure
V2V	–	Vehicle to vehicle

VANET	–	Vehicular ad hoc network
VCM	–	Vehicular channel model
VSCC	–	Vehicle Safety Communications Consortium
WAVE	–	Wireless Access for Vehicular Environment
WLAN	–	Wireless Local Area Network
WME	–	Wave Management Entity
WSMP	–	Wave Short Message Protocol
WSSUS	–	Wide Sense Stationary Uncorrelated Scattering
ZCOR	–	Zero-Coordination Opportunistic Routing